BEHAVIOR OF REINFORCED CONCRETE INFILLED FRAMES UNDER DYNAMIC LOADING: PART 1

APPROVED BY
SUPERVISING COMMITTEE:

____

Richard E. Klingner

____

Michael E. Kreger

BEHAVIOR OF REINFORCED CONCRETE INFILLED FRAMES UNDER DYNAMIC LOADING: PART 1

by

TAREK REFAAT BASHANDY, B.S.E.

THESIS

Presented to the Faculty of the Graduate School of

The University of Texas at Austin

in Partial Fulfillment

of the Requirements

for the Degree of

MASTER OF SCIENCE IN ENGINEERING

THE UNIVERSITY OF TEXAS AT AUSTIN
May 1995

To Refaat and Suzan

ACKNOWLEDGMENTS

This research program was conducted at the Phil M. Ferguson Structural Engineering Laboratory, located at J.J. Pickle's research center of the University of Texas at Austin. Funding of this project was provided by the U.S. Army Construction Engineering Laboratory (USACERL). The research report was a result of joint effort of a team consisting of the author and Nestor Rubiano. This thesis is based on the research report Some material presented here was a result of the team work, and will also be presented in a separate thesis written by Mr. Rubiano.

The author wishes to express his gratitude to Dr. Richard Klingner for his guidance throughout the author's study at the University of Texas. No part of this thesis would have been possible without his assistance, encouragement and suggestions in planning. In addition, special thanks to Dr. Kreger for his valuable advice and for being my second reader.

The assistance of the entire staff of the Ferguson laboratory is greatly appreciated. Special thanks to Cindy for her help in formatting the thesis.

Finally, there are no words the author can use to thank his father and mother for their encouragement and support throughout his life. You will always be my best friends.

Tarek Refaat Bashandy

December 12, 1994

ABSTRACT

BEHAVIOR OF REINFORCED CONCRETE INFILLED FRAMES UNDER DYNAMIC LOADING: PART 1

by

Tarek Refaat Bashandy, M.S.E.

The University of Texas at Austin, 1995

Supervising Professor: Richard E. Klingner

Many buildings used by the U.S. Army are classified as reinforced concrete frames with masonry infill walls. There is therefore a need to develop reliable analysis tools to predict the real strength and the dynamic response of such infilled frames. For that reason, a comprehensive multi-year study was carried out by the staff of the U.S. Army Construction Engineering Research Laboratories (USACERL). In that study, several half-scale specimens consisting of reinforced concrete frames (bare and with masonry infill), were subjected to simulated earthquake motions using a shaking table. Both in-plane and out-of-plane motions were applied to virgin specimens, previously damaged specimens, and repaired specimens. In the study reported here (carried out at the University of Texas at Austin) no additional experimental work was performed. In this study, the experimental data obtained by the USACERL was used to evaluate both the in-plane and out-of-plane behavior of infilled frames. Load-displacement characteristics were obtained; and maximum loads, deflections and internal strains were measured and assessed. Dynamic response was predicted analytically, using various mathematical idealizations. Finally, simplified analytical idealizations were developed to predict the strength and stiffness of infilled frames.

TABLE OF CONTENTS

LIST OF FIGURES

LIST OF TABLES

CHAPTER 1 INTRODUCTION

Approximately 40% of the buildings inventoried recently by the U.S. Army were classified as concrete frames with infill shear walls (Al-Chaar et al, 1994). Those buildings were designed and constructed following different specifications and construction practices, and the infill panels were not usually intended to be part of the structural system. Therefore, the real strength of these structures and their ability to withstand moderate and large earthquakes must be evaluated. Evaluation of the buildings' seismic resistance requires accurate models for predicting the behavior of infilled frames subjected to in-plane and out-of-plane loads. The in-plane strength and stiffness of the infills is likely to dominate the overall seismic response of the building, while their out-of-plane strength will determine whether or not individual panels will collapse under strong lateral motions.

Because of this need, a research program was initiated in 1992 to develop methods for assessing the seismic vulnerability of existing infilled-frame structures. From early 1992 through May 1993, the U.S. Army Construction Engineering Research Laboratories (USACERL) carried out a series of shaking-table tests on half-scale models of infilled reinforced concrete frames. The original objective of those tests was to aid in the development of engineering models for estimating the load-deflection behavior of the infilled frames under earthquake ground motions, considering elastic and inelastic response, in-plane and out-of-plane response, and the effects of damage due to in-plane excitation on the out-of-plane strength.

A large amount of data was gathered during that test program, including accelerations, displacements, and internal deformations of the specimens. As part of the research study reported here, those data are thoroughly interpreted and analyzed. State-of-the-art analytical models are used to explain the experimental findings. Finally, simplified engineering models are developed for use by designers in predicting the in-plane and out-of-plane strength and stiffness of the infills.

In this thesis, a detailed description of the test specimens and setup is presented. The experimental results obtained from the series of tests are then reviewed and interpreted. Several analytical models used to predict the response of infills are presented, and the specimens' behavior is compared with those analytical predictions. Finally, simplified engineering models are developed and applied.

1.1 Objectives and Scope

The main objective of this thesis is to verify and interpret the experimental findings obtained by the USACERL staff, and to predict such results analytically using both complex and simple idealizations. No additional experimental work was performed at The University of Texas at Austin.

The terminal objectives of this thesis are:

a) Describe the test program, the characteristics of the specimens, and the test setup and procedure,

b) Present the results of the shaking-table tests,

c) Synthesize and evaluate the observed responses,

d) Compare the experimental response with analytical predictions, and

e) Develop simplified engineering models for estimating the earthquake response of the infilled frames.

CHAPTER 2 BACKGROUND INFORMATION ON EXPERIMENTAL PROGRAM

2.1 General Background

In 1992 and 1993, Ghassan Al-Chaar and Steven Sweeney of USACERL performed a series of earthquake-simulated dynamic tests on small-scale reinforced concrete frames infilled with masonry panels. One set of test specimens, referred to from now on as "weak frames," (Figure 2.3) was intended to represent buildings designed by the 1956 ACI Code and old construction practices. A second set of specimens, referred to as "strong frames," (Figure 2.2) was designed by the 1989 ACI Code, and was intended to represent modern buildings. In this section, the test program, specimens, test setup and testing procedure are reviewed.

2.2 Overall Experimental Program

The overall experimental program is summarized in Table 2.1. As shown in that table, the experimental program consisted of tests on 8 "Models." Each Model consisted of a frame (strong or weak, bare or infilled, and tested in- or out-of-plane). For each type of frame, the sequence described below was followed.

First, a bare frame specimen consisting of two parallel frames was tested in-plane (Figure 2.1). Gradually increasing levels of ground motion were applied parallel to the frames. Their dynamic properties were measured and a certain level of damage was produced in the specimens. The frames were then infilled with masonry, and the same type of excitation was again applied. Their dynamic properties were again measured, and the maximum ground motion was gradually increased until the infills cracked. Finally, one infilled frame of the specimen was rotated 90 degrees and subjected to out-of-plane ground motions until severe cracking occurred.

For the strong-frame specimen, the infill was repaired after this out-of-plane excitation and subsequently retested to evaluate the effectiveness of the repair method. The weak-frame specimen was not repaired.

Finally, a strong infilled frame, to which no previous in-plane excitation had been applied, was tested out-of-plane until severe damage was apparent, to estimate the effect of in-plane ground motions on out-of-plane response. No specimen was tested in-plane after applying out-of-plane excitations; therefore, the effects of out-of-plane excitation on in-plane response cannot be assessed.

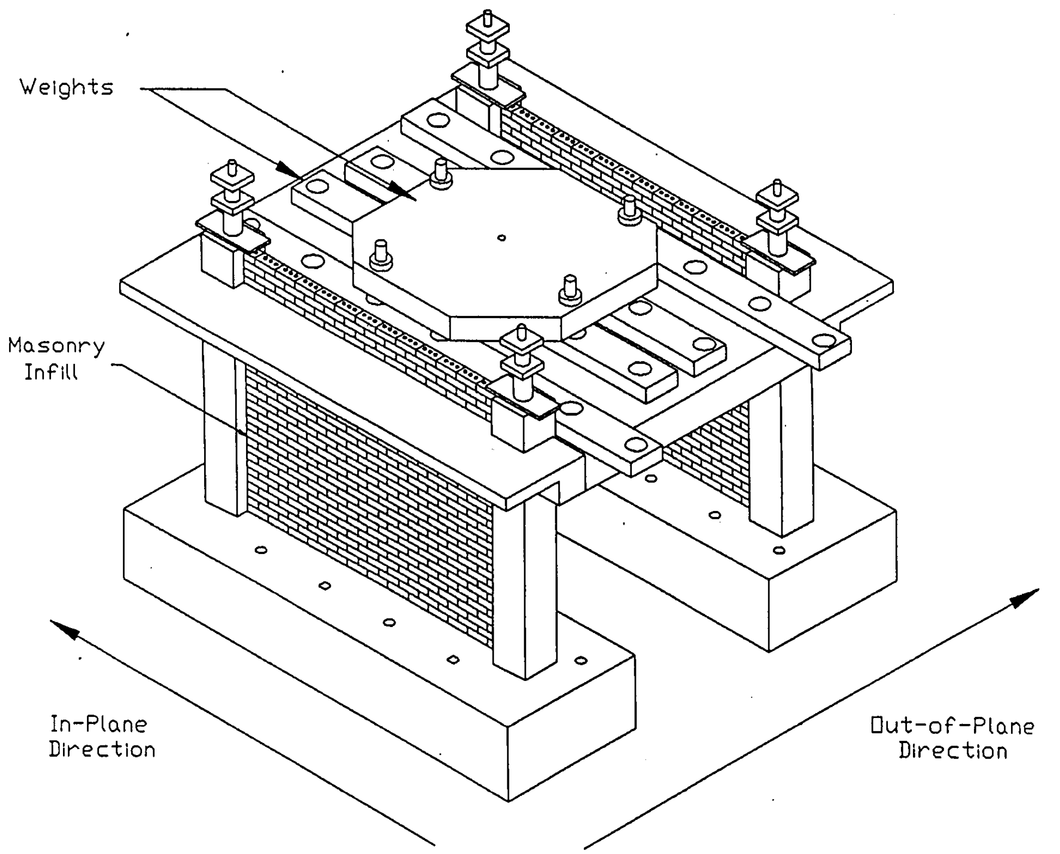

Figure 2.1 Test Setup

Table 2.1 Overall Experimental Program Table

Frame Type	In-Plane Seismic Tests		Out-of-Plane Seismic Tests	
	Bare Frame	**Infilled Frame**	**Unrepaired**	**Repaired**
Strong Frame	Model #1	Model #2	Model #3 Model #5 (Virgin)	Model #4
Weak Frame	Model #6	Model #7	Model #8	Not tested

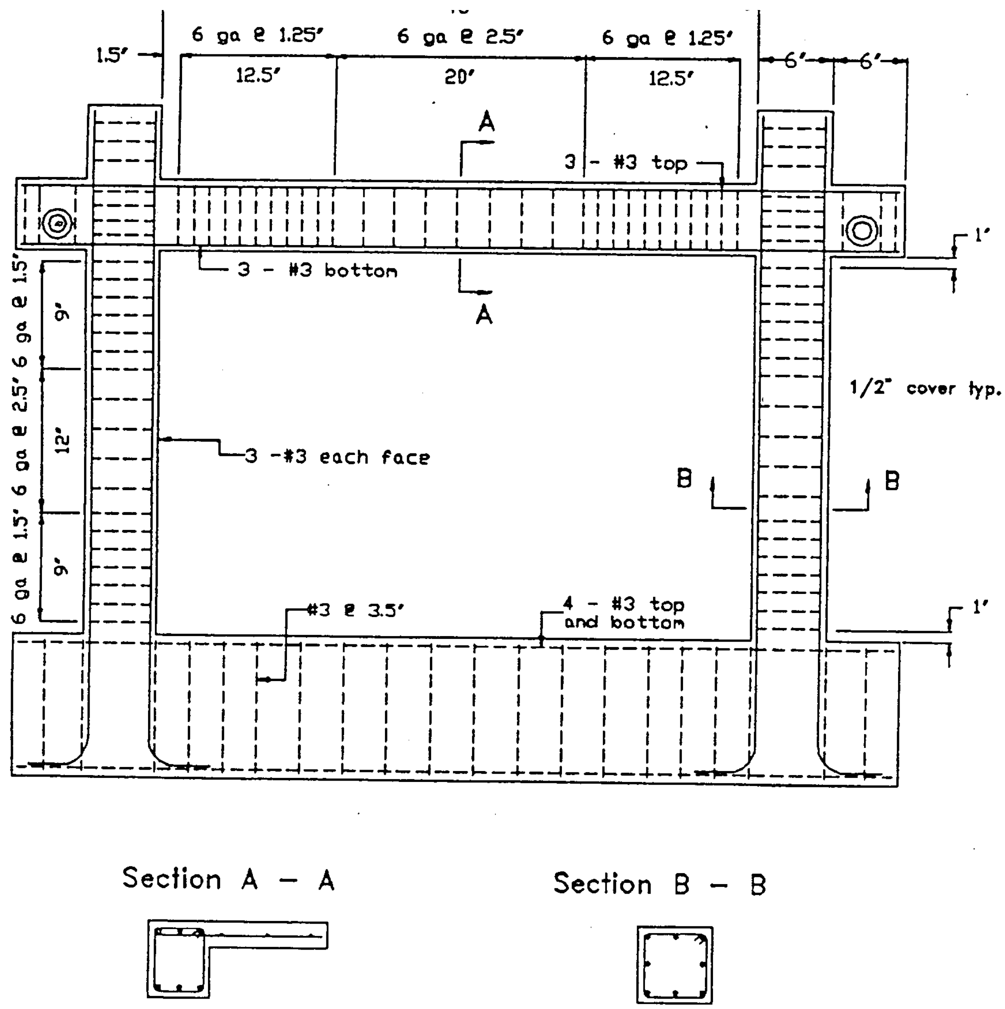

Figure 2.2 Geometry and Reinforcement of the Strong Frame

2.3 Description of Specimens and Test Setup

The specimens were half-scale models of bare and infilled reinforced concrete frames. Each specimen consisted of two parallel one-story, one-bay frames, connected at their top levels by a stiff concrete slab. The slab was attached to the top beams by transverse steel rods. The frame columns were founded on massive beams that were rigidly connected to the shaking-table floor. Figure 2.1 shows the layout and dimensions of the frames and the structural elements. Infills, with a height-to-thickness ratio of 18, were made of half-scale clay brick laid with a Type N mortar. The measured masonry prism compressive strength was 5000 psi (34.5 MPa).

To simulate the effects of the vertical gravity loads generated by overlying stories, post-tensioning cables were threaded through each column in order to increase their axial load. In addition, masses of 8.0 kips (36.5 kN) and 6.0 kips (26.7 kN) were added to the slab of the strong- and weak-frame specimens respectively. These masses were intended to simulate the lateral inertial forces generated in the full-scale prototype under base excitation.

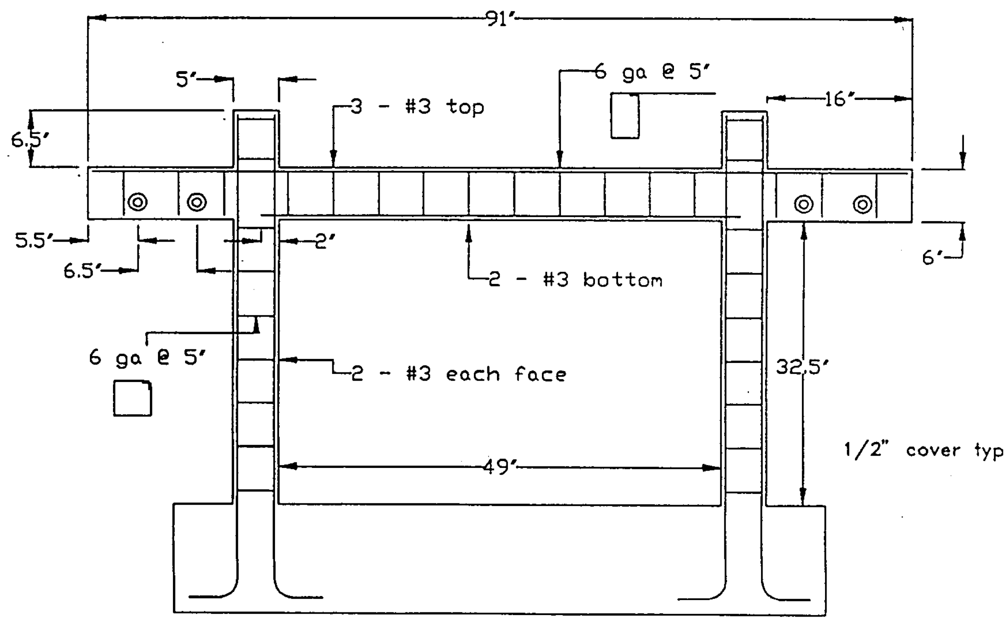

Figure 2.3 Geometry and Reinforcement of the Weak Frame

Ground accelerations were input to the specimens using the USACERL Biaxial Shock Testing Machine (BSTM). The foundation beams of the specimens were rigidly attached to the shaking table to avoid sliding of the frames. At very small time increments, accelerations and displacements were recorded at various locations and reinforcing-bar strains were measured at critical zones of columns and beams.

2.4 Testing Procedure

The first series of tests, performed on strong-frame specimens, comprised Models #1 through #5. The bare-frame specimen (Model #1) was subjected to a series of in-plane ground motions until cracks appeared in the structural elements. Varying levels of axial prestress were applied to the columns of this specimen during the tests.

Infills were then added to its frames, and the specimen was re-named Model #2. A new series of gradually increasing in-plane ground motions was applied to this model until the infills cracked. One infilled frame of this specimen was then rotated 90 degrees and its tip was fixed with cables to the shaking-table floor.

This specimen, named Model #3, was subjected to a series of out-of-plane ground motions until severe cracking occurred in the infills. After this, the masonry infill was repaired on both sides by 1/4-inch x 1/4-inch x 23-gage steel wire mesh, covered by a 1/4-inch (6.35-mm) ferrocement coating designed for high compressive strength and high workability. The steel mesh was not anchored to the infill nor the frame; all bond between the infill and the coating was achieved at the coating-infill interface itself.

This repaired specimen was named Model #4; it was subjected to a new series of increasing out-of-plane ground motions until severe damage occurred. Tables 2.2 through 2.5 describe the sequence of seismic tests for these models, including the span, the maximum base acceleration (A_{max}), the axial prestress in the columns (P_t) and remarks made by the experimenters.

Table 2.2 Seismic Tests for Model #1

Test #	**DATE**	**SPAN (%)**	**A_{max} (g)**	**P_t (kips)**	**Remarks**
1	3/3/92	10.0	—	0.0	Time scale = 1.4142. BAD TEST
2	3/3/92	25.0	0.192	0.0	
3	3/3/92	55.0	0.378	0.0	
4	3/3/92	—	0.379	0.0	
5	3/3/92	55.0	0.372	6.0	
6	3/3/92	55.0	0.375	9.0	Cracks
7	3/3/92	55.0	0.371	12.0	
8	3/3/92	8.0	-0.311	12.0	Filtered. f_c = 2 Hz
9	3/3/92	20.0	-0.838	12.0	Filtered
10	3/3/92	30.0	-1.204	12.0	Filtered
11	3/3/92	40.0	0.984	12.0	Filtered
12	3/3/92	55.0	0.394	12.0	Unfiltered.
13	3/4/92	55.0	0.384	9.0	Unfiltered
14	3/4/92	55.0	0.380	6.0	Unfiltered
15	3/4/92	55.0	0.386	3.0	Unfiltered

Table 2.3 Seismic Tests for Model #2

Test #	**DATE**	**SPAN (%)**	**A_{max} (g)**	**P_t (kips)**	**Remarks**
16	6/8/92	10.0	-0.389	0.0	Filtered
17	6/8/92	30.0	-1.198	0.0	
18	6/8/92	60.0	-3.317	0.0	D9 data bad for this & previous tests.
19	6/8/92	90.0	-5.933	0.0	

Table 2.4 Seismic Tests for Model #3

Test #	**DATE**	**SPAN (%)**	**A_{max} (g)**	**P_t (kips)**	**Remarks**
20	7/9/92	10.0	0.304	0.0	Filtered
21	7/9/92	30.0	0.906	0.0	Recording problems.
22	7/10/92	60.0	1.834	0.0	Filtered.
23	7/10/92	90.0	2.786	0.0	
24	7/10/92	10.0	-0.334	0.0	Filtered (new) fc = 4 Hz.
25	7/10/92	30.0	-1.098	0.0	

Table 2.5 Seismic Tests for Model #4

Test #	**DATE**	**SPAN (%)**	**A_{max} (g)**	**P_t (kips)**	**Remarks**
26	1/7/93	30.0	-1.194	0.0	
27	1/7/93	60.0	-3.142	0.0	
28	1/7/93	90.0	-8.418	0.0	
29	1/7/93	10.0	-0.927	0.0	
30	1/7/93	30.0	-3.738	0.0	A15 = 3.80g
31	1/7/93	60.0	-8.597	0.0	
32	1/8/93	60.0	—	0.0	ABORTED
33	1/8/93	45.0	-2.747	0.0	A15 max = -10.72g

The second series of tests was performed on a "virgin" infilled frame, referred to as Model #5. Gradually increasing levels of out-of-plane shaking were applied until severe damage to the panel was apparent. No previous in-plane ground motions had been applied to this specimen. Table 2.6 describes the sequence of seismic tests for Model #5.

Table 2.6 Seismic Tests for Model #5

Test #	**DATE**	**SPAN (%)**	**A_{max} (g)**	**P_t (kips)**	**Remarks**
34	2/18/93	30.0	-0.579	0.0	
35	2/18/93	60.0	-1.558	0.0	A16 peak = -3.40g
36	2/18/93	90.0	-3.472	0.0	Filtered. Change input. Accels. saturated
37	2/18/93	10.0	-0.460	0.0	
38	2/18/93	45.0	-3.907	0.0	
39	2/18/93	60.0	-4.124	0.0	
40	2/18/93	75.0	4.884	0.0	

A third series of tests, performed on weak-frame specimens, consisted of Models #6 through #8, and followed a sequence similar to that of the first series of tests. Model #6 was a bare-frame specimen, tested in-plane. Fairly constant axial prestress was applied to the columns during all seismic tests of this Model.

It was then infilled with masonry, and re-named Model #7. This Model was tested in-plane until its infills cracked; one of its panels (Model #8) was rotated and excited out-of-plane. However, Model #8 was not repaired after the out-of-plane excitation. Tables 2.7 through 2.9 describe the sequence of the seismic tests for these models.

Table 2.7 Seismic Tests for Model #6

Test #	**DATE**	**SPAN (%)**	**A_{max} (g)**	**P_t (kips)**	**Remarks**
41	4/30/93	10.0	0.082	8.0	Filtered.
42	4/30/93	20.0	0.139	8.0	
43	4/30/93	30.0	0.203	8.0	
44	4/30/93	50.0	0.316	8.0	
45	4/30/93	70.0	0.443	8.0	
46	4/30/93	30.0	-1.119	8.0	Switch to 2 Hz filtered El Centro
47	4/30/93	40.0	-1.563	8.0	

Table 2.8 Seismic Tests for Model #7

Test #	**DATE**	**SPAN (%)**	**A_{max} (g)**	**P_t (kips)**	**Remarks**
48	5/18/93	20.0	-0.785	0.0	
49	5/18/93	40.0	-1.609	0.0	
50	5/18/93	60.0	-3.044	0.0	
51	5/18/93	75.0	-6.384	0.0	
52	5/18/93	85.0	-7.254	0.0	Severe damage, especially in East infill.

Table 2.9 Seismic Tests for Model #8

Test #	**DATE**	**SPAN (%)**	**A_{peak} (g)**	**P_t (kips)**	**Remarks**
53	5/20/93	50.0	-2.235	0.0	There was a problem with A9
54	5/20/93	75.0	-7.021	0.0	
55	5/20/93	90.0	-6.624	0.0	
56	5/20/93	20.0	-1.917	0.0	
57	5/20/93	50.0	-7.150	0.0	Retensioned the four bracing cables
58	5/20/93	70.0	7.985	0.0	

All seismic tests were performed by subjecting each specimen to a series of earthquake records scaled from the North-South component of the El Centro 1940 ground motion. In some cases, high-pass filters with cut-off frequencies ranging from 2.0 to 4.0 Hz were used to remove the low-frequency components of the shaking-table input, permitting the application of higher maximum shaking-table accelerations without exceeding the table's velocity or displacement limits.

CHAPTER 3 OVERALL EXPERIMENTAL RESULTS

3.1 General Description of Experimental Results

A total of 8 models were tested following the program summarized in Table 2.1 and described in detail in Section 2.4. Fifty-eight seismic tests were performed on the different models using increasing levels of ground motion. Test specimens were fully instrumented: accelerations, displacements and strains were recorded. All displacements were absolute (measured with respect to a fixed datum on the laboratory floor).

The global load-displacement response of each model is presented in (Bashandy et al 1994). In this chapter the response of tests that are believed to represent the experimental behavior of the tested models will be discussed in detail. Chapter 4 provides a summary of all test results, and the conclusions derived from them.

3.2 Data Reduction Process

All experimental data recorded during the tests were processed and converted to engineering units by the USACERL research staff. As a result, computer-readable files were produced containing the time history of absolute displacements and accelerations at several locations on the specimens.

Each specimen had a unique instrumentation configuration for acceleration and displacement measurement. The base shear or inertial force acting on a specimen was computed as the response acceleration at the top of the frame times the effective mass of the structure. Displacements relative to the base of the specimens were obtained by subtracting the shaking table's displacement from the absolute displacement at the desired location.

3.3 Synopsis of Overall Experimental Results

3.3.1 Synopsis of Overall Experimental Results for Model #1

Using this strong bare frame, 15 in-plane seismic tests were conducted. Load-displacement diagrams, plotted at the center of the north side of the slab and at the east top beam, are evaluated below for the selected seismic tests.

- *Seismic Test #9*: The peak ground acceleration for this test was 0.84g. This test has relatively regular load-displacement diagrams, with higher values of both base shear and tip displacement than in the previous tests. Load-displacement diagrams for Test #9 are shown in Figures 3.1 and 3.2. A peak base shear of about 13 kips (58 kN) and a maximum lateral displacement of about 0.90 inches (23 mm) were reached. An average backbone stiffness of 180 kips/inch (31.5 kN/mm) was measured. From the two load-displacement diagrams, it is apparent that the frame did not yield. Finally, comparison of these two figures shows that the specimen's recorded response was reasonably consistent at the two different locations.

- *Seismic Test #10*: The peak ground acceleration for this test was 1.20g. This test has a regular load-displacement diagram, with higher values of both base shear and tip displacement than in the previous tests. Figures 3.3 and 3.4 show the load-displacement response at two locations on the specimen. A maximum base shear of 19 kips (84.5 kN) was reached, corresponding to a maximum displacement of about 0.17 inches (4.3 mm). Both diagrams have a backbone stiffness of about 140 kips/inch (24.5 kN/mm). As before, no yielding of the frame is apparent, and both figures show consistent force-displacement behavior measured at different locations on the specimen.
- *Seismic Test #11*: The peak ground acceleration for this test was 0.98g. Figures 3.5 and 3.6 show the load-displacement response for this test. Both of these diagrams show an approximate backbone stiffness of 120 kips/inch (21.0 kN/mm), a maximum load of 20 kips (89.0 kN) (which seems to be the yielding load of the frame), and a maximum displacement of about 0.3 inches (7.6 mm). The load-displacement diagram at the center of the north side of the slab, shown in Figure 3.5, suggests that some yielding of the frame occurred. This behavior, however, is not as obvious in Figure 3.6. The consistency of the displacements and accelerations, measured at different locations on the specimen, is relatively apparent from these diagrams.

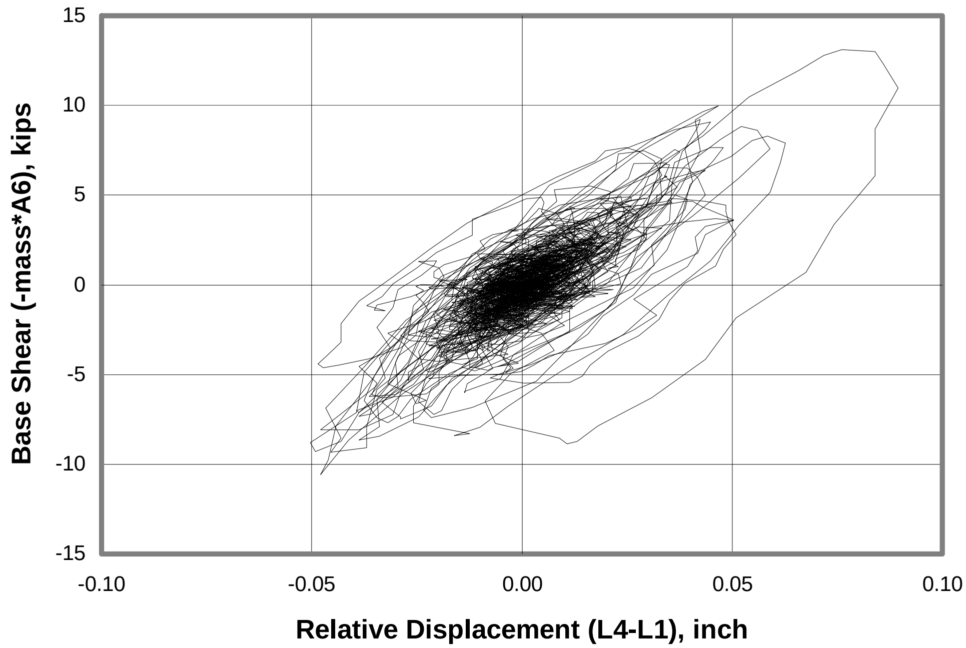

Figure 3.1 Load-Displacement Response at Center of North Side of the Slab for Model #1, Seismic Test #9

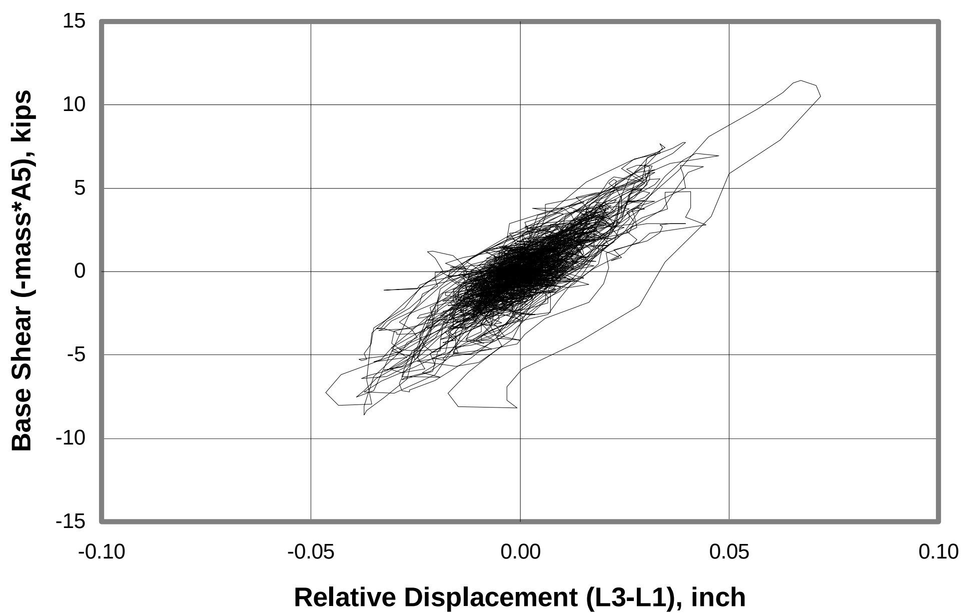

Figure 3.2 Load-Displacement Response at the Center of the Top East Beam for Model #1, Seismic Test #9

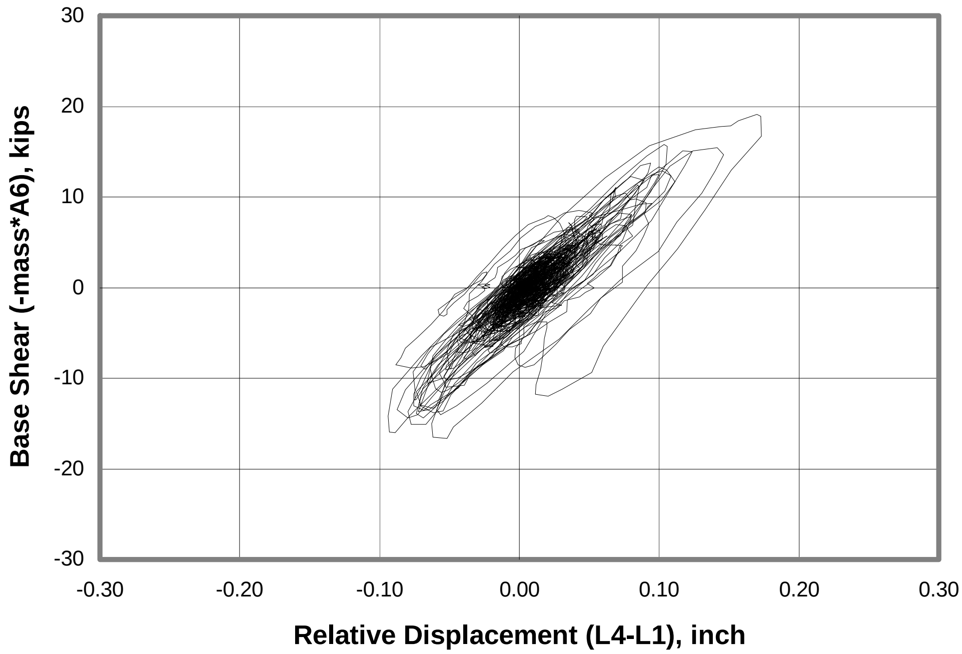

Figure 3.3 Load-Displacement Response at Center of North Side of the Slab for Model #1, Seismic Test #10

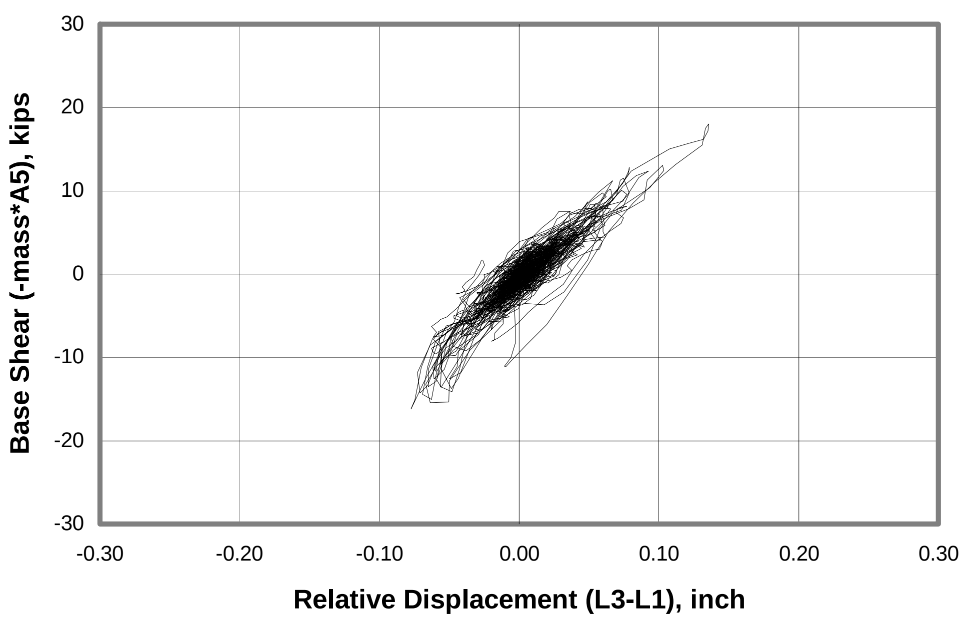

Figure 3.4 Load-Displacement Response at the Center of the Top East Beam for Model #1, Seismic Test #10

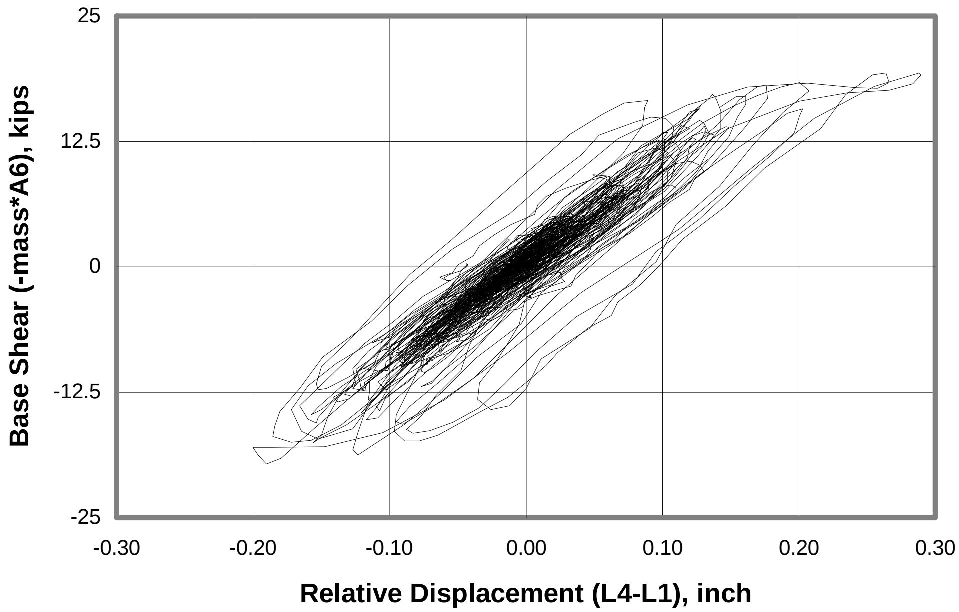

Figure 3.5 Load-Displacement Response at Center of North Side of the Slab for Model #1, Seismic Test #11

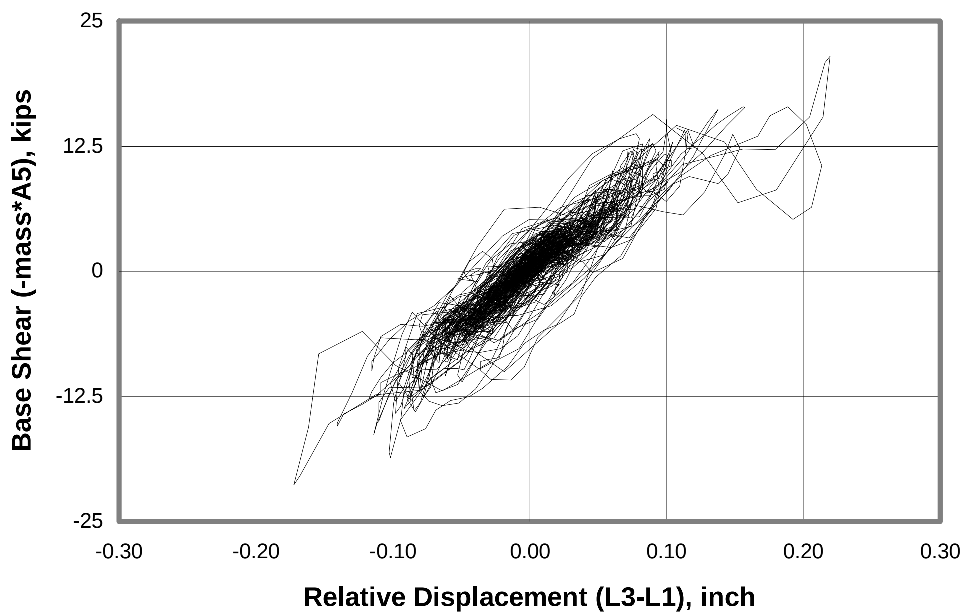

Figure 3.6 Load-Displacement Response at the Center of the Top East Beam for Model #1, Seismic Test #11

3.3.2 Synopsis of Overall Experimental Results for Model #2

This specimen was constructed by infilling the strong bare frames of Model #1. Four in-plane seismic tests were conducted. Load-displacement diagrams, plotted at the center of the north side of the slab and at the east top beam, are evaluated below for the selected seismic tests.

- *Seismic Test #18:* The peak ground acceleration for this test was 3.32g. Figures 3.7 and 3.8 show the load-displacement response at two locations on the specimen. In contrast with the above tests, load-displacement diagrams for Test #18 at the center of the slab are very similar to those taken from the east top beam. However, values of tip displacements for both diagrams are unrealistically high (2 to 6 inches or 50.8 to 152.4 mm), and are accompanied by inconsistent values of base shear. Nevertheless, the load level reached is relatively high (40 kips or 177.9 kN). Based on the load-displacement diagrams, yielding of the structure cannot be predicted.

- *Seismic Test #19:* The peak ground acceleration for this test was 5.93g. Figures 3.3 and 3.4 show the load-displacement response at two locations on the specimen. For this test also, load-displacement diagrams at the center of the slab are very similar to those at the east top beam. Values of tip displacements are also very high (over 10 inches, or 254 mm), accompanied by inconsistent values for base shear. Moreover, the load-displacement pattern shows an unusual shape which suggests a displacement saturation (that is, the gages reached the end of their travel). However, the load levels reached are again very high (over 50 kips or 222.4 kN). Based on the load-displacement diagrams, yielding of the structure cannot be predicted.

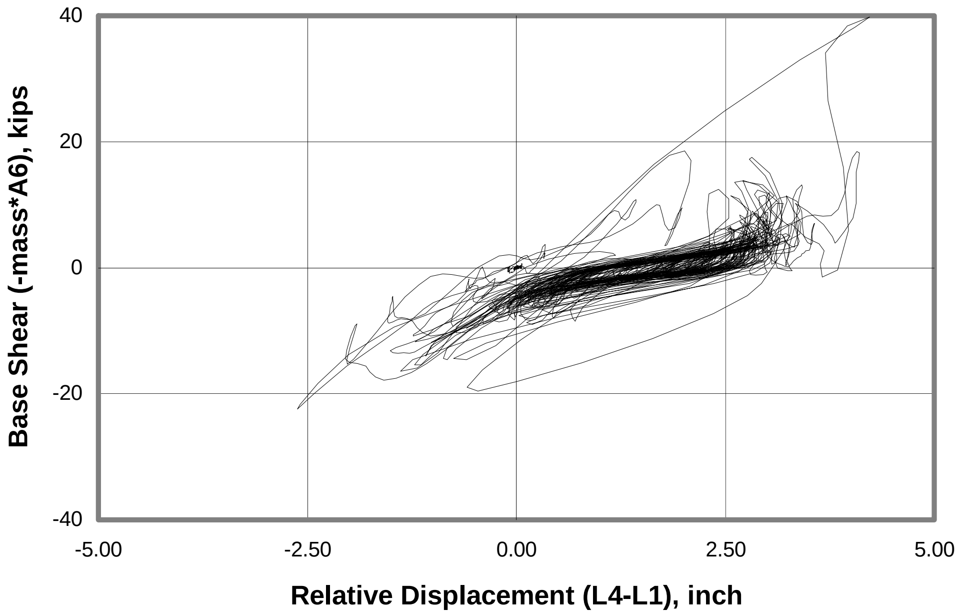

Figure 3.7 Load-Displacement Response at Center of North Side of the Slab for Model #2, Seismic Test #18

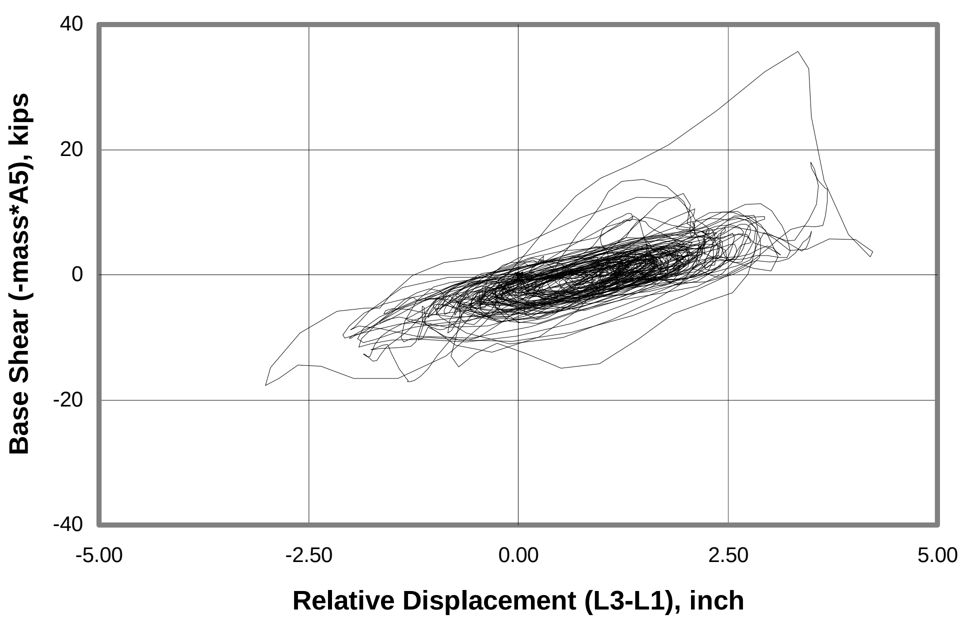

Figure 3.8 Load-Displacement Response at the Center of the Top East Beam for Model #2, Seismic Test #18

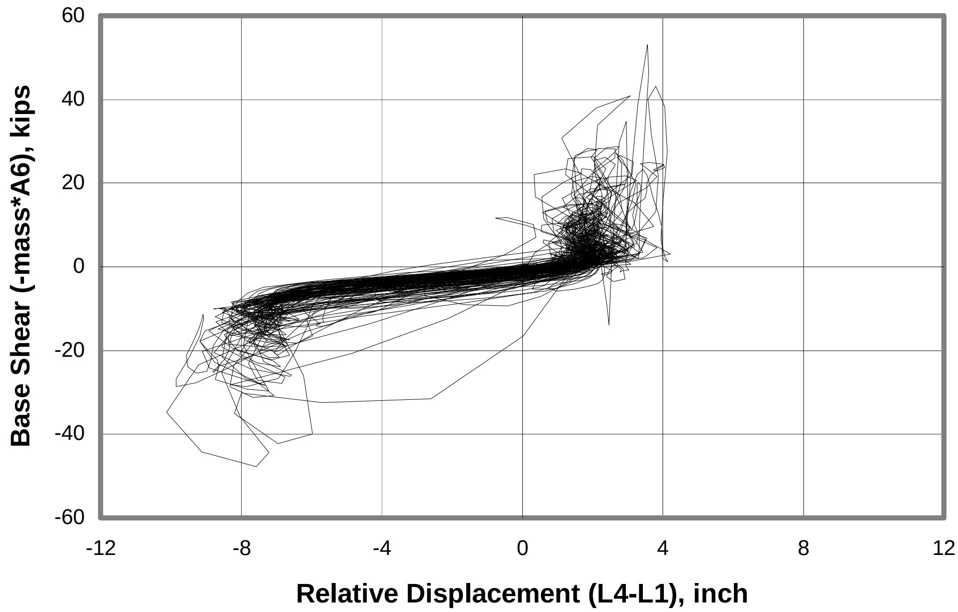

Figure 3.9 Load-Displacement Response at Center of North Side of the Slab for Model #2, Seismic Test #19

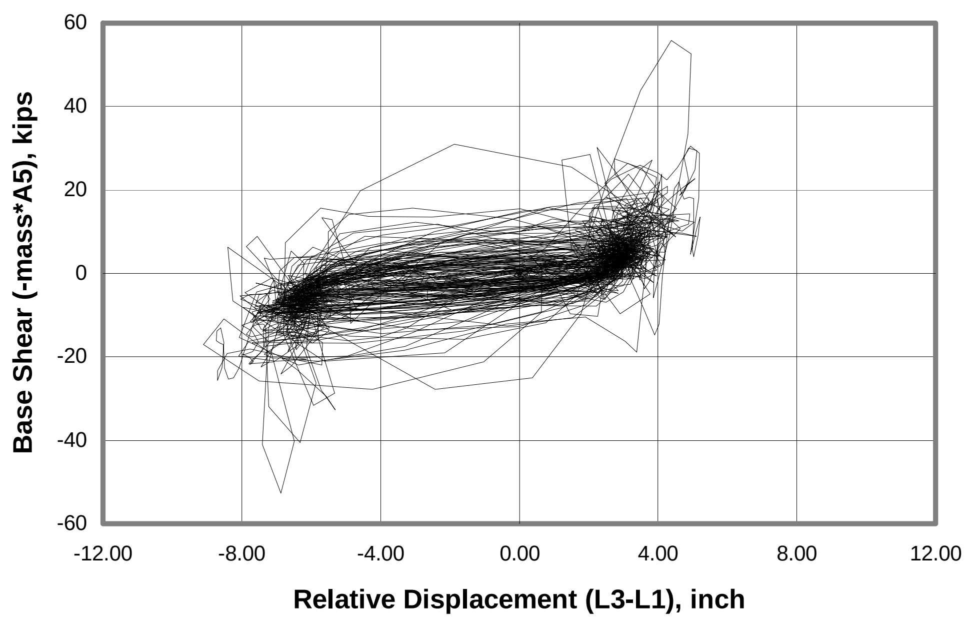

Figure 3.10 Load-Displacement Response at the Center of the Top East Beam for Model #2, Seismic Test #19

3.3.3 Synopsis of Overall Experimental Results for Model #3

This specimen consisted of the unrepaired north infilled frame of Model #2. The frame was rotated 90 degrees, and 6 out-of-plane seismic tests were conducted. Figure 3.11 shows the locations of accelerometers and strain gages on the infill.

Since horizontal out-of-plane displacements of the infill were not measured, it is not possible to generate an out-of-plane load-displacement diagram for the infilled frame. Therefore, load-displacement diagrams were plotted only for the frame (at the center of the north beam and at the right beam-column joint), for each seismic test. However, these diagrams (not shown here) do not represent the real out-of-plane behavior of the infill because the tips of the frame columns were tied to the lab floor by cables as explained above.

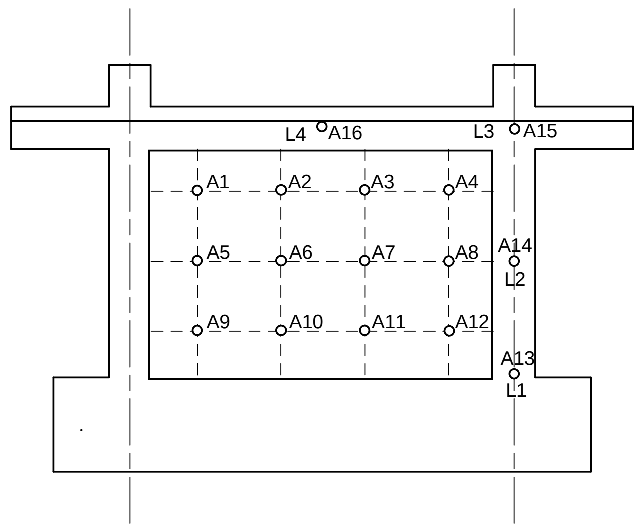

Figure 3.11 Accelerometer and Strain Gage Locations for Model #3

In spite of the lack of information on the infill deflections, their out-of-plane loads may be evaluated using the 12 accelerometers installed on their surface. Moreover, the relative lateral loads on different regions of the infill may be obtained, since the accelerometers were spaced uniformly on the infill surface.

Table 3.1 summarizes the maximum accelerations recorded for each accelerometer for all tests of this model. The recorded acceleration maxima are consistent over most of the infill surface, with a slight tendency to be higher at the top of the infill. The recorded acceleration peaks for the lower right corner invariably differ from the rest. This suggests a systematic problem with the accelerometer located in that region.

A maximum average acceleration of 6.0g was recorded on the infill for Seismic Tests #23 and #25. For these tests, maximum recorded base accelerations were 2.79g and 1.10g, respectively. Since the infill has a weight of about 0.20 kips (0.88 kN), the resulting out-of-plane load is estimated as 1.2 kips (5.3 kN). This force is a lower bound to the out-of-plane strength of the infill, since no collapse occurred during the test.

Table 3.1 Peak Out-of-Plane Response Accelerations (g) for Model #3

Test	A_{base}	--- TOP	---	---	---	----- MIDDLE	---	---	---	----- BOTTOM	---	---	---
#	A13	A1	A2	A3	A4	A5	A6	A7	A8	A9	A10	A11	A12
20	0.304	-0.417	-0.429	-0.426	-0.414	-0.419	-0.427	-0.425	-0.404	-0.393	0.411	-0.161	0.287
21	0.906	-0.766	0.751	0.762	0.759	-0.758	0.757	0.755	-0.781	-0.724	0.763	-0.179	0.887
22	1.834	-3.945	-4.107	-4.172	-4.119	-3.794	-3.933	-3.961	-3.838	-3.449	-3.583	-1.679	1.798
23	2.786	-5.441	-5.021	-5.009	-5.506	-6.062	-5.480	-5.613	-5.886	-5.975	-6.203	-1.604	2.700
24	-0.334	-1.874	-2.004	-1.971	-1.792	-1.665	-1.880	-1.821	-1.517	-1.225	-1.305	1.068	-0.274
25	-1.098	-5.862	-6.196	-6.227	-5.776	-4.870	-6.070	-5.898	-4.853	-4.129	-4.117	3.343	-0.839

3.3.4 Synopsis of Overall Experimental Results for Model #4

Using this strong repaired infilled frame, eight out-of-plane seismic tests were conducted.

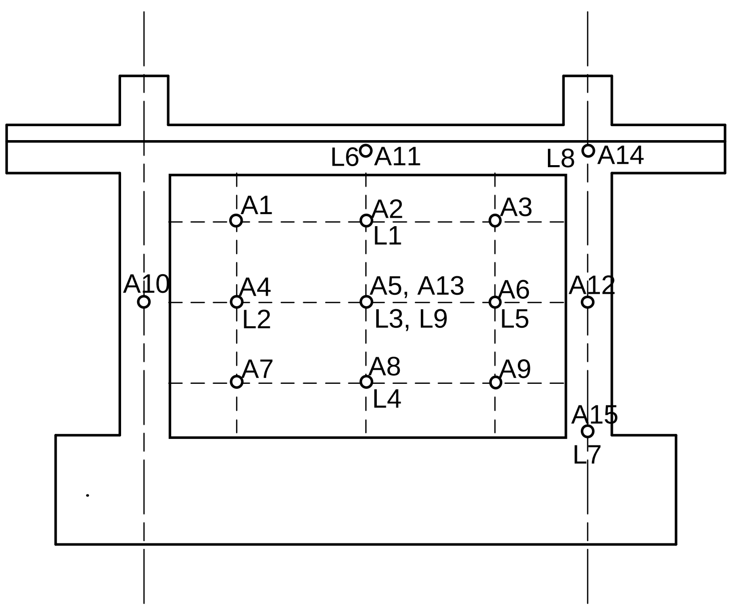

Figure 3.12 Accelerometer and Strain Gage Locations for Model #4

Figure 3.12 shows the locations of accelerometers and strain gages on the plane of the infill.

Load-displacement diagrams (not shown here) were plotted at the center of the top beam and at the right beam-column joint for each seismic test. Again, these do not represent the actual out-of-plane behavior of the specimen, due to the support given by the cables attached to the top of the frame.

As for Model #3, out-of-plane loads may be calculated using acceleration records. As before, a consistent pattern of accelerations was recorded, with a clear tendency toward higher accelerations at the top of the specimen. Table 3.2 summarizes the maximum accelerations recorded by each accelerometer for all tests of this model.

For Seismic Test #31, a maximum average acceleration of 10.0g was recorded on the infill, with a peak acceleration of 11.1g at the center of the infill. The maximum recorded base acceleration for this test was 8.60g.

The average out-of-plane lateral load is therefore estimated as 2.0 kips (8.9 kN), while the peak load at the center of the infill is 2.2 kips (9.8 kN). These forces, again, are only lower bounds to the out-of-plane strength of the infill, since no collapse occurred during the test.

Table 3.2 Peak Out-of-Plane Response Accelerations (g) for Model #4

Test	A_{base}	- - - - - - TOP - - - - - -			- - - - MIDDLE - - - -			- - - BOTTOM - - -		
#	A15	A1	A2	A3	A4	A5	A6	A7	A8	A9
26	-1.194	-1.324	-1.276	-1.428	-1.292	-1.322	-1.333	-0.464	-1.212	-1.241
27	-3.142	-3.778	-3.748	-3.887	-3.543	-3.639	-3.591	-3.174	-3.269	-3.281
28	-8.418	-8.816	-7.130	-8.768	-8.215	-7.879	-7.748	-5.437	-6.866	-7.190
29	-0.927	-1.302	-1.516	-1.749	-1.165	-1.355	-1.421	-0.995	-1.127	-1.132
30	-3.738	-5.622	-6.249	-6.418	-4.555	-5.030	-4.832	-3.667	-4.043	-4.073
31	-8.597	10.157	10.179	-9.392	9.456	11.096	9.596	-7.964	8.862	-8.601
33	-2.747	-5.011	-7.189	-5.444	-4.611	-5.454	-4.733	-4.678	-4.880	-4.530

In contrast to Model #3, for Model #4 out-of-plane displacements were measured at various locations on the infill. Hence, load-displacement diagrams were plotted at the center of the infill, for each of the Seismic Tests. In the following discussions, only Seismic Tests with base accelerations over 3.50g will be considered since load-displacement characteristics of tests with lower accelerations are generally not useful for evaluating the overall response of the specimen.

- *Seismic Test #28:* The peak ground acceleration for this test was 8.42g. Figure 3.13 shows the load-displacement response of Model #4 for this test. Figure 3.13a was plotted using the out-of-plane displacement of the center of the infill relative to the base of the specimen while Figure 3.13b used the out-of-plane displacement relative to the average displacement of the surrounding frame ("L_{avg}"). Comparison of these two figures reveal a great difference of the two relative displacements.

- *Seismic Test #30:* The peak ground acceleration for this test was 3.74g. Figure 3.14 shows the load-displacement response of Model #4 for this test. As before, Figure 3.14a was plotted using the out-of-plane displacement of the center of the infill relative to the base of the specimen, and Figure 3.14b used the out-of-plane displacement relative to the average displacement of the surrounding frame. In this case, the two figures are almost identical, indicating that the frame motion is equal to the base input motion. However, load-displacement patterns imply unrealistic large displacements and low or zero stiffness.

- *Seismic Test #31:* The peak ground acceleration for this test was 8.60g. Figure 3.15 shows the load-displacement response of Model #4 for this test. Figure 3.15a was plotted using the out-of-plane displacement of the center of the infill relative to the base of the specimen, and Figure 3.15b used the out-of-plane displacement relative to the average displacement of the surrounding frame. As before, the two figures are almost identical, indicating that the frame motion is equal to the base input motion. Displacements are again very large.

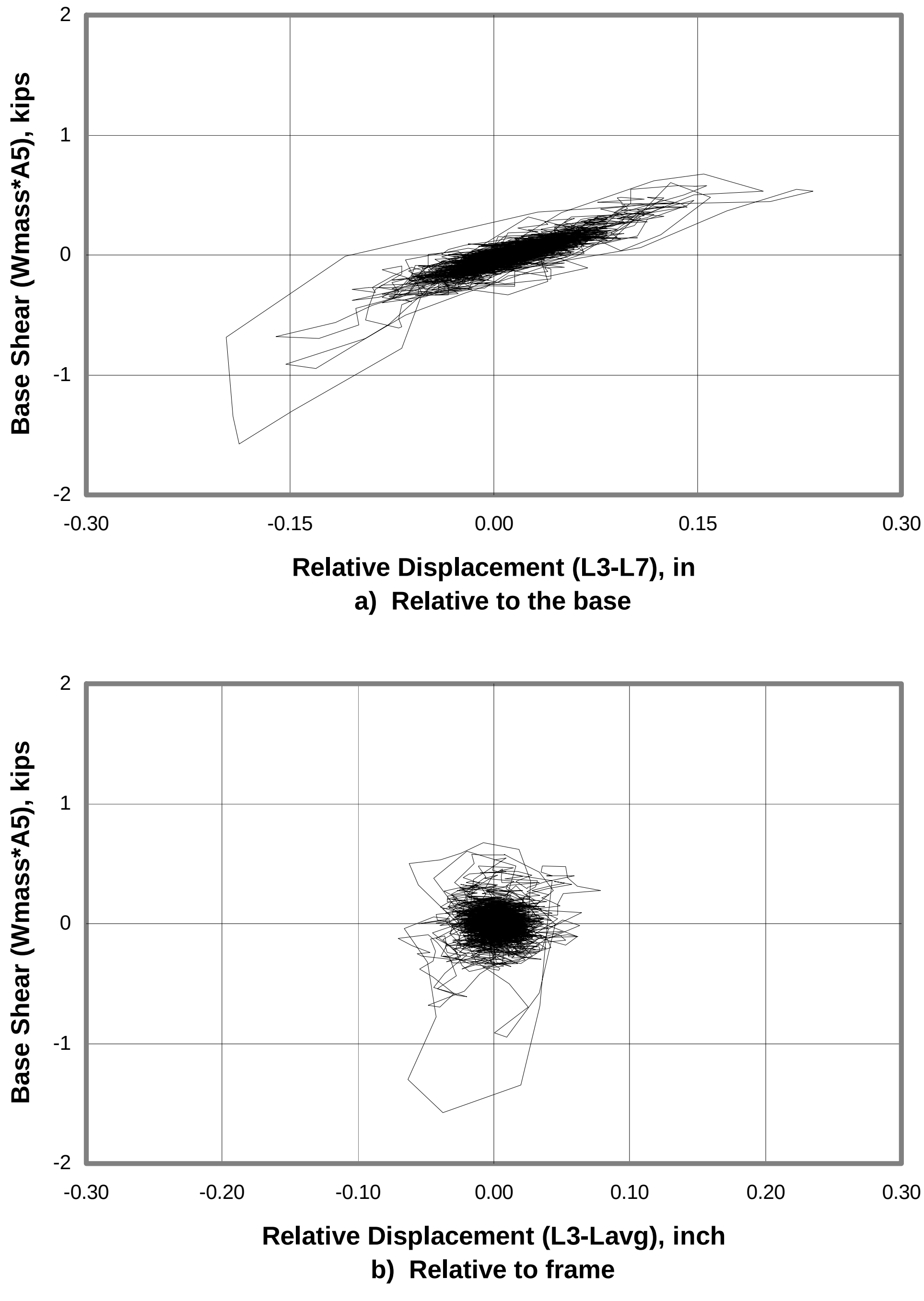

Figure 3.13 Load-Displacement Response at Center of Infill for Model #4, Seismic Test #28

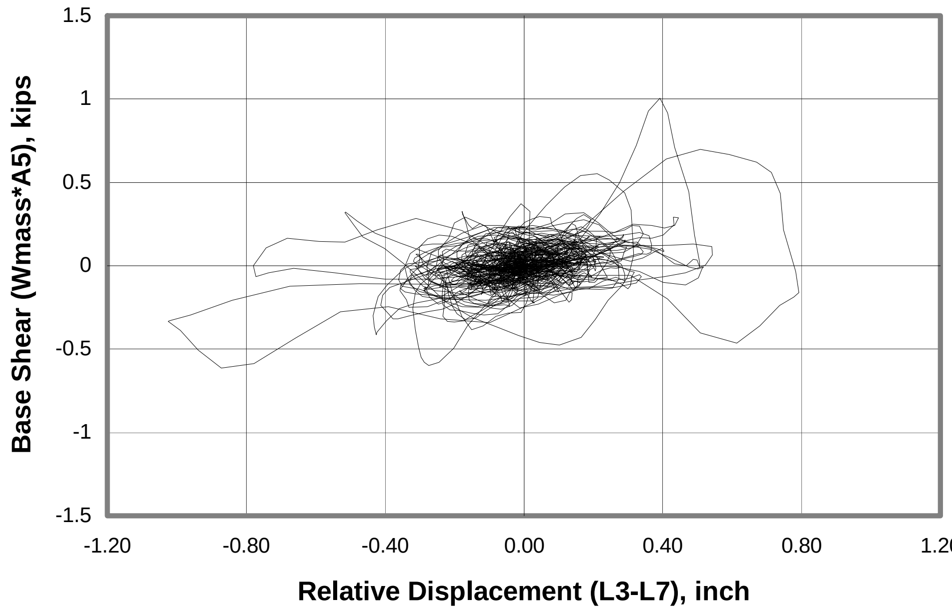

a) Relative to the base

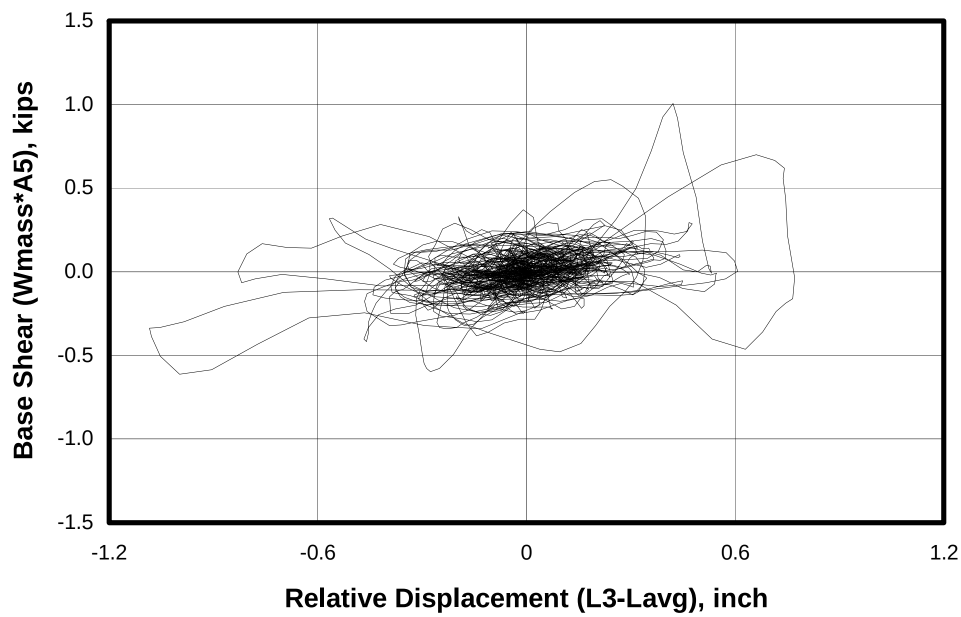

b) Relative to the frame

Figure 3.14 Load-Displacement Response at Center of Infill for Model #4, Seismic Test #30

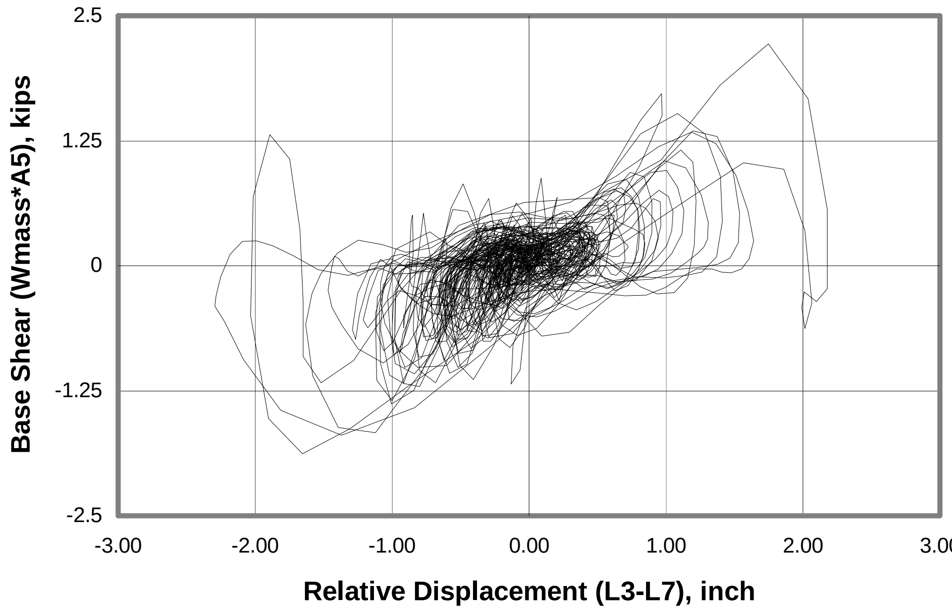

a) Relative to the base

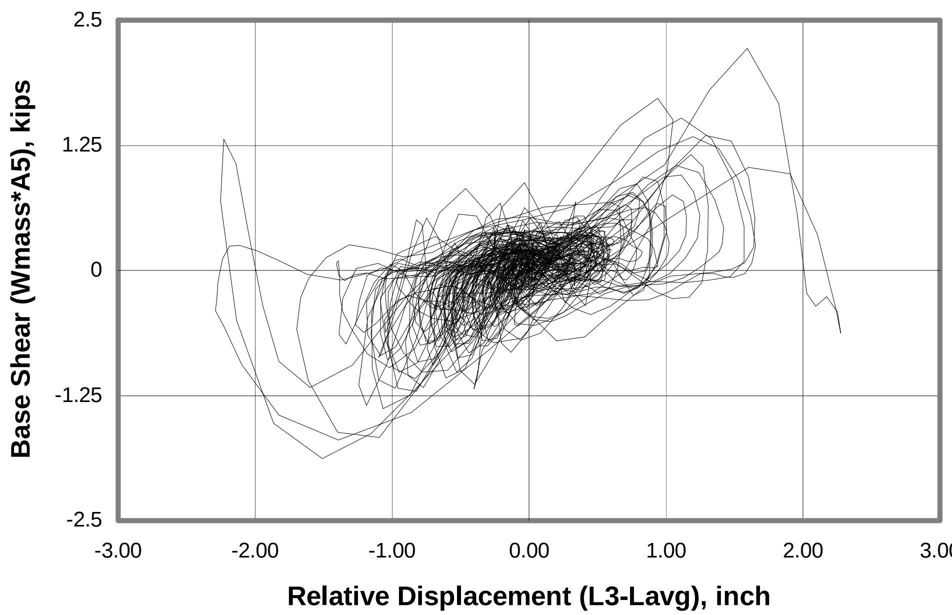

b) Relative to the frame

Figure 3.15 Load-Displacement Response at Center of Infill for Model #4, Seismic Test #31

3.3.5 Synopsis of Overall Experimental Results for Model #5

Using this virgin strong infilled frame, 7 seismic out-of-plane tests were conducted. Figure 3.16 shows the locations of accelerometers and strain gages on the infill.

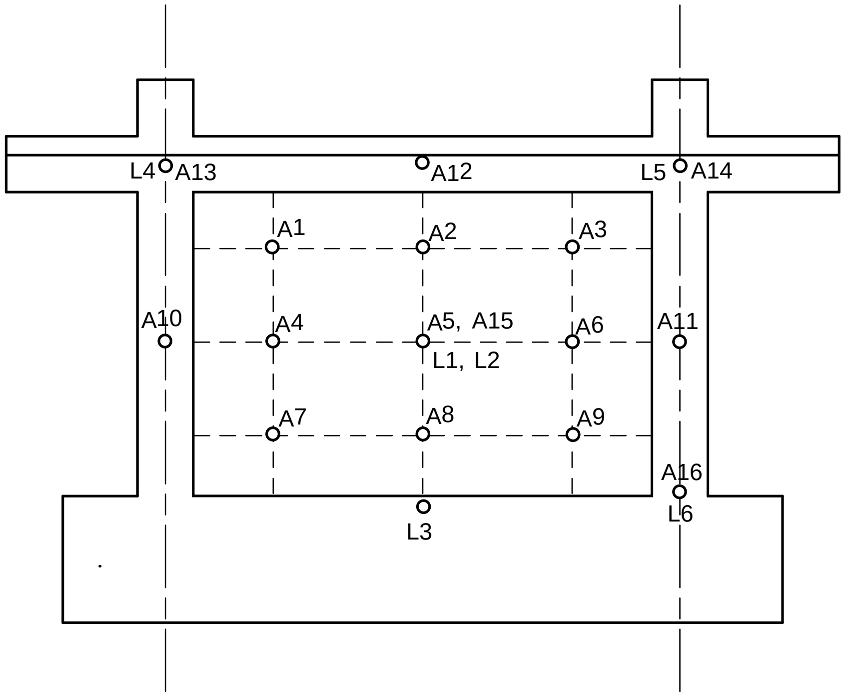

Figure 3.16 Accelerometer and Strain Gage Locations for Model #5

Table 3.2 summarizes the maximum accelerations recorded for each accelerometer for all tests of this model. As before, out-of-plane response accelerations recorded on the infill were larger at the top than at the bottom.

A maximum average acceleration of 5.0g was recorded on the infill during Seismic Tests #39 and #40, for which the maximum recorded base accelerations were 4.12g and 4.88g respectively. A lower bound to the average out-of-plane strength is therefore estimated as 1.0 kip (4.4 kN).

Load-displacement diagrams were plotted at the center of the infill for each seismic test. In general, they show unrealistic patterns and inconsistent displacement levels. In the following discussions, only Seismic Tests #39 and #40 will be considered.

- *Seismic Test #39:* The peak ground acceleration for this test was 4.12g. Figure 3.17 shows the load-displacement response of Model #5 for this test. Figure 3.17a was plotted using the out-of-plane displacement at the center of the infill, measured with the "main" gage L2, relative to average displacement of the surrounding frame (L_{avg}).

Figure 3.13b, on the other hand, was plotted using the "backup" gage L1. Both figures show a similarly unrealistic pattern.

- *Seismic Test #40:* The peak ground acceleration for this test was 4.88g. Figure 3.18 shows the load-displacement response of Model #5 for this test. As before, Figure 3.18a was plotted using the out-of-plane displacement at the center of the infill, measured with the "main" gage L2, relative to average displacement of the surrounding frame (L_{avg}), and Figure 3.13b was plotted using the "backup" gage L1. In this case, the load-displacement pattern is consistent for both diagrams. However, some cycles exhibit very large displacements on only one side of the infill.

Table 3.3 Peak Out-of-Plane Response Accelerations (g) for Model #5

Test	A_{base}	- - - TOP - - - - - -			- - - MIDDLE - - - -			- BOTTOM - - -		
#	A16	A1	A2	A3	A4	A5	A6	A7	A8	A9
34	-0.579	-0.675	-0.668	-0.698	-0.635	-0.635	-0.623	-0.577	-0.586	-0.586
35	-1.558	-1.754	-1.831	-1.960	-1.677	-1.740	-1.738	-1.542	-1.596	-1.630
36	-3.472	-4.419	-4.515	-4.522	-3.566	-3.758	-3.653	-3.232	-3.357	-3.472
37	-0.460	-0.585	-0.601	-0.602	-0.548	-0.549	-0.533	-0.480	-0.499	-0.484
38	-3.907	-4.440	-4.545	-4.519	-3.805	-3.967	-4.089	-3.753	-3.790	-3.843
39	-4.124	-5.016	5.053	-4.938	4.677	4.788	4.633	4.160	4.140	4.216
40	4.884	5.179	4.349	-4.712	4.440	4.550	4.437	4.022	4.162	-4.234

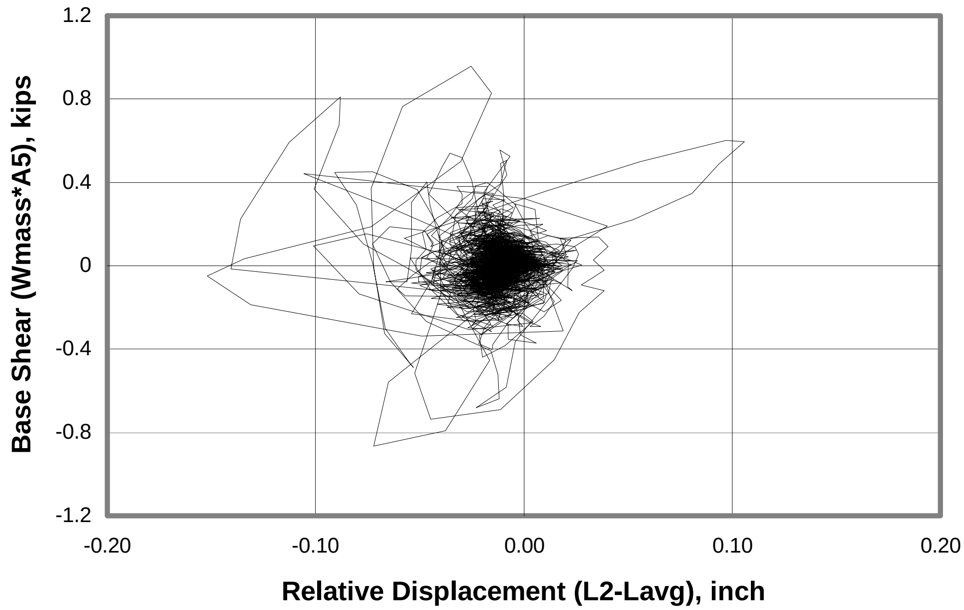

a) Using Main Displacement Gage

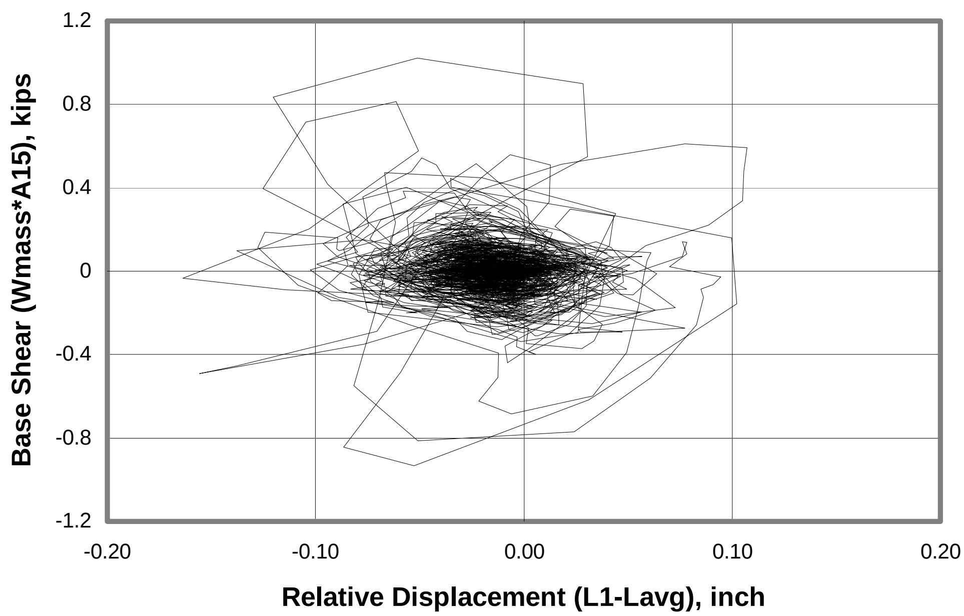

b) Using Backup Displacement Gage

Figure 3.17 Load-Displacement Response at Center of Infill (Backup) for Model #5, Seismic Test #39

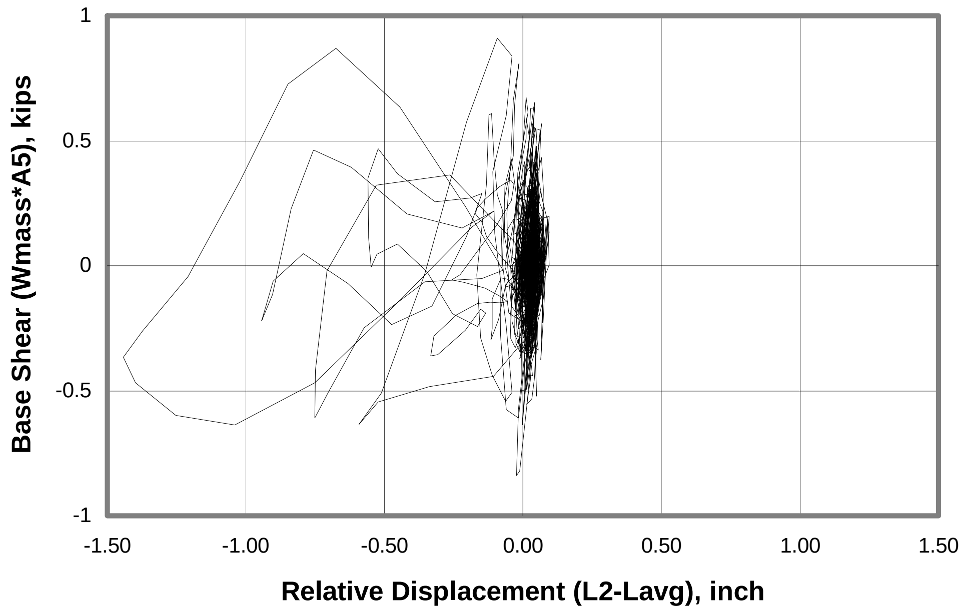

a) Using Main Displacement Gage

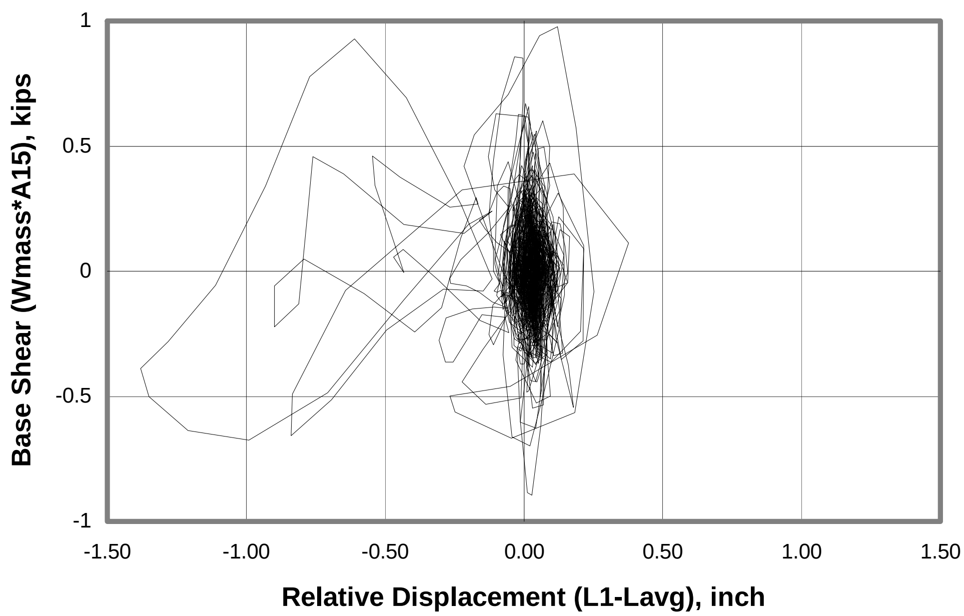

b) Using Backup Displacement Gage

Figure 3.18 Load-Displacement Response at Center of Infill (Backup) for Model #5, Seismic Test #40

3.3.6 Synopsis of Overall Experimental Results for Model #6

Using this weak bare frame, 7 seismic in-plane tests were conducted. Load-displacement diagrams, plotted at the center of the north side of the slab and at the top mass, are evaluated below for the selected seismic tests.

- *Seismic Test #45:* The peak ground acceleration for this test was 0.44g. Load-displacement diagrams for this test are shown in Figures 3.19 and 3.20. Base shears are low, and a linear elastic response of the frame is apparent.
- *Seismic Test #46:* The peak ground acceleration for Test #46 was 1.12g. Load-displacement diagrams for this test, shown in Figures 3.21 and 3.22, exhibit an expected pattern, with a relatively low but consistent average stiffness of 47 kips/inch (8.2 kN/mm). The peak load was about 16 kips (71.2 kN), with a maximum displacement of 0.37 inches (9.4 mm). A linear elastic response of the frame is clear.
- *Seismic Test #47:* The peak ground acceleration for this test was 1.56g. Load-displacement diagrams, shown in Figures 3.23 and 3.24, display an initial stiffness consistent with that obtained in Seismic Test #46, followed by a degraded stiffness. The peak load for Test #47 was about 22 kips (97.9 kN), and the maximum displacement was 0.7 inches (17.8 mm). As before, the response is generally linear elastic. In this case, however, some yielding of the frame is apparent near the peak load.

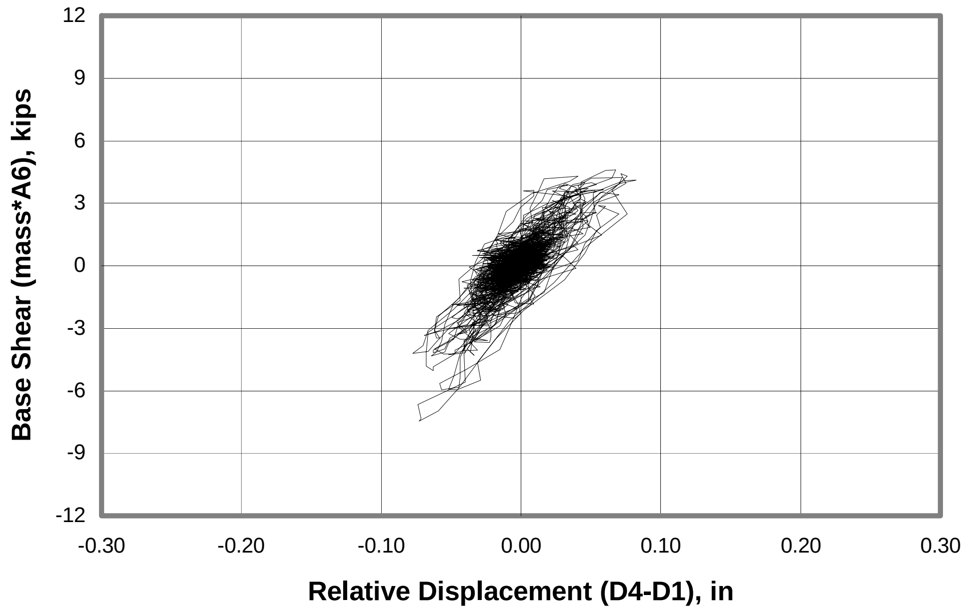

Figure 3.19 Load-displacement Response at Center of North side of the Slab for Model #6, Seismic Test #45

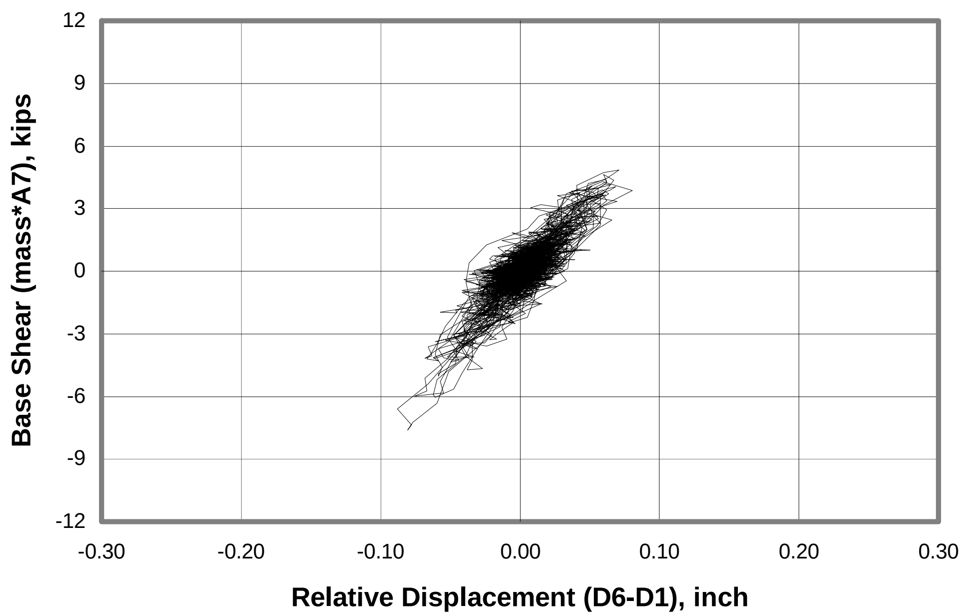

Figure 3.20 Load-Displacement Response at the Top Mass for Model #6, Seismic Test #45

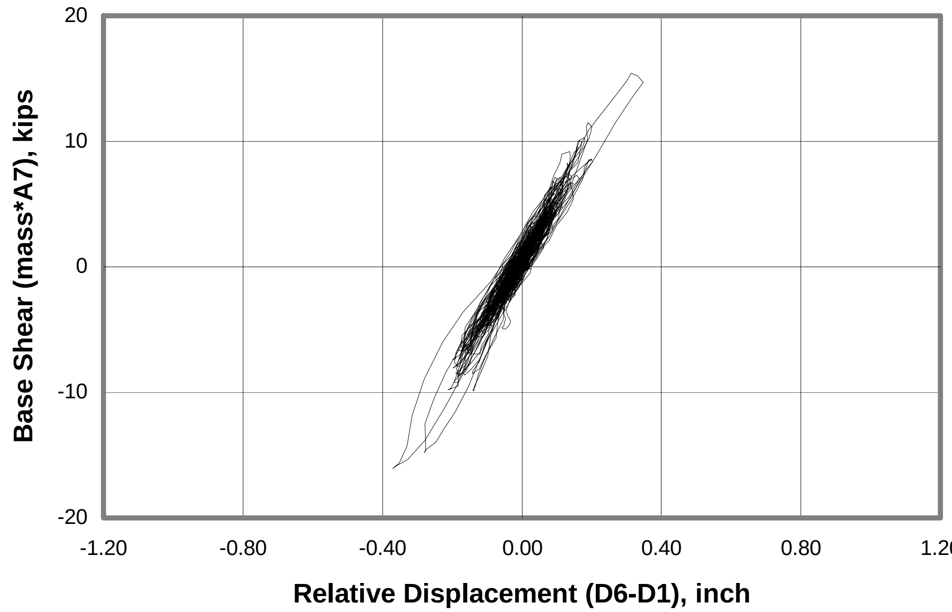

Figure 3.22 Load-Displacement Response at the Top Mass for Model #6, Seismic Test #46

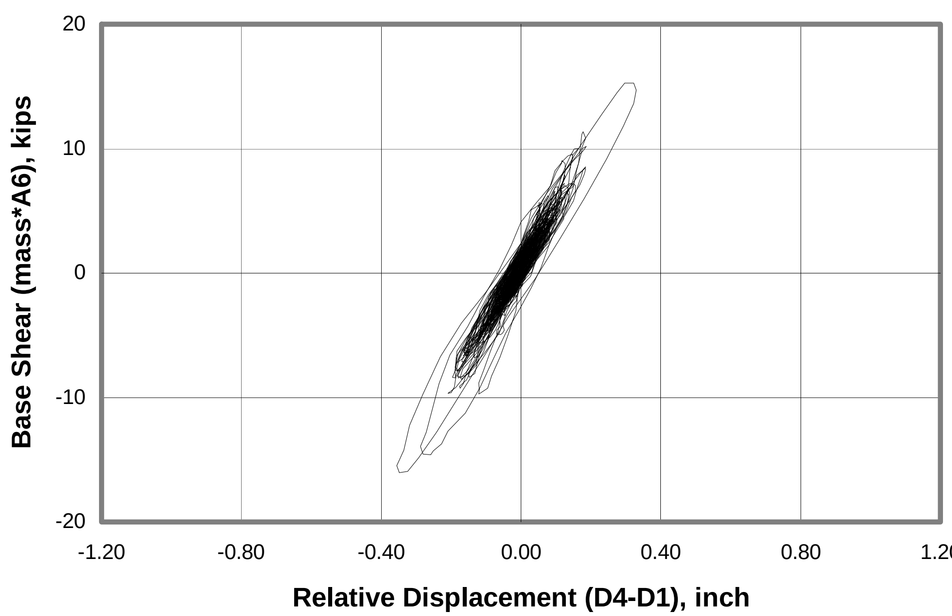

Figure 3.21 Load-Displacement Response at Center of North Side of the Slab for Model #6, Seismic Test #46

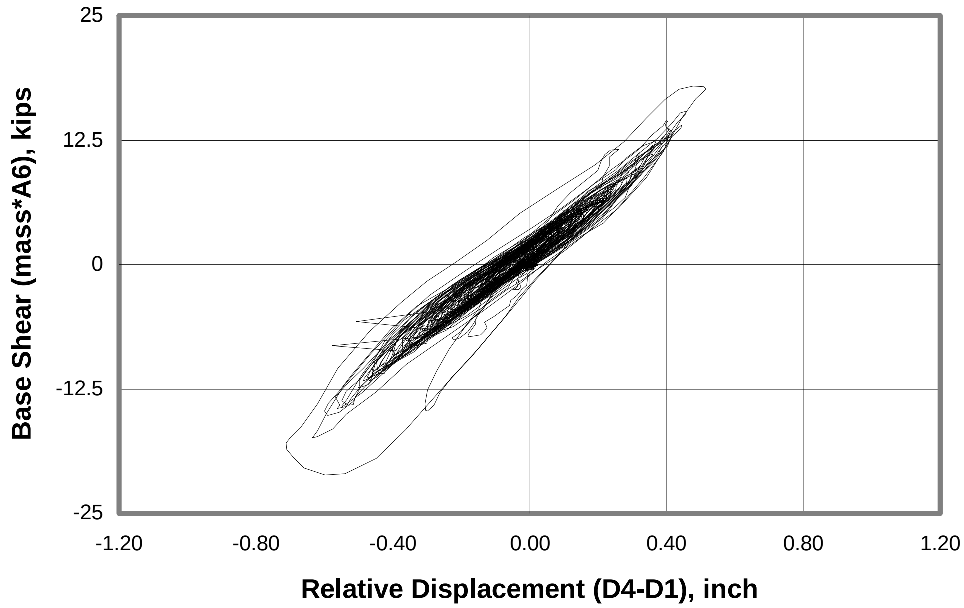

Figure 3.23 Load-Displacement Response at Center of North side of the Slab for Model #6, Seismic Test #47

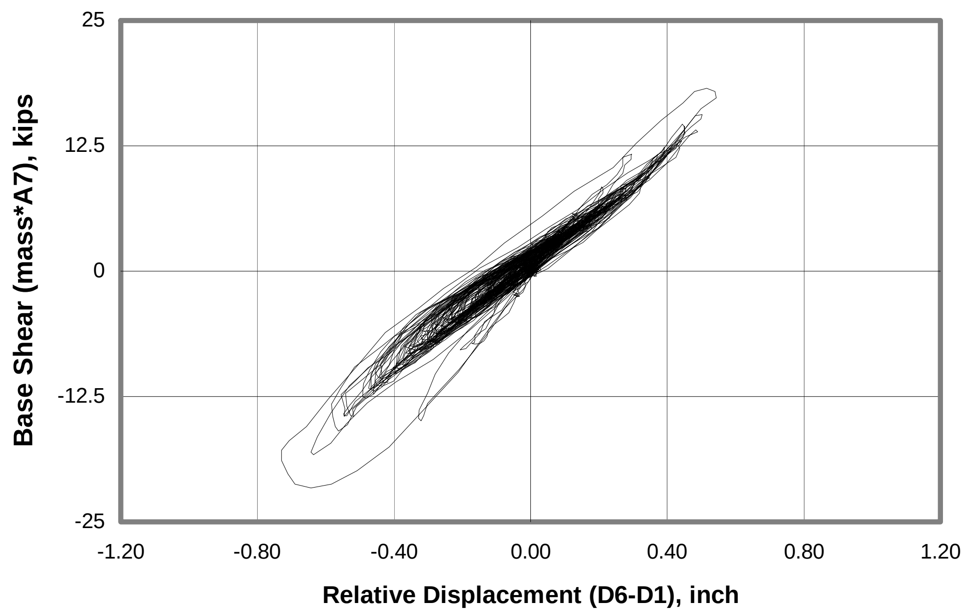

Figure 3.24 Load-Displacement Response at the Top Mass for Model #6, Seismic Test #47

3.3.7 Synopsis of Overall Experimental Results for Model #7

Using this weak infilled frame, 5 seismic in-plane tests were conducted. Load-displacement diagrams, plotted at the top mass and at the north side of the slab are evaluated below for the selected seismic tests:

- *Seismic test #51:* The peak ground acceleration for this test was 6.38g. Load-displacement diagrams are shown in Figures 3.25 and 3.26. In this case, very similar patterns were obtained for both diagrams (top mass and north side of the slab). A single large loop with a maximum stiffness of about 200 kips/inch (35.0 kN/mm) and a peak base shear of 60 kips (266.9 kN) is accompanied by small cycles with base shears under 25 kips (111.2 kN) and very low stiffness (under 100 kips/inch, or 17.5 kN/mm). Maximum displacements reach 0.4 inches (10.2 mm). The frame apparently yielded at the peak load during this test.
- *Seismic test #52:* The peak ground acceleration for this test was 7.25g. Load-displacement diagrams, shown in Figures 3.27 and 3.28, display base shears generally under 30 kips (133.4 kN) and displacements under 0.6 inch (15.2 mm). However, a single large loop shows a maximum base shear over 60 kips (266.9 kN) and a displacement of about 0.90 inches (23 mm). Average stiffness is 50 kips/inch (8.8 kN/mm) near the zero-load region. For large displacements, the stiffness increases to over 100 kips/inch (17.5 kN/mm). Some of the small cycles suggest an initial stiffness of 200 kips/inch (35.0 kN/mm) or more, consistent with previous tests. As for Seismic Test #51, yielding of the frame is apparent at peak load.

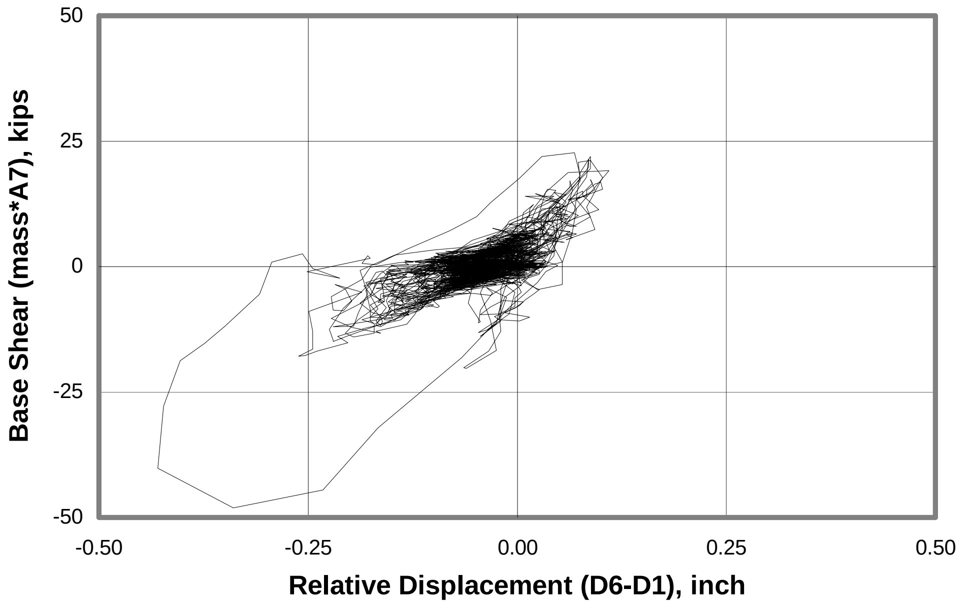

Figure 3.25 Load-Displacement Response at the top mass for Model #7, Seismic Test #51

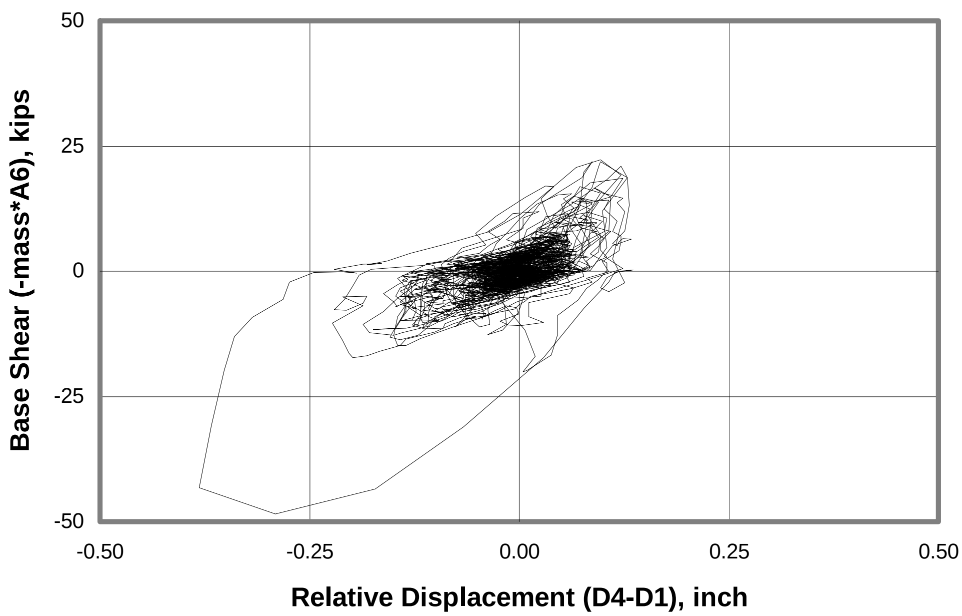

Figure 3.26 Load-Displacement Response at Center of North side of the Slab for Model #7, Seismic Test #51

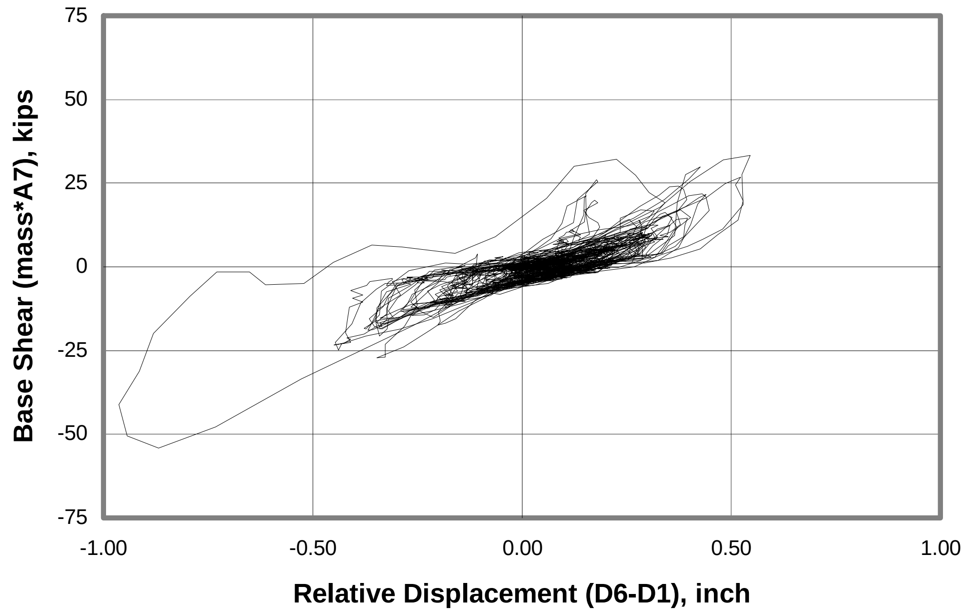

Figure 3.27 Load-Displacement Response at the Top Mass for Model #7, Seismic Test #52

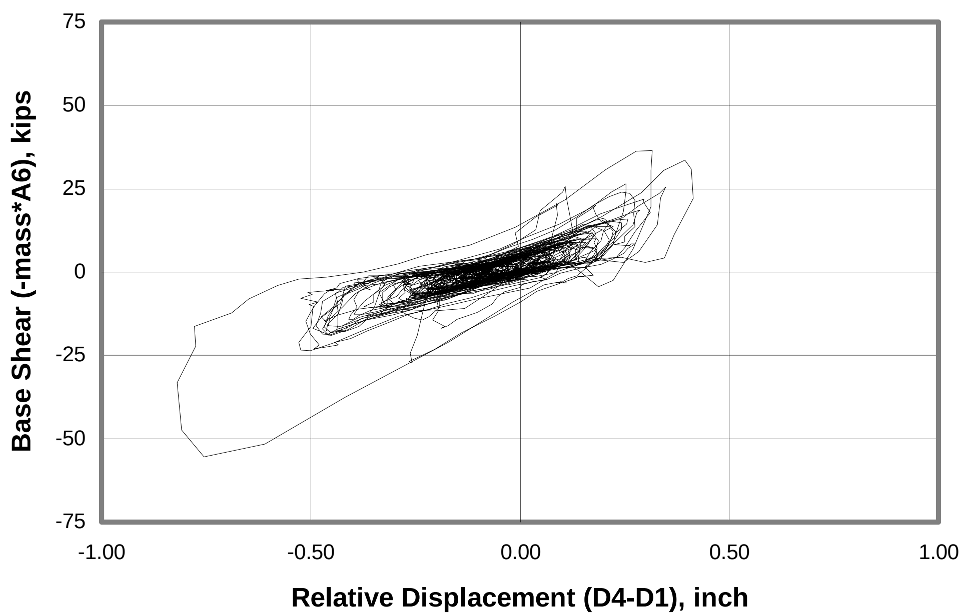

Figure 3.28 Load-Displacement Response at Center of North Side of the Slab for Model #7, Seismic Test #52

3.3.8 Synopsis of Overall Experimental Results for Model #8

Using this unrepaired weak infilled frame, 6 seismic out-of-plane tests were conducted. Figure 3.29 shows the location of the accelerometers and strain gages on the infill.

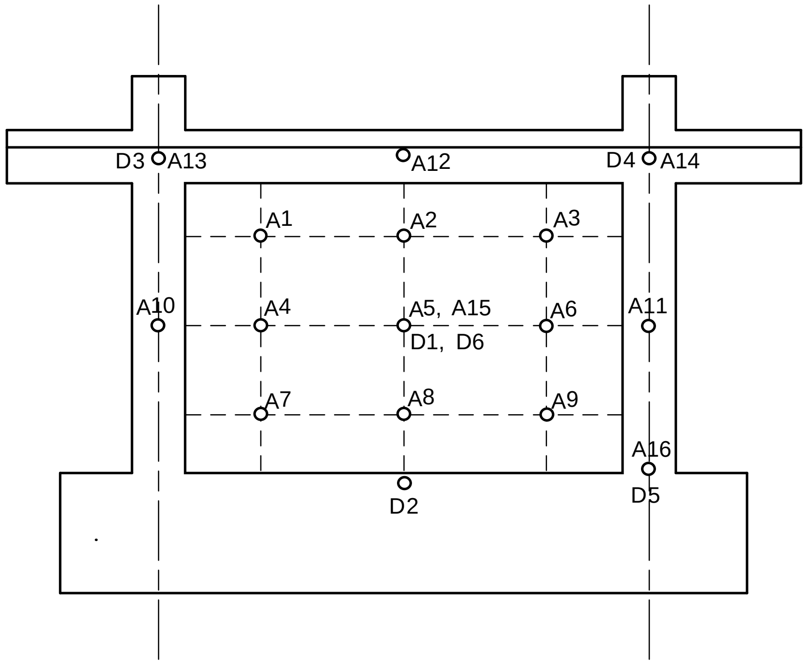

Figure 3.29 Accelerometer and Strain Gage Locations for Model #8

Load-displacement diagrams, plotted at the center of the infill, are evaluated below for the selected seismic tests.

- *Seismic Tests #54 and #55:* Peak ground accelerations for these tests were 7.02g and 6.62g respectively. Load-displacement diagrams for Seismic Test #54 (not shown here) and for Seismic Test #55 (Figure 3.30) are similar to each other, with several small hysteresis loops and a single large cycle. An average maximum response acceleration of about 8.0g was recorded. The maximum out-of-plane load was therefore estimated as 1.6 kips (7.1 kN). For these tests, the measured maximum lateral displacement at the center of the infill is about 0.3 in (7.6 mm). From the load-displacement diagrams, an average lateral stiffness of about 10 kips/inch (1.8 kN/mm) was obtained.

- *Seismic Test #57:* The peak ground acceleration for this test was 7.15g. The load-displacement diagram, shown in Figure 3.31, is similar to the diagrams obtained for

Seismic Tests #54 and #55. In this case, however, several relatively large hysteresis cycles were recorded. A maximum average acceleration of about 8.50g was recorded. The maximum out-of-plane load is therefore estimated as 1.7 kips (7.5 kN). The measured maximum lateral displacement at the center of the infill, in this case, was about 0.35 inches (8.9 mm). From the load-displacement diagrams an average lateral stiffness of about 10 kips/inch (1.8 kN/mm) was obtained.

- *Seismic Test #58:* The peak ground acceleration for this test was 7.99g. In this case, the load-displacement diagram, shown in Figure 3.32, displays several large cycles. The maximum recorded response acceleration was 10.0g corresponding to an out-of-plane applied load of 2.0 kips (8.9 kN). The maximum base acceleration was 8.0g. The maximum measured lateral displacement of the center of the infill was 0.6 inches (15.2 mm). The average lateral stiffness was estimated from the load-displacement diagram as 8.0 kips/inch (1.4 kN/mm).

Table 3.4 Peak Out-of-Plane Response Accelerations (g) for Model #8

Test	A_{base}	- - - -- TOP - - - - - -			- MIDDLE - - - -			- BOTTOM - - -		
#	A16	A1	A2	A3	A4	A5	A6	A7	A8	A9
53	-2.235	-2.834	-2.708	-2.801	-2.678	-2.844	-2.665	-2.356	-2.400	3.392
54	-7.021	-8.212	-7.272	-8.322	-7.523	-7.752	-6.773	-6.994	-7.017	-9.928
55	-6.624	-8.500	-7.925	-8.920	-7.666	-7.940	-6.902	-6.895	-7.065	9.634
56	-1.917	-3.168	-3.298	-3.223	-3.006	-3.182	-3.027	-2.092	-2.181	-2.223
57	-7.150	-8.779	-8.612	-9.322	-8.596	-8.085	-7.154	-7.625	-7.793	9.628
58	7.985	9.261	10.051	-9.369	-8.512	9.590	-8.696	8.326	-8.444	-8.984

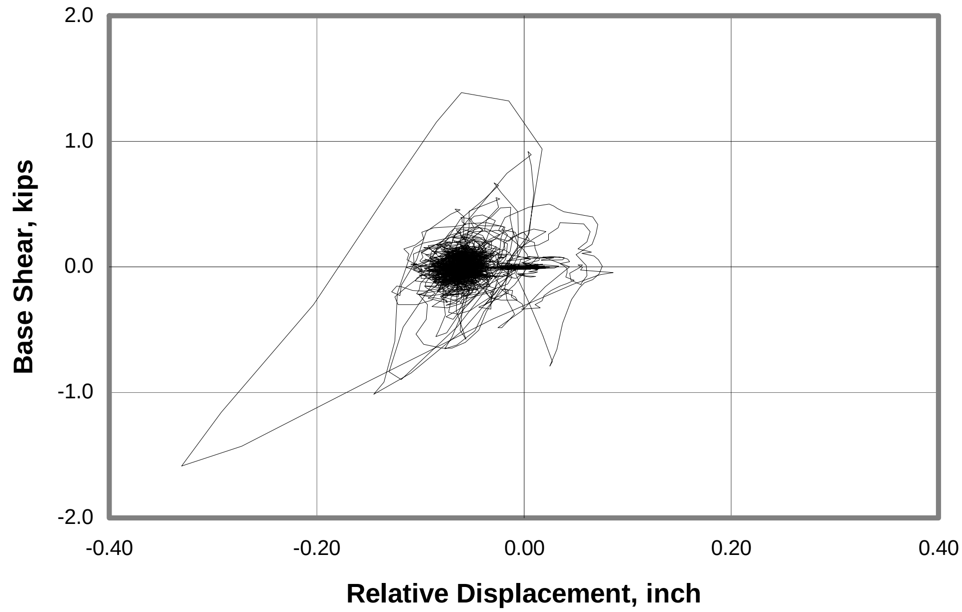

Figure 3.30 Load-Displacement Response at Center of Infill for Model #8, Seismic Test #55

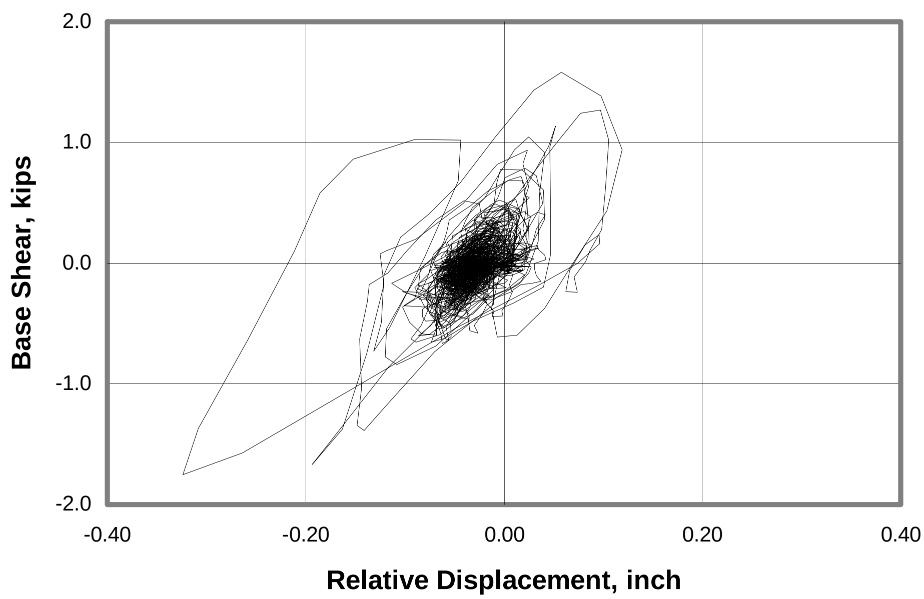

Figure 3.31 Load-Displacement Response at Center of Infill for Model #8, Seismic test #57

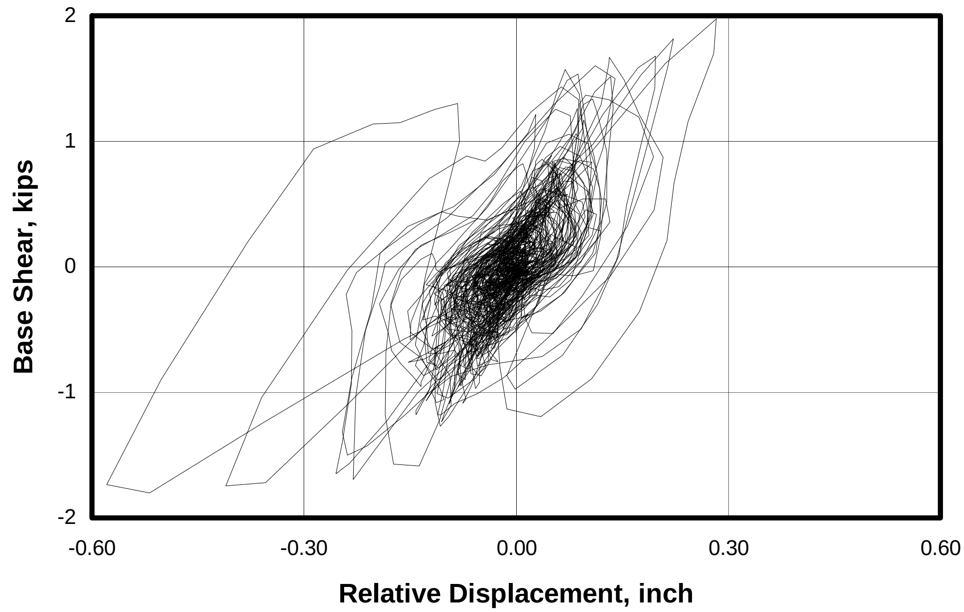

Figure 3.32 Load-Displacement Response at Center of Infill for Model #8, Seismic Test #58

CHAPTER 4 ANALYSIS OF OVERALL EXPERIMENTAL RESULTS

4.1 Individual Specimen Response

Based on the previous observations on the shaking-table test data, several conclusions were reached regarding the individual response of each Model.

1) Model #1 (in-plane, strong bare frame):

   a) Seismic Tests #1-#8 and #12-#15 were either aborted or had very low levels of base shear, with irregular and inconsistent load-displacement patterns. Therefore, they do not represent the behavior of this specimen well.

   b) Seismic Tests #9, #10 and #11 show reasonable and consistent load-displacement patterns, as well as stiffness, strength and displacement values. An average backbone stiffness for the uncracked bare frame of 120 to 140 kips/inch (21.0 to 24.5 kN/mm) is obtained from these diagrams, relatively close to the estimated stiffness of 170 kips/inch (29.8 kN/mm) for cracked sections. Maximum measured load and displacement were 20 kips (89.0 kN) and 0.3 inches (7.6 mm) respectively. Because of the internal consistency of the overall load-displacement results and the agreement with simple strength models, these results are believed to represent faithfully the experimental behavior of the strong bare frame.

2) Model #2 (in-plane, strong infilled frame):

   a) Seismic Tests #16 and #17 had low levels of input ground motion. They showed very inconsistent response at various locations of the specimen, accompanied by very low values of stiffness compared to the bare-frame specimen (Model #1). Consequently, these tests are not believed to represent the real behavior of this specimen.

   b) Seismic Tests #18 and #19 show unrealistically large displacements, and consequently, extremely low stiffness. However, the load levels (30 to 40 kips, or 133 to 178 kN) seem reasonable, and are believed to represent the experimental strength of the strong infilled frame.

3) Model #3 (out-of-plane, strong infilled frame):

   a) Out-of-plane displacements of the infill were not measured. Therefore, stiffness was not computed and load-displacement diagrams were not constructed. However, load levels, computed from the measured infill accelerations, were fairly constant over the surface with an average value of 1.2 kips (5.3 kN). This load may be considered a lower bound to the out-of-plane strength of the infill, since no collapse occurred during the Test.

4) Model #4 (out-of-plane, strong repaired frame):

   a) The out-of-plane load-displacement patterns obtained do not represent the behavior of the specimen well. Maximum lateral load levels imposed on the infill were over 2.0 kips (8.9 kN).
   b) The repair technique used during the test program proved to be effective since load levels could be increased from 1.2 kips (5.3 kN) for Model #3 to 2.0 kips (8.9 kN) for this Model, that is, an increment of about 70%.
   c) The test setup for out-of-plane excitation, using cables to tie the tip of the frame to the BSTM floor, was adequate since infill displacements measured relative to the base of the specimen were practically identical to the infill displacements measured relative to the frame.

5) Model #5 (out-of-plane, virgin strong infilled frame)

   a) The out-of-plane load-displacement patterns obtained do not represent well the behavior of the specimen. Maximum lateral load levels imposed on the infill were about 1.0 kip (4.4 kN).

6) Model #6 (in-plane, weak bare frame):

   a) Seismic Tests #41 through #45 had low levels of input ground motion and unreliable load-displacement patterns. Consequently, these tests are not believed to represent the real behavior of this specimen.
   b) Tests #46 and #47 show good load-displacement diagrams at the top slab. An average stiffness of 47 kips/inch (8.2 kN/mm) was measured. Maximum measured load and displacement were 22 kips (97.9 kN) and 0.7 inches (17.8 mm) respectively.

7) Model #7 (in-plane, weak infilled frame):

   a) Seismic Tests #48 and #49 had low levels of input ground motion and unreliable load-displacement patterns. Therefore, these tests do not represent the real behavior of this specimen.

   b) Seismic Test #50 suggests a stiffness value close to 300 kips/inch (52.5 kN/mm). These values were measured from a single hysteresis loop with maximum base shear of 30 kips (133 kN).

   c) Seismic Tests #51 and #52 show good load-displacement patterns at the top slab, with maximum loads reaching 60 kips (267 kN). Stiffness levels are generally under 200 kips/in, (35 kN/mm) suggesting a degrading behavior for this specimen. The maximum lateral displacement is 0.9 inches (22.9 mm).

8) Model #8 (out-of-plane, weak infilled frame):

   a) Seismic Tests #53 and #56 had low levels of input ground motion and unreliable load-displacement patterns. Therefore, these tests are not believed to represent the real behavior of this specimen.

   b) Seismic Tests #54, #55, #57 and #58 show consistent and believable load-displacement patterns. The peak out-of-plane load was 2.0 kips (8.9 kN), and the maximum displacement was 0.6 inches (15.2 mm). Average stiffness was estimated as 10 kips/inch (1.8 kN/mm).

4.2 Conclusions Regarding In-Plane Response of Bare Frames

1) In-plane, bare-frame tests involving very low levels of base acceleration (under 0.5g) clearly show load-displacement characteristics that are inconsistent with each other, and not useful for evaluating specimen behavior. These “poor” load-displacement patterns are apparently due to the precision of the instruments.

2) Tests with higher levels of ground input acceleration were useful. The average in-plane stiffness for these tests was about 130 kips/inch (22.8 kN/mm) in the case of the strong-frame specimen, and about 50 kips/inch (8.8 kN/mm) for the weak-frame specimen. The maximum base shear in both cases was about 20 kips (89 kN).

4.3 Conclusions Regarding In-Plane Response of Infilled Frames

1) Again in this case, tests involving low levels of base acceleration (under 2.0g) show "poor" load-displacement characteristics.

2) Tests with higher levels of ground input acceleration were useful. An initial stiffness of about 300 kips/inch (52.5 kN/mm) was measured for the weak infilled frame. For subsequent tests, a degraded stiffness of less than 200 kips/inch (35 kN/mm) was measured. Maximum base shear was about 60 kips (267 kN).

4.4 Conclusions Regarding Out-of-Plane Response of Infilled Frames

1) Tests with low levels of ground input acceleration (generally under 4.0g) show load-displacement characteristics that are inconsistent with each other, and not useful for evaluating specimen behavior.

2) Tests with higher levels of ground input acceleration were useful. Maximum out-of-plane shears reached 2.0 kips (8.9 kN), corresponding to an equivalent uniform load of 190 lb/ft^2 (9.1 kPa). A maximum out-of-plane displacement at the middle center of the infill was 0.60 inches (15 mm). The average stiffness was then estimated as 10 kips/inch (1.8 kN/mm).

CHAPTER 5 COMPARISON WITH ANALYTICAL IDEALIZATIONS

5.1 General Remarks Regarding Analytical Idealizations

In this chapter, the half-scale in-plane specimens whose behavior was described previously, are analyzed. Four computer programs were used. The programs RCCOLA (Mahin 1977, Farahany 1983) and DRAIN-2DX (Kanaan 1975) were used to idealize the bare frames; and the programs FEM/I (Ewing 1987) and LPM/I (Kariotis 1992) were used to idealize the infilled frames.

- RCCOLA was used to calculate the moment-curvature behavior of beams and columns for subsequent input into DRAIN-2DX.
- DRAIN-2DX was used to analyze the response of the weak and strong bare frames, excited with the ground accelerations obtained from the shaking table data.
- FEM/I was used to calculate the response of the infilled concrete frame, in a static push-over analysis (Figure 5.7).
- LPM/I was used to analyze the response of the weak and strong infilled frames, excited by the ground accelerations obtained from the shaking table data.

Further information about the above computer programs and the analytical idealizations used is given in Appendix A.

5.2 Analytical Idealization for Bare Frame Specimens

5.2.1 Idealization for Model #1

Model #1 (strong bare frame, excited in-plane) was idealized using the beam-column elements of DRAIN-2DX. Moment-rotation behavior was derived using RCCOLA. Further details are given in Appendix A.

The Idealization had a calculated fundamental period of 0.097 seconds, and a calculated initial lateral stiffness of 110 kips/inch (19.3 kN/mm), close to that obtained from the diagrams plotted using the actual test data (120 kips/inch--21.0 kN/mm). Calculated histories of base shear versus tip displacement (in response to the shaking table input) are shown in Figures 5.1, 5.2, and 5.3.

Calculated responses were compared with those observed experimentally. For all three tests, analytical idealizations predicted no significant yielding. The predicted load-displacement pattern was almost linear elastic. However, corresponding diagrams plotted using the actual test data showed wider loops, implying more energy dissipation than predicted. The maximum predicted base shear for the three tests was within about 15% of that obtained from test results. A single response peak was noticed in the diagram for Test #10, due to a spike in the excitation. However the diagram plotted using the actual test data shows that this excitation spike had less effect on the actual structure.

Although the differences between the maximum predicted tip displacement and the actual test were more significant (within about 25%), the overall results from the computer idealization are acceptable.

5.2.2 Idealization for Model #6

Model #6 (strong bare frame, excited in-plane) was idealized using the same procedure as Model #1, described in Section 5.2.1.

The idealization had a calculated fundamental period of 0.133 seconds and an initial lateral stiffness of 45 kips/inch (7.9 kN/mm), close to the values obtained from the diagrams plotted for using the actual test data (47 kips/inch, or 8.2 kN/mm). Calculated histories of base shear versus tip displacement (in response to the shaking table input) are shown in Figures 5.4, 5.5, and 5.6.

Calculated responses were compared with those observed experimentally. The analytical idealization predicted slight yielding for Test #45, and more significant yielding in Tests #46 and #47. The actual extent of yielding was less. As a result, the maximum predicted tip displacement was greater than that obtained from the actual test results. For Test #47, the computer idealization predicted a maximum displacement of 1.1 inches (28 mm). The actual recorded maximum displacement was 0.7 inches (18 mm). The effect of peaks in ground acceleration was greater when the structure was yielding. These peaks in ground acceleration caused a few larger loops in the base shear - tip displacement diagrams plotted using the actual test data, but its effect was obviously less than for the computer idealization.

The maximum base shear predicted by the analytical idealization was very close to that obtained from the actual test results for Tests #46 and #47 (within about 5%), and was much higher for Test #45 (100% difference). In the latter test, the earthquake excitation was very low, and the instrumentation did not have enough precision for this level of displacement and acceleration. This resulted in the irregular pattern shown in Figure 5.4 (a).

As discussed in Appendix A, the DRAIN-2DX elements used to idealize this frame were not able to predict any bond slip that might have occurred in bars at the end of the beam due to

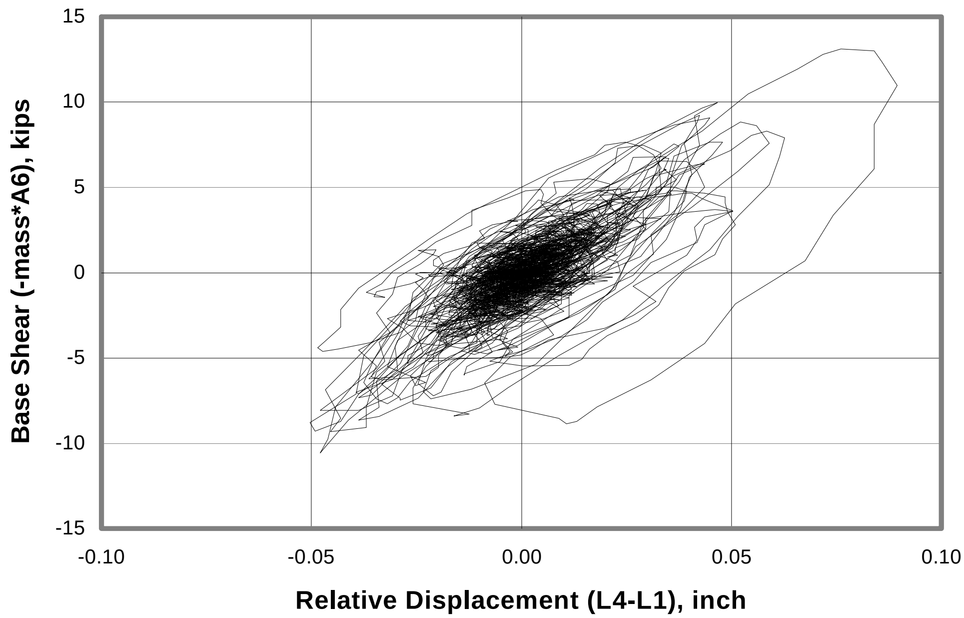

(a) Measured Load-Displacement Response for Model #1, Seismic Test #9

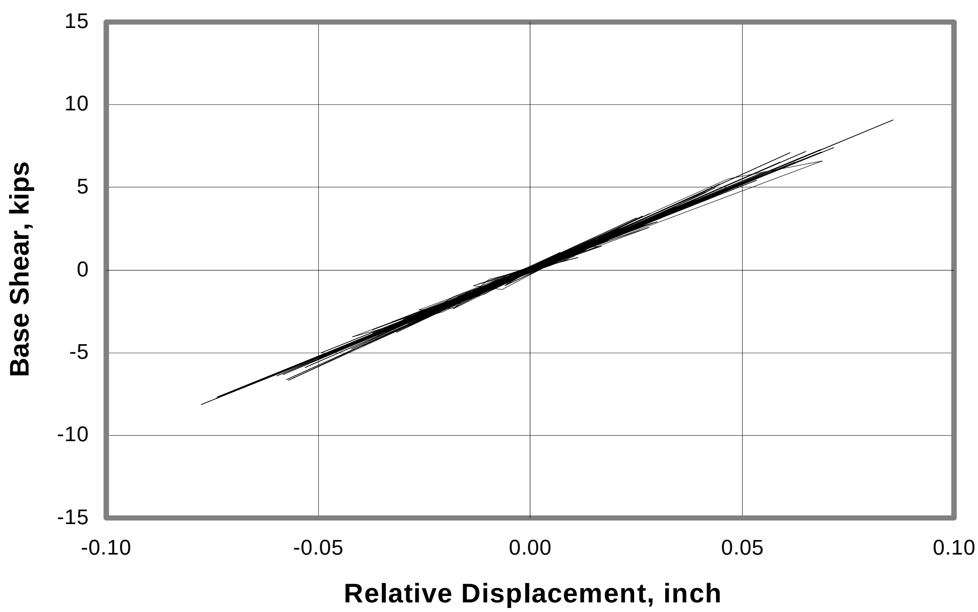

(b) Predicted Load-Displacement Behavior of Model #1, Seismic Test #9

Figure 5.1 Measured vs. Predicted Load-Displacement Behavior for Model #1, Seismic Test #9

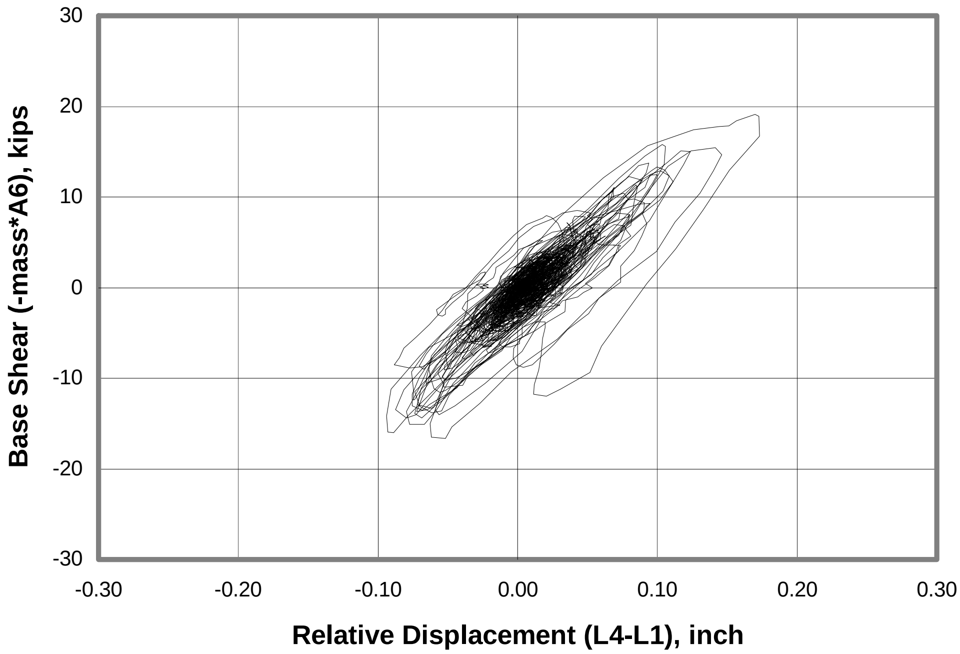

(a) Measured Load-Displacement Response for Model #1, Seismic Test #10

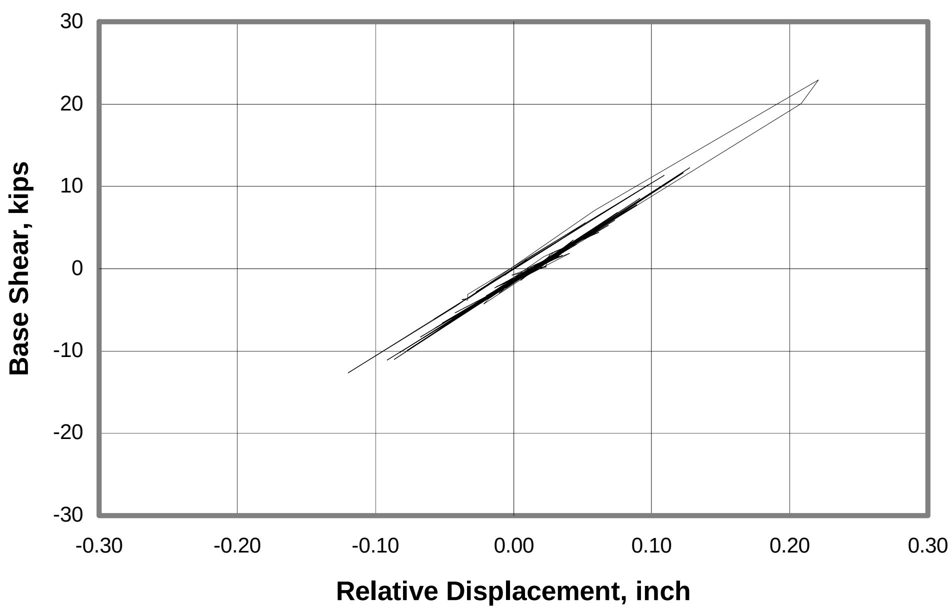

b) Predicted Load-Displacement Behavior of Model #1, Seismic Test #10

Figure 5.2 Measured vs. Predicted Load-Displacement Behavior for Model #1, Seismic Test #11

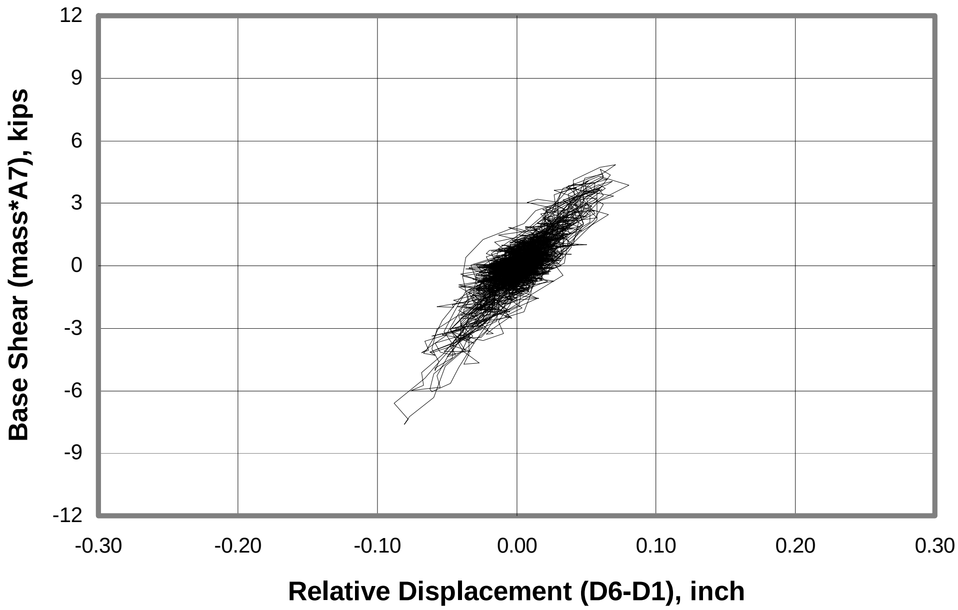

(a) Measured Load-Displacement Response for Model #6, Seismic Test #45

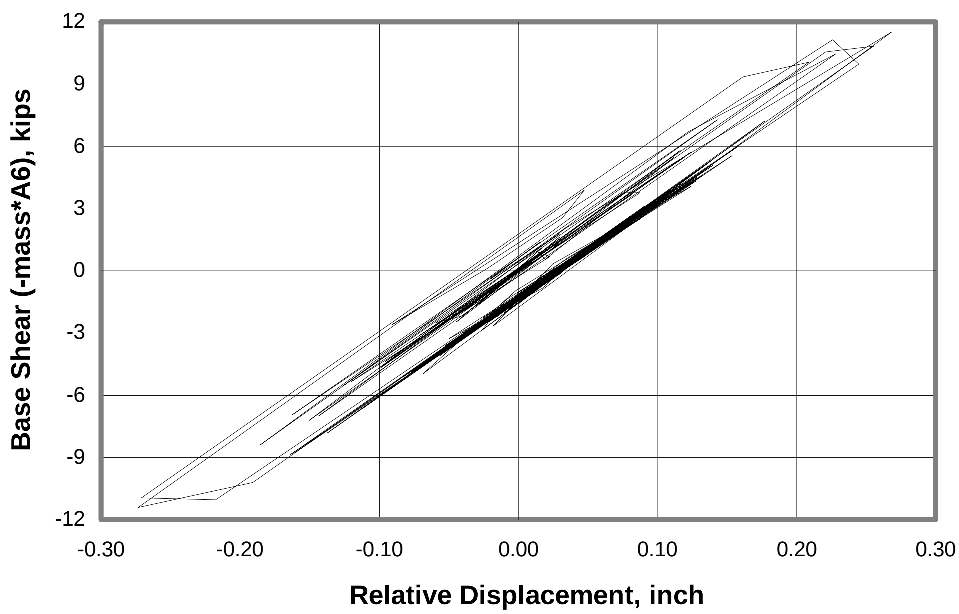

(b) Predicted-Load Displacement Behavior of Model #6, Seismic Test #45

Figure 5.3 Measured vs. Predicted Load-Displacement Behavior for Model #6, Seismic Test #45

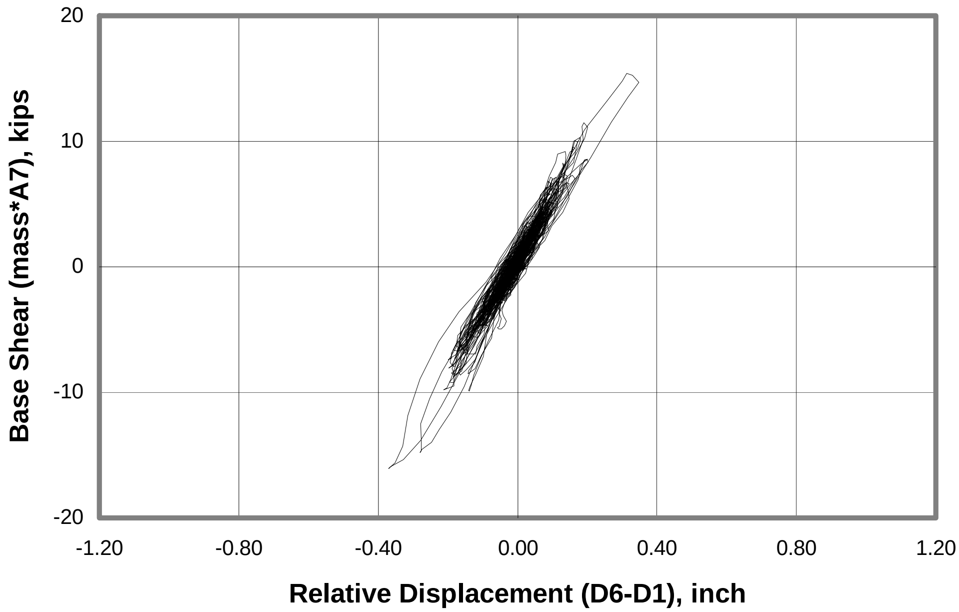

(a) Measured Load-Displacement Response for Model #6, Seismic Test #46

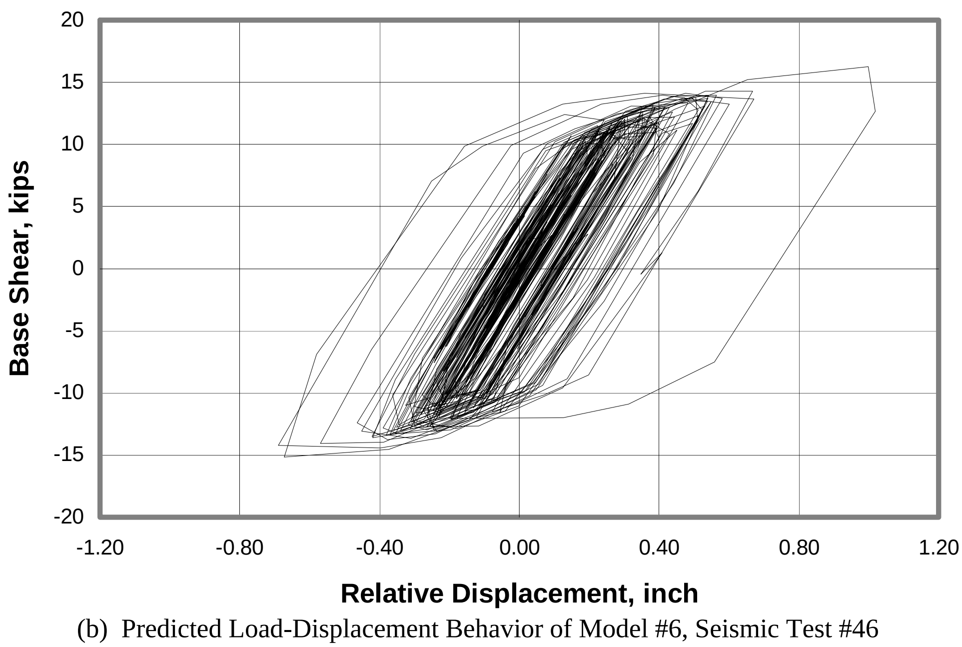

(b) Predicted Load-Displacement Behavior of Model #6, Seismic Test #46

Figure 5.4 Measured vs. Predicted Load-Displacement Behavior for Model #6, Seismic Test #46

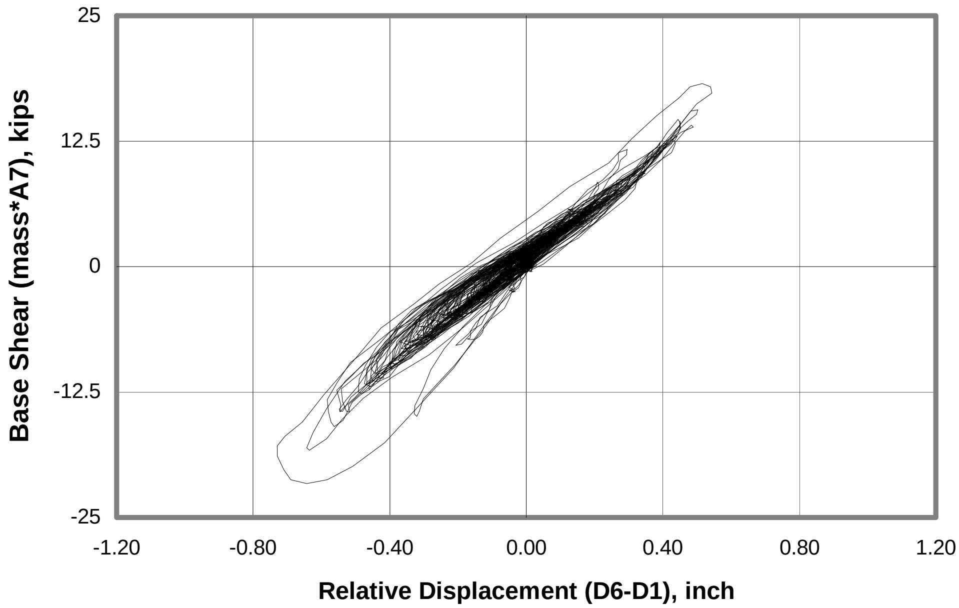

(a) Measured Load-Displacement Response for Model #6, Seismic Test #47

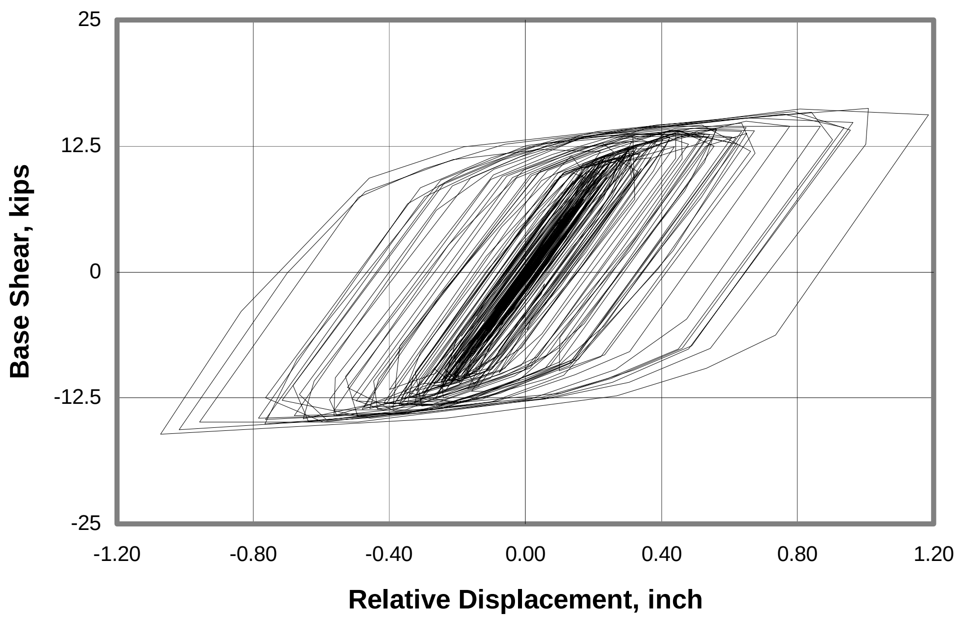

(b) Predicted Load-Displacement Behavior of Model #6, Seismic Test #47

Figure 5.5 Measured vs. Predicted Load-Displacement Behavior for Model #6, Seismic Test #47

insufficient development. Since the analytical predictions are close to the actual test results, no bond failure occurred for Model #6 (weak frame), and this idealization is believed to be adequate.

5.2.3 Conclusions Regarding Analytical Idealization of Bare Frames

1) As explained below, computer idealizations using DRAIN-2DX give acceptable predictions of the load-displacement behavior of the bare frames.

   a) The computer idealizations predict backbone stiffness and maximum base shear within 10% of the values obtained experimentally. Values for maximum tip displacement are less accurate, and can be 30% higher than the values obtained experimentally.

   b) The computer idealization exaggerates the effect of peaks in the ground acceleration, especially if the structure is yielding. Predicted displacements and base shears resulting from peaks were generally about 20% higher than those measured. Peaks in excitation while the structure was yielding caused tip displacement to be over estimated by about 50%.

2) Analysis assuming no bond slip or anchorage failure is apparently reasonable.

3) Computer idealization load-displacement predictions for tests with low excitation did not compare well with the measured response. This could be due to the inaccuracy of the measured response because of the limited sensitivity of the gages.

4) Developing elements which can idealize strength and stiffness degradation will give more accurate results

5.3 Analytical Idealization for Infilled Frames Loaded In-Plane

5.3.1 Idealization for Model #2

The programs FEM/I (Ewing 1987) and LPM/I (Kariotis 1992) were used to idealize Model #2 (strong infilled frame, excited in-plane). The finite element program FEM/I was used to calculate the response of the infilled concrete frame in a static push-over analysis. In this analysis, finite elements were used to represent the masonry infill and the reinforced concrete frame. The finite element model used assumes that tension cracks are smeared over the integration points of each element, and includes compressive strength reduction after tensile cracking occurs in orthogonal directions, but does not incorporate any stiffness degradation. Results of the finite element idealization are shown in Figure 5.7.

The program LPM/I was used for the dynamic analysis of Model #2. The infilled frame was idealized using Element 11 of LPM/I. Element 11 is a nonlinear, hysteretic, degrading envelope spring element. The characteristics of this element are described by force-deformation relations based on analysis and observation of cyclic experiments of reinforced masonry walls. The values of the spring parameters were obtained from the output of the push-over analysis performed by FEM/I. Figure 5.8 shows the force-displacement characteristics of Element 11, and how it relates to FEM/I output. Further details on the idealization of Model #2 are given in Appendix A.

The idealization had a calculated initial fundamental period of 0.023 seconds and an average lateral stiffness of 1820 kips/inch (320.3 kN/mm). Calculated histories of base shear versus tip displacement (in response to the shaking table input) are shown in Figure 5.9.

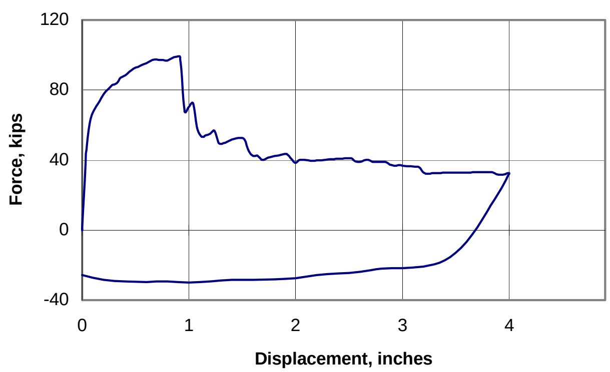

(a) Strong Infilled Frame (Model #2)

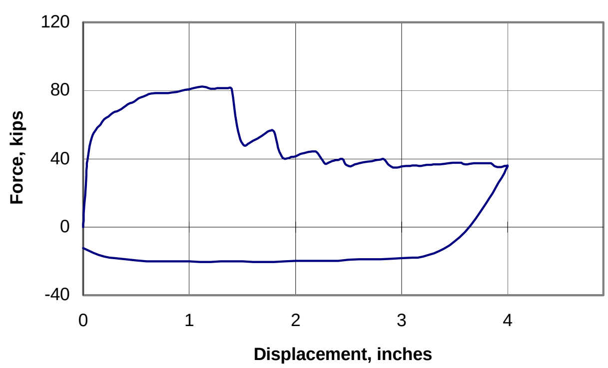

(b) Weak Infilled Frame (Model #7)

Figure 5.6 Push-Over Analysis as performed by FEM/I (Ewing 1987)

Calculated responses were compared with those observed experimentally. Analytical idealization predicted no significant yielding or energy dissipation, and the load-displacement pattern was almost linear elastic. One exaggerated loop was noticed, with almost twice the average tip displacement and base shear, resulting from a peak in the ground acceleration. Corresponding diagrams plotted using the actual test data showed wider loops, implying more energy dissipation. The same exaggerated loop existed in these recorded diagrams. The maximum predicted base shear was close to that obtained from the actual test data (37.5 kips, or 167 kN versus 40 kips, or 178 kN). However, the predicted maximum tip displacement was much lower than that obtained from the test data (0.025 inch, or 0.64 mm versus 4 inch, or 101 mm). Because the experimental value for the maximum tip displacement is unreasonable for an infilled frame (implying a 12.5% drift), and because the experimental load-displacement pattern is irregular, implying some problems with the displacement gages (which reached the end of their travel), the displacement values obtained experimentally are believed to be invalid, and the predicted lateral stiffness cannot be compared to that obtained experimentally.

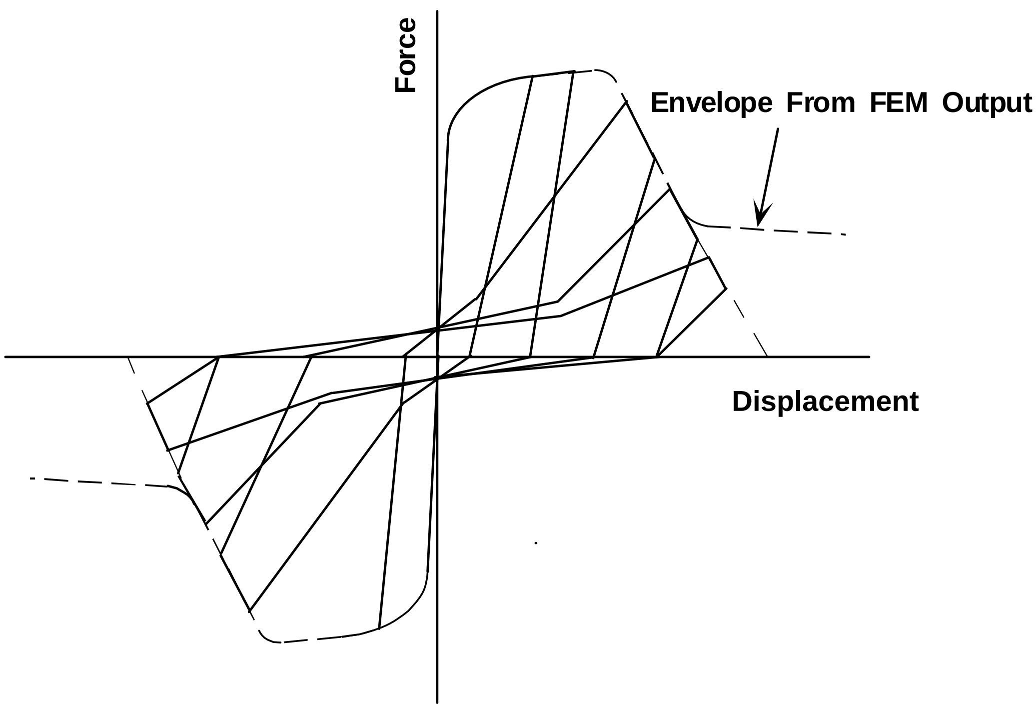

Figure 5.7 Force-Displacement characteristics of LPM/I Element11 (Kariotis 1992)

5.3.2 Idealization for Model #7

Model #7 (weak infilled frame, excited in-plane) was idealized using the same procedure as Model #2, described in Section 5.3.1.

The idealization had a calculated initial fundamental period of 0.023 seconds, and an average lateral stiffness of 1000 kips/inch (175 kN/mm). Although the predicted initial stiffness of this idealization is close to that of Model #2 (1550 kips/inch, or 271.3 kN/mm versus 1820 kips/inch or 318.5 kN/mm), the calculated average stiffness is much lower, because this model was excited up to the yield phase. Calculated histories of base shear versus tip displacement (in response to the shaking table input) are shown in Figure 5.10.

Calculated responses were compared with those observed experimentally. Both the predicted and the measured load displacement diagrams showed wide loops implying significant energy dissipation. A single peak (with about double the average maximum base shear) was noticed in both diagrams. The maximum predicted base shear was close to that obtained from the actual test data (61 kips, or 271.3 kN versus 55 kips or 244.64 kN). However, the predicted maximum tip displacement was much lower than that obtained from the test data (0.07 inch or 1.8 mm versus 0.98 inch or 25 mm). For the same reasons discussed in Section 5.3.1, the displacement values obtained experimentally are believed to be invalid, and the predicted lateral stiffness will not be compared to that obtained experimentally.

5.3.3 Conclusions Regarding Analytical Idealization of Infilled Frames Loaded In-Plane

1) The predicted initial stiffness for Model #2 was higher than that for Model #7 (1820 kips/inch, or 318.5 kN/mm versus 1550 kips/inch, or 271.3 kN/mm), although both models had the same infill. This shows that the stiffness of the confining frame has a significant effect on the behavior of infilled frames.

2) The computer idealization for infilled frames predicts the effect of peaks in ground accelerations to within 15% of the experimental value.

3) Patterns for the tip displacement-base shear diagrams plotted using experimental data are acceptable (they were similar to patterns plotted using predicted response). However values of tip displacements are very high (implying a 12.5% drift). There is an error factor in the values of the tip displacement varying between 12 and 160.

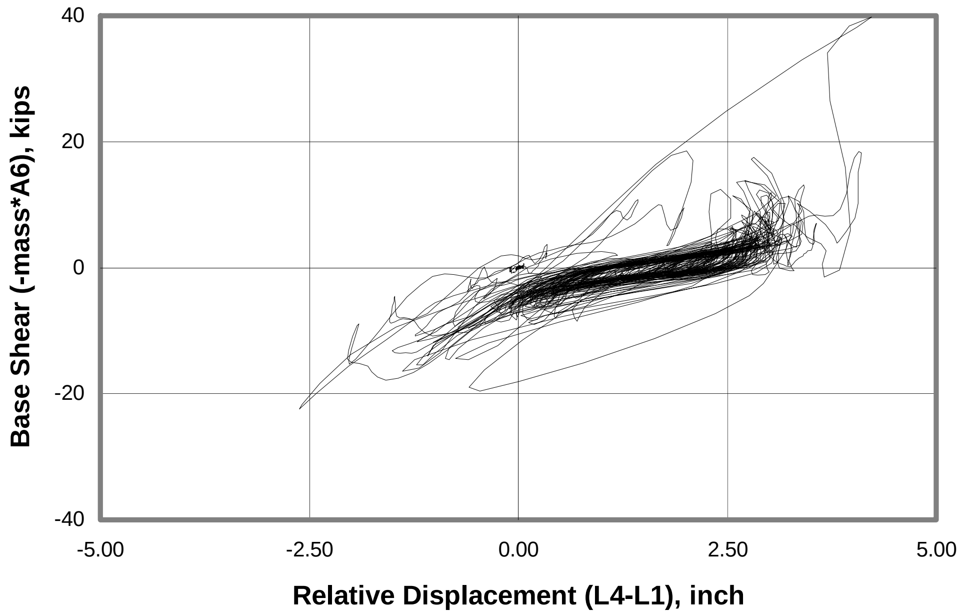

(a) Measured Load-Displacement Response for Model #2, Seismic Test #18

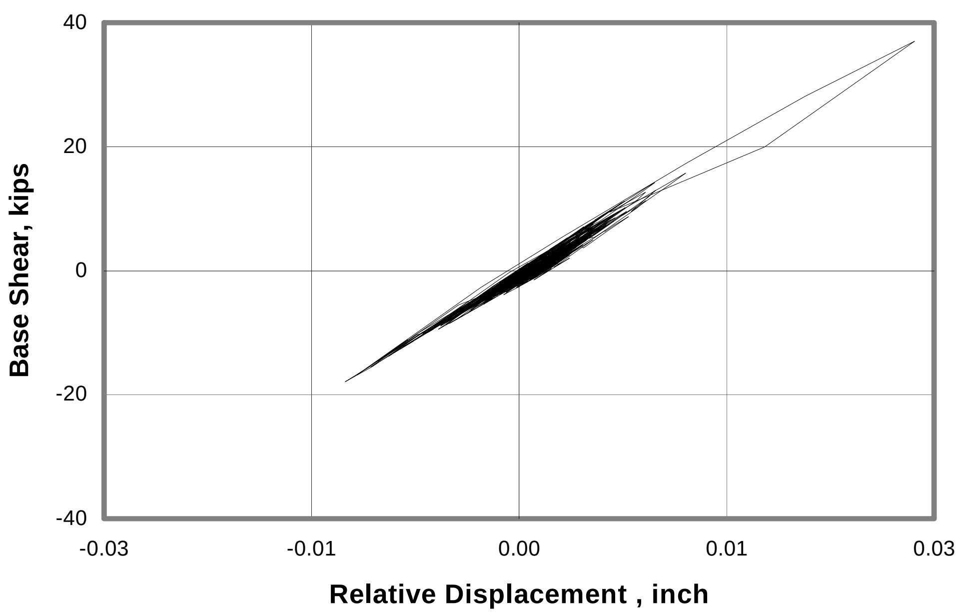

(b) Predicted Load-Displacement Behavior of Model #2, Seismic Test #18

Figure 5.8 Measured vs. Predicted Load-Displacement Behavior for Model #2, Seismic Test #18

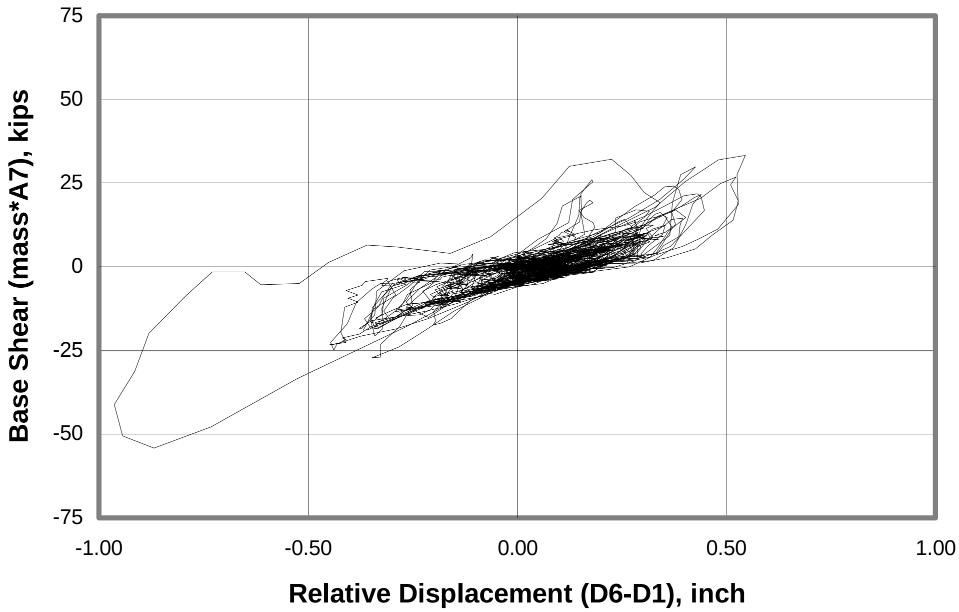

(a) Measured Load-Displacement Response for Model #7, Seismic Test #52

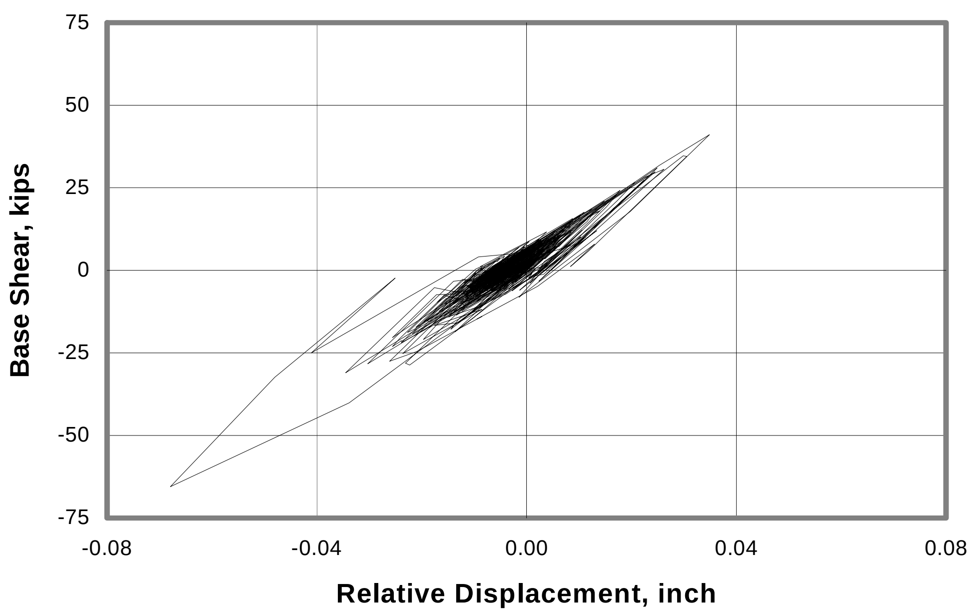

(b) Predicted Load-Displacement Behavior of Model #7, Seismic Test #52

Figure 5.9 Measured vs. Predicted Load-Displacement Behavior for Model #7, Seismic Test #52

CHAPTER 6 COMPARISON WITH SIMPLIFIED ANALYTICAL IDEALIZATIONS

6.1 General Remarks Regarding Simplified Analytical Idealizations

Studies of the behavior and strength of masonry infills excited in-plane have been of interest to researchers for the last several decades. Previous experimental and analytical research has led to the development of several methods for predicting the lateral stiffness and strength of infilled frames. The purposes of this chapter are:

- to discuss the in-plane behavior of infilled frames;
- to review proposed methods for predicting the lateral stiffness and strength of infilled frames;
- to modify these methods if required, and to recommend one method on the basis of accuracy and ease of use;
- and to present a method for determining the out-of-plane strength of cracked masonry infills.

6.2 Simplified Analytical Idealization of the In-Plane Behavior of Infilled Frames

The in-plane structural action of an infilled frame may be idealized in two ways:

1) As a shear wall, and
2) As an equivalent diagonal strut

Each of these is discussed below.

6.2.1 Shear Wall Idealization for In-Plane Behavior of Infilled Frames

In a shear wall idealization, the infilled frame may be viewed as an isolated shear wall whose in plane strength is due to vertical diaphragm action. However, this idealization neglects the interaction between the infill panel and the frame, and greatly underestimates the infilled frame strength and stiffness (Thomas, 1990). Previous research (Thomas, 1990) showed that the lateral stiffness and strength of an infilled frame is greater than the sum of the contributions of the frame and the infill, because of the difference between the flexural deformation pattern of the frame, and the shearing deformation pattern of the infill (Figure 6.4).

6.2.2 Equivalent Strut Idealization

In the equivalent strut idealization, the infilled frame is viewed as a frame braced by a compression diagonal (Stafford Smith, 1966). The equivalent strut idealization of the infilled frame can be justified as follows: Lateral deflection of the infilled frame causes a separation between the frame and the infill panel over part of their contact interface (Figure 6.4). Therefore, contact is maintained only at opposite corners, at the ends of a compression diagonal that forms through the infill panel. The infill panel acts like an equivalent strut, oriented along the infill panel's compression diagonal.

However, the equivalent strut idealization simplifies the load transfer between the frame and the infill panel (Stafford Smith, 1962). Load transfer actually takes place over an extended contact length, not just at one point at the corners of the infill panel. In spite of this, application of the equivalent strut theory is still justifiable. In most practical structures, the frame is very flexible compared to the infill panel, and any discrepancy caused by this simplification is insignificant (Stafford Smith, 1962).

The effect of this equivalent strut simplification was investigated by constructing three different finite-element idealizations for the infilled frame. In the first idealization, the actual properties of masonry were used to represent the whole infill. In the second idealization, finite elements were used to idealize the masonry forming a diagonal strut between the corners of the frame only, to show the effect of the equivalent strut idealization. In the third idealization, the tensile strength of the elements representing masonry units at the boundary of the infill was specified to be 10% of the actual masonry tensile strength, to show the effect of separation at the interface between the infill and the confining frame. Figure 6.1 shows that the results from the push-over analysis for the three idealizations are almost identical. This shows that the equivalent strut idealization accurately represents the behavior of infilled frames.

6.2.3 Simplified Idealization for Lateral Stiffness of Infilled Frames

Based on criteria of accuracy, consistency and simplicity, previous research (Thomas, 1990) recommended the use of Stafford Smith's equivalent strut method (Stafford Smith, 1966) for the prediction of the lateral stiffness of infilled frames. Furthermore, Stafford Smith's second strut method was preferred because of its simplicity and the availability of design graphs for it. Recent research (Angel, 1994) suggested the use of Holmes' (Holmes 1961, 1963) equivalent strut method for the prediction of the lateral stiffness. In this section both of Stafford Smith's methods, and Holmes' method will be discussed. Results from each method will be compared to results from finite element analysis, for both the strong and weak infilled frames (Models #2 and #7).

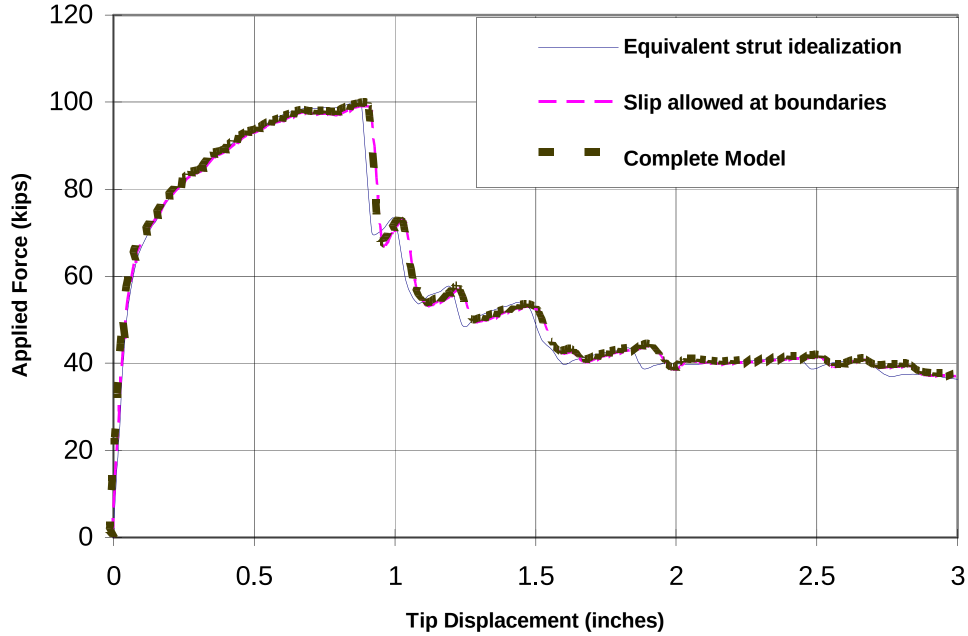

Figure 6.1 Effect of different equivalent-strut simplifications on finite element results for the Infilled frames

a) Stafford Smith's First Method (Stafford Smith, 1966):

This method will be referred to here as "SS1." Although this method is dimensionally consistent, only U.S. customary units will be used, to match the original form, and to make comparison with other methods easier. According to Stafford Smith, the stiffness of an infill panel is affected not only by the size, thickness proportions, and material of the panel, but also by the length and distribution of the applied load on the corner. As the frame stiffness increases, the contact length and consequently the effective stiffness also increases. Stafford Smith considered the possibility of rigid as well as pinned connections, even though the difference between calculated stiffness between the rigid and the pinned cases was presumed to be small in most cases (Stafford Smith, 1966).

For a rigid frame, it is possible to combine the effects of the strain energies of the tension in the windward column, A, the compression in the equivalent strut, B, and the bending of the frame, C. The lateral stiffness of the infilled frame can then be determined from the equivalent structure, as reviewed below (Stafford Smith, 1962).

The lateral stiffness of the infilled frame is given by

$$K = \frac{A + B + B}{C(A + B)} \tag{6.1}$$

where:

A is the strain energy from tension in the windward column, and is given by

$$A = \frac{h \tan 2\theta}{A_c E_f} \tag{6.2}$$

B is the strain energy from compression in the equivalent strut, and is given by

$$B = \frac{d}{w t E_i (\cos 2\theta)} \tag{6.3}$$

C is the strain energy from the bending of the frame and is given by

$$C = \frac{h^3 (3 I_b h + 2 I_c L)}{12 E_f I_c (6 I_b h + I_c L)} \tag{6.4}$$

h	=	height of column (inches)
θ	=	angle of diagonal to horizontal (degrees)
A_c	=	cross-sectional area of the column (inch^2)
E_f	=	elastic modulus of frame (ksi)
d	=	diagonal length of the infill panel (inches)
w	=	width of the equivalent strut (inches)
t	=	thickness of the infill panel (inches)
E_i	=	elastic modulus of infill panel (ksi)
I_b	=	moment of inertia of the beam (inch^4)
I_c	=	moment of inertia of column (inch^4)
L	=	length of beam (inches)

b) Stafford Smith's Second Method:

This method will be referred to here as "SS2." This method is not dimensionally consistent, and was formulated for U.S. customary units. The effect of the stiffness of the frame members in flexure compared to that of the infill panel in compression was considered by Stafford Smith in later studies (Stafford Smith 1966, 1967a, 1967b, 1969, 1978, Carter 1969, Riddington 1967). The stiffer the frame compared to the infill panel, the greater the contact length, and consequently the stiffer the infilled frame. To indicate the relative stiffness between infill panel and frame, Stafford Smith therefore defines a non-dimensional parameter, λ, analogous to that used in elastic foundation theory to express the stiffness of the foundation relative to an overlaying beam (Stafford Smith, 1966):

$$\lambda = \sqrt[4]{\frac{E_i \, t \sin\theta}{4 E_f \, I_c \, L}} \tag{6.5}$$

where

E	=	elastic modulus of infill panel (ksi)
E_f	=	elastic modulus of frame (ksi)
t	=	thickness of infill panel (inches)
θ	=	angle between diagonal and the horizontal (degrees)
I_c	=	moment of inertia of the column ($inch^4$)
L	=	Length of beam (inches)

Given an expression for relative stiffness, λL, a relationship can be derived for α, the length of contact between infill and frame after lateral load has been applied:

$$\frac{\alpha}{L} = \frac{\pi}{2\lambda L} \tag{6.6}$$

where

α = contact length between frame and panel during loading (inches)

L = length of the infill panel (inches)

This relationship was adapted from the equation for the contact length of a free beam on an elastic foundation, subjected to a concentrated load; it compares very closely with more complex relationships derived considering triangular and parabolic stress distributions over the contact length, and also agrees with experimental results (Stafford Smith, 1966).

In relating the contact length to an effective width of the equivalent strut, Stafford Smith found that theoretical predictions of effective width were consistently higher than experimental values. For design purposes, he therefore adopted a set of curves based on experimental results (Figure 6.2). The equivalent width of the compression diagonal can be found by entering the charts with a computed relative stiffness.

The area of the equivalent strut is then the product of the width and thickness of the infill panel:

$$A_{strut} = w \cdot t \tag{6.7}$$

Once the area of the equivalent strut has been determined, the lateral deflection of the resulting braced frame can be calculated by conventional methods.

c) Holmes' Method:

Although this method is dimensionally consistent, only U.S. customary units will be used, to match the original form, and to make comparison with other methods easier. Holmes considered a single frame-infill specimen subjected to a horizontal shear force P. This force produces a compressive resultant, $H/\cos\theta$ in the infill, as illustrated in Figure 6.4. By considering the forces in

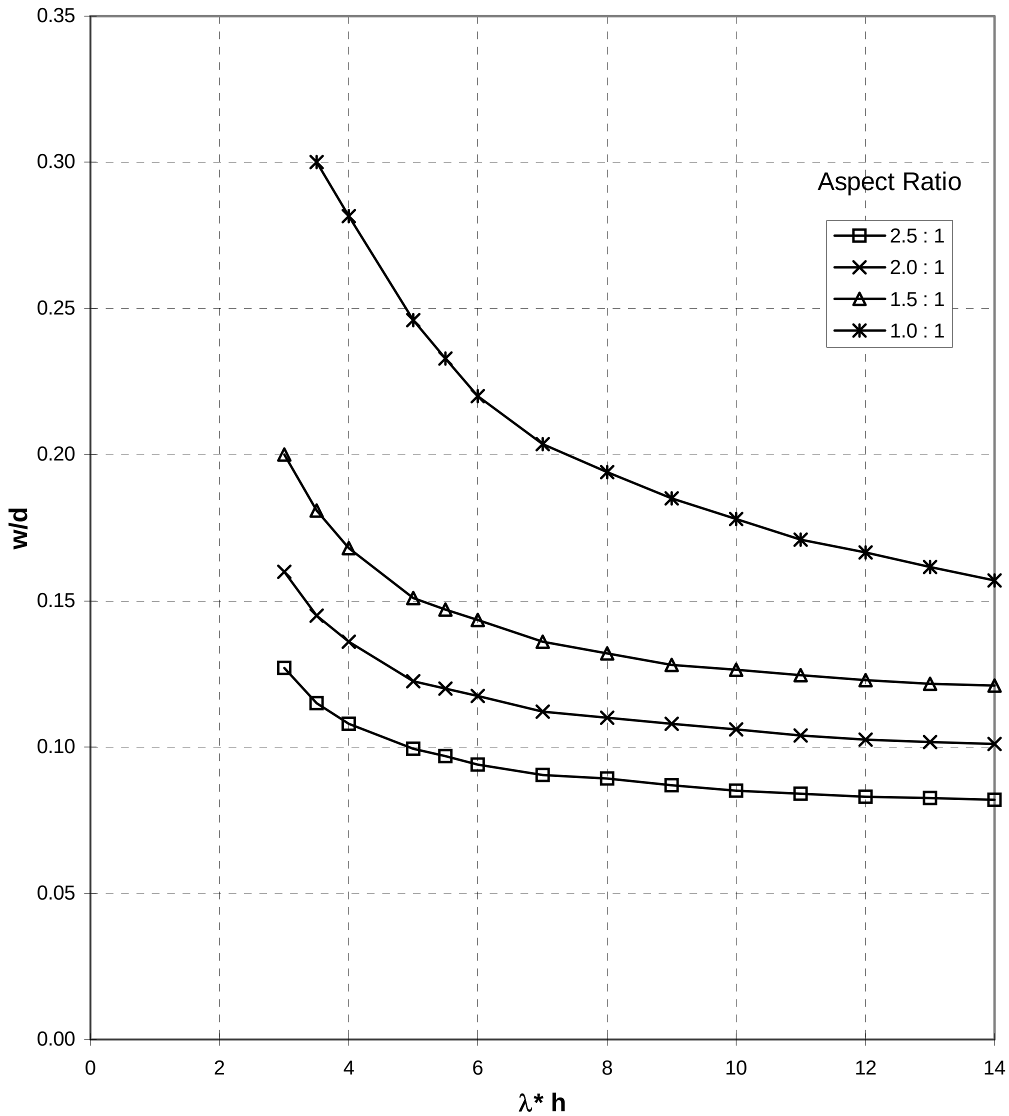

Figure 6.2 w/d as a Function of λh for Different Aspect Ratios (Stafford Smith 1966)

the frame and the infill panel separately, the horizontal force causing failure may be determined by evaluating the shortening of the equivalent strut. The expression proposed to evaluate the horizontal stiffness of the specimen is given by

$$K = \frac{24E\,I_c}{h^3\left[1+\left(\frac{I_c}{I_b}\right)\cot\theta\right]} + \frac{t\,f_c'}{3\varepsilon_c} \tag{6.8}$$

where

E_f	=	elastic modulus of frame (ksi)
I_c	=	moment of inertia of column ($inch^4$)
I_b	=	moment of inertia of the beam ($inch^4$)
θ	=	angle between diagonal and the horizontal (degrees)
ε_c	=	strain in infill at failure
h	=	height of the frame (inches)
A	=	cross-sectional area of the equivalent strut ($inch^2$)
f'_c	=	diagonal compressive strength of the infill panel (ksi)

The above equation suggests that the in-plane stiffness of an infilled frame depends primarily on the relative geometry of the frame and the thickness of the infill along with the mechanical properties of both the masonry panel and the frame. The compressive area of the equivalent strut was determined to be primarily dependent on the thickness and the aspect ratio of the infill panel. The specimen behavior prediction assumes an idealized linear relationship for the force-deflection up to crushing of the masonry at which failure of the system occurs.

The lateral stiffnesses of the strong and the weak infilled frames were calculated using both Stafford Smith methods, and Holmes' method. In Table 6.1, results are compared with the finite element idealization. The finite element stiffness was matched closely by Stafford Smith's second method (SS2), and by Holmes' method. Of these, Stafford Smith's second method (SS2) is recommended, because it considers the relative stiffness of the frame and the infill in estimating the contact length between them, giving a more accurate value for the effective width of the equivalent strut. In contrast, Holmes' method uses a constant value for the width of the equivalent strut, which may lead to inaccurate results in some special cases. The stiffness obtained by the SS2 method is close to the experimentally determined initial stiffness. Previous research shows that the stiffness of infilled frames exposed to cyclic loads eventually degrades to about half this initial value (Angel, 1994).

Table 6.1 Predicted Specimen Stiffness, kips/inch

Model	Predicted Stiffness			
	Finite element	Simplified Methods		
		SS1	SS2	Holmes
Strong frame	743	388	690	634
Weak frame	653	335	580	617

6.2.4 Simplified Idealization For Predicting the In-Plane Strength of Infilled Frames

Previous research (Thomas, 1990) recommended the use of Liauw and Kwan's (Liauw, 1982, 1983a, 1983b, 1985) method for determining the lateral strength of the infilled frames. This recommendation is based on the same criteria mentioned in Section 6.2.1. The predictions of this method were rather conservative (low) in some cases, but they were also very consistent (Thomas, 1990). In this section Liauw and Kwan's method will be discussed, and also an older method proposed by Holmes (Holmes, 1963). Results from each method will be compared to results from the push-over analyses performed using the finite element idealizations, for both the strong and weak infilled frames (Models #2 and #7). The predicted lateral strength will not be compared to results from the dynamic tests, as the infilled frames tested in-plane were not excited up to their lateral strength.

a) Liauw and Kwan's method for predicting the in-plane strength of infilled frames

Liauw and Kwan combined plastic theory with nonlinear finite element analysis to arrive at collapse loads for infilled frames. They addressed concerns that they maintained had been ignored in previous studies by Wood (Wood, 1978). These included multi-story design and the distinction between integral and non-integral infill panels.

According to Liauw and Kwan, Wood's failure to differentiate between integral and non-integral frames led to wide discrepancies between his theoretical predictions and experimental results (Liauw, 1983). Wood did include a penalty factor to lower the effective crushing stress of the infill panel to account for its lack of plasticity (Wood, 1978). According to Liauw and Kwan, Wood's over-estimation of the collapse shear is due to the assumption of excessive friction at the interface between the infill panel and the frame, and to neglect of separation between infill panel and frame in the composite shear mode.

According to Liauw and Kwan, friction has an insignificant effect, and should be considered only as reserve strength . Therefore, only three failure modes exist for the non-integral infilled frame, as shown in Figure 6.3.

1) Corner crushing with failure in columns

2) Corner crushing with failure in beams

3) Diagonal crushing

The collapse shears for each failure mode in single-story, non-integral infilled frames are as follows:

Mode 1:
$$H_u = \sigma_c t\, h \sqrt{\frac{2\left(M_{pj} + M_{pc}\right)}{\sigma_c\ t\, h^2}} \tag{6.9}$$

Mode 2:
$$H_u = \frac{\sigma_c t\, h}{\tan\theta} \sqrt{\frac{2\left(M_{pj} + M_{pc}\right)}{\sigma_c\ t h^2}} \tag{6.10}$$

Mode 3:
$$H_u = \frac{4M_p}{h} + \frac{\sigma_c\ th}{6} \tag{6.11}$$

where

H_u = in-plane design strength of infill panel (kips)

h = story height (inches)

M_{pb}= plastic moment of the beam (inch-kip)

M_{pc}= plastic moment of the columns (inch-kip)

M_p = the smaller of M_{pb} and M_{pc} (inch-kip)

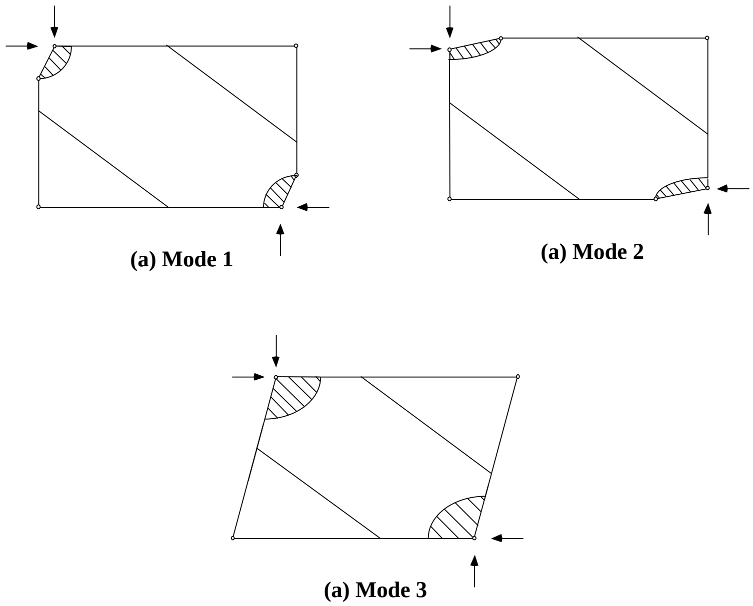

Figure 6.3 Collapse modes for infilled frames (Liauw and Kwan 1983)

The collapse shear is the minimum value from the above three equations.

Plastic theory can be applied to multi-story infilled frames as well as single-story ones, because the collapse modes for both are basically the same. However, many different possible combinations of failure modes are possible, and the evaluation of ultimate load can become quite complex. A simplified procedure was developed by Liauw and Kwan for the story-by-story design of multi-story infilled frames. Equations for predicting the collapse shears for lower stories (that is, all stories except the top one) in integral and non integral infilled frames are listed in the following equations:

Mode 1:
$$H_u = \sigma_c \, t \, h \sqrt{\frac{4 M_{pc}}{\sigma_c \, t h^2}} \tag{6.12}$$

Mode 2:
$$H_u = \frac{\sigma_c \, t h}{\tan\theta} \sqrt{\frac{4 M_{pb}}{\sigma_c \, t h^2}} \tag{6.13}$$

Mode 3:
$$H_u = \frac{4 M_{pc}}{h} + \frac{\sigma_c \, t h}{6} \tag{6.14}$$

The lateral strength of both the strong and the weak infilled frames were calculated using Liauw's methods for both single and multi-story frames, and were compared with the results from the finite element idealization (Table 6.2). As expected, the predictions of this method were low.

b) Holmes' Method:

This method is based on the analysis of the results of small-scale and full-scale tests of steel infilled frames, performed by Holmes (Holmes, 1963). As in Holmes' stiffness method, the infill has been replaced by an equivalent strut leaving the frame itself to carry the forces, as shown in Figure 6.4. By equating the change in the length of the diagonal AC of the frame to the shortening of the equivalent strut, the load causing failure is given by

$$H = \frac{24 E I_c \, \varepsilon'_c \; d}{h^3 \left[1 + \left(\frac{I_c}{I_b} \right) \cot\theta \right]} \cos\theta \; + \; \frac{t \, d \; f'_c \;\; \cos\theta}{3} \tag{6.15}$$

where

E_f = elastic modulus of frame (ksi)

I_c = moment of inertia of column ($inch^4$)

I_b = moment of inertia of the beam ($inch^4$)

d = diagonal length of the infill panel (inches)

θ = angle between the diagonal and the horizontal (degrees)

ε'_c = strain in infill at failure

h = height of the frame (inches)

A = cross-sectional area of the equivalent strut ($inch^2$)

f'_c = diagonal compressive strength of the infill panel (ksi)

The first term on the right-hand side of the above equation represents the load carried by the frame alone, calculated on an elastic basis. However, this value should be limited by the peak strength of the bare frame, which is given by the lesser of $\frac{4M_{pc}}{h}$ or $\frac{4M_{pb}}{h}$, where M_{pc} and M_{pb} are the fully plastic moments of the columns and the beams respectively, and h is the height of the frame. The value of the lateral strength obtained by this method, shown in Table 6.2, is much higher than that predicted by the finite element idealization.

Table 6.2 Predicted Specimen In-Plane Strength, kips

Model	Predicted Strength			
		Simplified Methods		
	Finite Element	Liauw	Holmes	CERL
Strong Frame	96.0	64.0	155.4	96.9
Weak Frame	82.2	48.7	152.4	80.8

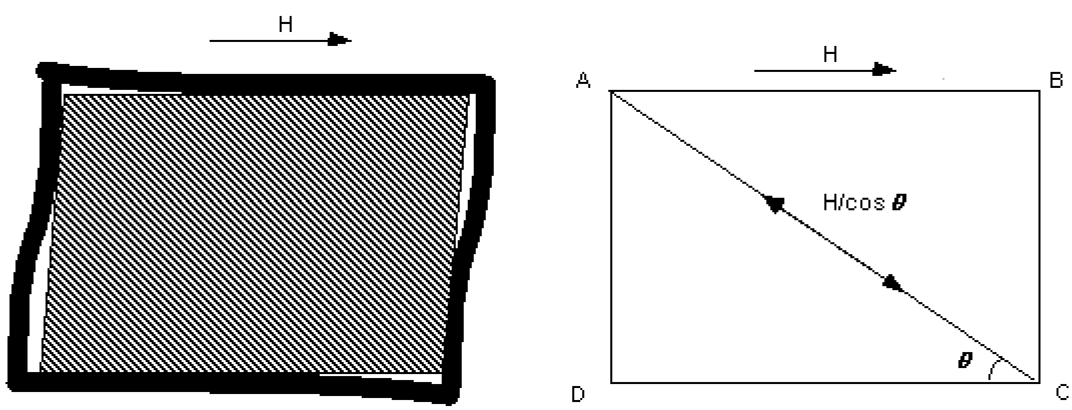

Figure 6.4 Structural Action of an Infilled Frame with a Horizontal Shear Force, H

The main reason for the high value of the estimated collapse load for the infilled frame under study in Holmes' method is that the area of the equivalent strut is exaggerated. In Holmes' method, the width of the equivalent diagonal strut is fixed to one-third the length of the infill diagonal, irrespective of the relative stiffness of the frame and the infill in the estimation of the contact length between them. An expression based on Holmes' method, and modified for the effect of relative frame-infill stiffness on the width of the equivalent diagonal strut, is

$$H = \frac{24EI_c\,\varepsilon_c'\,d}{h^3\left[1+\left(\frac{I_c}{I_b}\right)\cot\theta\right]}\cos\theta + A\,f_c'\,\cos\theta \tag{6.16}$$

where A is the area of the diagonal strut obtained using the curves proposed by Stafford Smith (Method SS2), as described in Section 6.2.3. This method will be referred to here as the "CERL method." As shown in Table 6.2, predictions of this method are very close to those obtained by the finite element idealization,. The use of the new expression (CERL Method) is recommended for the estimation of the lateral strength of the infilled frames.

6.3 Simplified Analytical Predictions of the Out-of-Plane Strength of Infills

6.3.1 Effect of Arching Action on the Out-of-Plane Strength of Infills

Masonry infills have been observed to withstand much larger lateral loads than would be predicted on the basis of conventional bending analysis. Previous experimental work showed that fixed-end brick beams have 3 to 6 times the load-carrying capacity of simply supported beams, due to arching action (McDowell, 1956a).

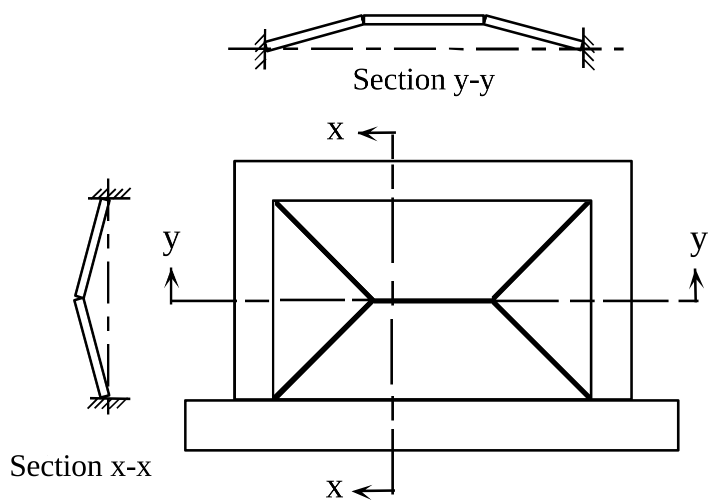

Figure 6.5 Deflected Shape of a Typical Infill During Out-of-Plane test

When considering arching, the stress-strain properties of masonry in compression are important. In previous research, different stress distributions were assumed. Some workers have assumed a triangular stress distribution (McDowell, 1956a); others, rectangular (Dawe, 1990); and still others, elasto-plastic (McDowell, 1956a). In the method presented here, an equivalent rectangular stress block based on Eremin's theory (McDowell, 1956b) was used. Eremin assumed a uniform compressive stress equal to the maximum compressive stress for masonry over the whole compression area, thus overestimating the compressive force and the effect of arching action. The equivalent stress block used in this study considers the difference between the assumed and the actual stress distributions. The effect of using an equivalent stress block is investigated further in Appendix B.

Figure 6.5 shows the deflected shape at collapse of infills surrounded by reinforced concrete frames and loaded out-of-plane in recent similar research (Angel, 1994). This type of deformed shape is highly idealized although similarities with a typical infill crack pattern are clear (Figure 6.9). This cracking pattern shows that the arching action exists in both the vertical and the horizontal directions. The strength prediction method developed in this section will consider both arching and two-way action and is based on the described yield-line pattern.

6.3.2 Proposed Method for Predicting the Out-of-Plane Strength of Infills

A typical deflected masonry segment is shown in Figure 6.6. According to Eremin (McDowell, 1956b), the lateral strength is obtained at a deflection, x_y, at which a compressive stress f'_c (the ultimate compressive strength of the mortar or the masonry, whichever is weaker) exists at points m, n and o. The deflection is given by

$$x_y = \frac{t\, f'_c}{E\, \varepsilon_m} \tag{6.17}$$

where

$$\varepsilon_m = \frac{L' - \frac{h}{2}}{L'} \tag{6.18}$$

and L' is the length of the diagonal shown in Figure 6.6.
The resisting moment associated with the deflection, x_y, is given by

$$M_y = 0.85 f'_c \ \left(0.85c\right)\left[t - x_y - 0.85c\right] \tag{6.19}$$

As in Eremin's approach, the bearing width, c, is chosen so that the moment, M_y, is a maximum. Differentiating M_y with respect to c, one obtains

$$c = \frac{1}{1.7}\left(t - x_y\right) \tag{6.20}$$

or

$$a = \frac{1}{2}\left(t - x_y\right) \tag{6.21}$$

where a is the width of the equivalent compressive block. Substituting in Equation 6.19,

$$M_y = \frac{0.85 f'_c}{4}\left(t - x_y\right)^2 \tag{6.22}$$

Figure 6.6 corresponds to the deflection pattern of Figures 6.7 and 6.8a. However, according to the yield line pattern shown in Figure 6.7, there is another shape for the deflected segment (Figure 6.8b). The corresponding moment for this segment will also be given by Equation 6.22.

The lateral strength of a segment is obtained by equating the external work to the internal work done when the segment is subjected to a virtual deflection δ (Figure 6.7).

$$\frac{wh\delta}{2} = \left(\frac{M_y}{2} + \frac{M_y}{2}\right)\frac{\delta}{h/2} + \left(\frac{M_y}{2}\right)\frac{2\delta}{h/2} \tag{6.23}$$

or

$$w = \frac{8 M_y}{h^2} \tag{6.24}$$

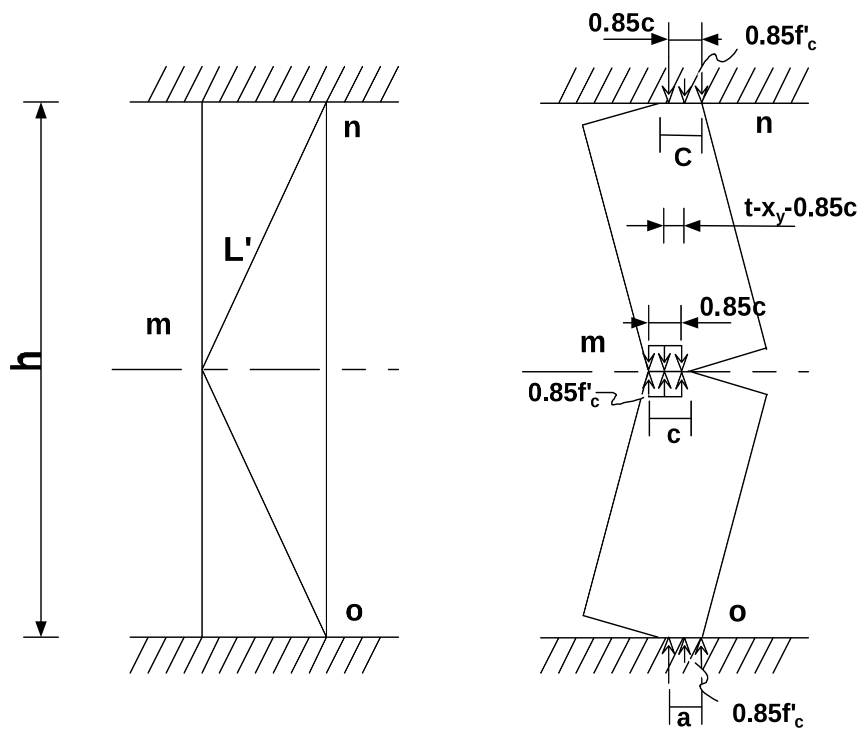

Figure 6.6 Stresses in Masonry Segments with Out-of-Plane Deflection

for the segment shown in Figure 6.8(a), and

$$w\left[\left((h-2x)\,\delta+2x\frac{\delta}{2}\right)\right]=4\left(\frac{M_y}{2}\right)\frac{\delta}{x} \tag{6.25}$$

or

$$w=\frac{2\,M_y}{hx-x^2} \tag{6.26}$$

for the segment shown in Figure 6.8(b)

As the deflections of strips are described by the yield line pattern shown in Figure 6.6, all horizontal and some vertical strips will not experience the deflection x_y associated with the maximum moment M_y. According to Eremin, the resisting moment is directly proportional to the out-of-plane deflection, up to x_y (calculated from Eq. 6.17). The resisting moment at any out-of-plane deflection, $\delta(x)$, less than x_y, is given by

$$M(x) = \frac{\delta(x)}{x_y} M_y \tag{6.27}$$

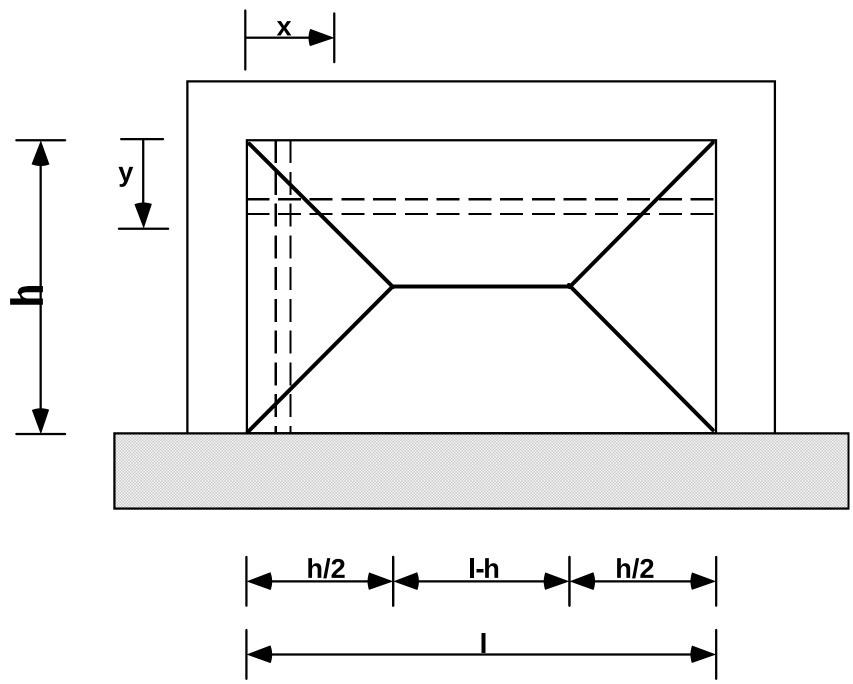

Figure 6.7 Yield Line Pattern of an Infill

From the yield line pattern shown in Figure 6.7, for vertical strips

$$\delta(x) = \frac{x}{h/2} x_{yv} = \frac{2x}{h} x_{yv} \tag{6.28}$$

and for horizontal strips,

$$\delta(y) = \frac{y}{h/2} x_{yh} = \frac{2y}{h} x_{yh} \tag{6.29}$$

where x_{yv} and x_{yh} are obtained from Equation 6.17, substituting h as the height of the infill and the length of the infill respectively.

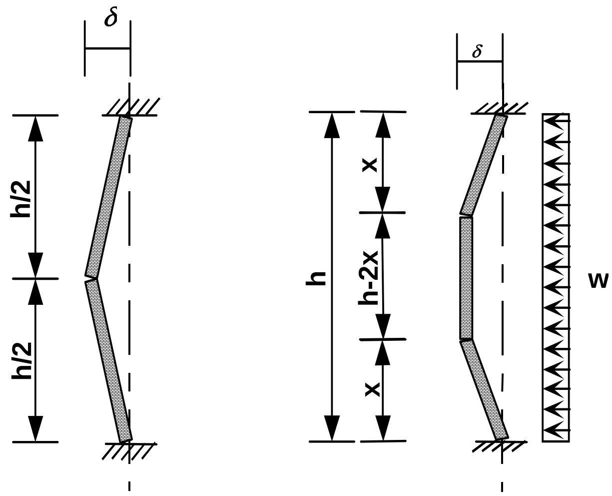

Figure 6.8 Deflected Segments Under Lateral Loads

Substituting in Equation 6.26 for vertical strips:

$$w(x) = \frac{4\,M_{yv}}{h}\frac{x}{hx - x^2} \tag{6.30}$$

Similarly, for horizontal strips:

$$w(y) = \frac{4\,M_{yh}}{h}\frac{y}{ly - y^2} \tag{6.31}$$

M_{yv} and M_{yh} are obtained by substituting the values of x_{yv} and x_{yh} respectively in Equation 6.22. The resistance of horizontal segments as given by Equation 6.31 is associated with the maximum out-of-plane deflection for a horizontal strip, x_{yh}. In rectangular panels, the maximum out-of-plane deflection (at the center of the panel) is governed by the crushing of masonry in the center vertical strips, at a center deflection equal to x_{yv}. Failure will occur before horizontal strips can reach the lateral deflection x_{yh}, required to develop a moment equal to M_{yh}. Equation (6.31) must therefore be modified to

$$w(y)=\frac{4\,M_{yh}}{h}\,\frac{y}{ly-y^2}\left(\frac{x_{yv}}{x_{yh}}\right) \tag{6.32}$$

The total force resisted by the infill, W, can be obtained from the summation of the forces resisted by the horizontal and vertical strips

$$W=\frac{8M_{yv}}{h}\left(l-h\right)+2\left(\int_{0}^{h/2}\frac{4M_{yv}}{h}\,\frac{1}{h-x}\,dx\right)h+2\left[\int_{0}^{h/2}\frac{4M_{yh}}{h}\left(\frac{x_{yv}}{x_{yh}}\right)\frac{1}{l-y}\,dy\right]l \tag{6.33}$$

or

$$W=8\,\frac{M_{yv}}{h}\,(l-h)+8\,M_{yv}\ln(2)+8\,\frac{M_{oh}}{h}\left(\frac{x_{yv}}{x_{yh}}\right)\ln\left(\frac{l}{l-h/2}\right)l \tag{6.34}$$

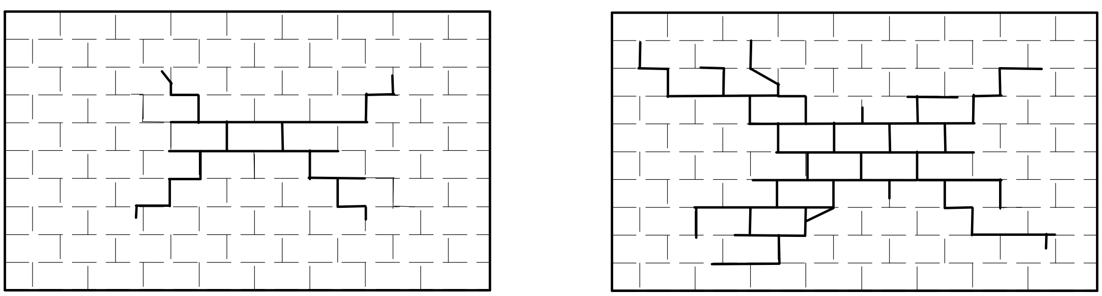

Moderate Damage Severe damage

Figure 6.9 Degrees of Infill Cracking Damage as Described by Angel (Angel 1994)

6.3.3 Effect of Previous In-Plane Damage on Out-Of-Plane Strength of Infills

The out-of-plane strength calculation of Equation 34 is consistent with moderate in-plane damage in the form of an x-shaped yield line pattern. Recent experimental research (Angel, 1994) showed that out-of-plane strength can be significantly decreased by severe in-plane damage. Angel used experimental data to develop reduction factors that depended on the panel slenderness ratio and the magnitude of existing in-plane damage in the panel being evaluated. He proposed visual inspection to differentiate between severe and moderate damage (Figure 6.9). Based on those factors, a reduction factor, R, was developed, and results are presented in Table 6.3. That reduction factor was obtained from the ratio between the reduction factors for moderate and severe cracking, as proposed by Angel, and should be multiplied by the out-of-plane strength (as given by Equation 6.34) in the cases of severe in-plane damage only.

Table 6.3 Reduction Factors for Severe In-Plane Damage (based on Angel 1994)

h/t	R
5	0.997
10	0.945
15	0.889
20	0.830
25	0.776
30	0.735

6.3.4 Effects of Confining Frame Stiffness

According to Angel (Angel 1994), predicted out-of-plane behavior also depends on the stiffness of the confining frame. Angel developed expressions for a reduction factor to account for the flexibility of the confining frame for panels at edge locations (for the cases of exterior bays). These expressions are as follows:

$$R_2 = 0.357 + 7.14 \times 10^{-8} EI \qquad \text{For } 2.0\times10^6 \text{ kip-inch} \le EI \le 9\times10^6 \text{ kip-inch} \quad (6.35)$$

$$R_2 = 1 \qquad \text{For } EI > 9\times10^6 \text{ kip-inch} \quad (6.36)$$

However, the above expressions will not cause significant reductions for the case of reinforced concrete confining frames for most practical dimensions.

This reduction factor cannot be used directly with the scaled specimen because it does not consider the effect of the confining member's length on its stiffness. If the reduction factor computed using the above equations is multiplied by the cube of the ratio between the column height of this specimen and the column height of real buildings (33 inches, or 838 mm versus 120 inches or 3048 mm), it will give no reduction in the out-of-plane strength due to the confining frame stiffness.

6.3.5 Comparison between Experimental Data and Arching Theory as Developed in this Study

In Table 6.4, the maximum experimentally determined out-of-plane lateral strength of infilled frames was compared to the strength predicted using the arching theory developed here, and also to that predicted using Angel's.

Table 6.4 Predicted versus Observed Out-of-Plane Strength of Infills, psf

	Test results	Arching theory	Angel's Theory
Lateral Strength	190	1775	1787

The lateral strength as predicted by both methods is significantly higher than that obtained experimentally. According to one test observer (Sweeney), the infilled frames were excited out-of-plane up to their lateral strength. However, another test description (Al-Chaar, 1994) states that the infilled frames were loaded out-of-plane up to cracking of the panel only. According to Al-Chaar, the difference between the test results and the estimated out-of-plane strength is due to two important factors:

1) In the dynamic tests, the panels were excited only up to cracking while the above theories estimate ultimate out-of-plane strength.

2) Although the panels cracked in the assumed "X" pattern, slight relative displacements were observed between panel segments defined by those planes. These relative displacements between segments increase the effective slenderness ratio of the infill, and the contact thickness between the masonry segments along the cracked sections is less than predicted. The effect of decreasing the effective slenderness ratio causes the out-of-plane strength to decrease (Angel, 1994).

6.3.6 Effects of the Yield Line Pattern on Calculated Out-of-Plane Strength of Infill Panels

Although experimental results showed that previous in-plane loading cracked the panels in an "X" pattern, Angel developed his arching theory using a unit one-way strip that is cracked horizontally at mid-height, and described this idealization as "The worst case situation" (evidently, the lowest predicted strength). However, based on results of this study, the case cited by Angel does not appear to be the worst case. Using the new arching theory developed here and assuming an "X" yield line pattern and including two way action, the lateral strength of this infill was 17% lower than that calculated assuming a horizontal crack at mid-height. This can be explained as follows:

In an "X" yield line pattern, only the center vertical strips reach the displacement corresponding to the maximum lateral strength due to arching action. Vertical strips at a horizontal distance h/2 from the confining frame will have less lateral deformation (Figure 6.7), and thus less arching action and less lateral strength, causing a decrease in the total lateral strength for the infill. The contribution of horizontal strips to the total lateral resistance is usually small (10% for the infills under investigation) and neglecting it will not overcome the exaggeration in the prediction of the lateral strength due to the assumption of a center crack allowing all vertical strips to reach the deformation corresponding to the maximum lateral strength. The reason for the low contribution of horizontal strips is that they have higher displacement capacities (due to their length) and the lateral displacement at maximum strength (which is governed by the shorter vertical strips) usually develops low strains, and thus low compression and a little arching action in these strips.

6.3.7 Example of Calculation for the Out-of-Plane Strength of Infills

The following example is adapted from Angel (1994). For ease of comparison with the original, it has been carried out in U.S. customary units.

Suppose that a reinforced concrete building with infilled frames has been damaged by an earthquake. It has been determined that the concrete frame did not sustain serious damage. However, the masonry infills are cracked and must be evaluated for out-of-plane strength in the event of a future earthquake.

The infill panel to be investigated is 20 feet long x 15 feet high x 7-3/8 inches thick, and has no openings. The interface between the infill and the surrounding Frame is determined to be sound. The infill material is brick, constructed in two wythes with a medium strength Type N PCL mortar. A series of masonry compression tests and shove tests are carried out to determine the mechanical properties of the infill masonry. The compression tests, carried out in accordance with ASTM E447, provide values for the masonry compressive strength (f'_c). Values of the masonry modulus of elasticity (E_m) can be found in ACI 530-92/ASCE 5-92/TMS 402-92 knowing the mortar type and the unit strength. Results are presented in Table 6.5 .

Table 6.5 Example (Infill properties)

Physical properties	Mechanical Properties

t = 7-3/8 inches	f ′$_c$ = 1000 psi
h = 180 inches	E_m = 750
L = 240 inches	f_a = 40 psi
h/t = 25	f_v = 200 psi

The out-of-plane strength is obtained by substituting in Eq. (6.34). The different factors are calculated as follows

a) Vertical direction

$$L' = \sqrt{(h/2)^2 + t^2} = \sqrt{(90)^2 + 7.375^2} = 90.3 \ \ inches$$

$$\varepsilon_m = \frac{L' - h/2}{L'} = \frac{90.3 - 90}{90.3} = 3.32\times10^{-3}$$

$$x_{yv} = \frac{(7.375)(1)}{(750)(3.32E-3)} = 2.96 \ \ inches$$

$$M_{yv} = \frac{0.85\times1}{4}(7.375 - 2.96)^2 = 4.14 \ \ kip-inch/inch$$

b) Horizontal direction

$$L' = \sqrt{(l/2)^2 + t^2} = \sqrt{(120)^2 + 7.375^2} = 120.23 \quad inches$$

$$\varepsilon_m = \frac{L' - l/2}{L'} = \frac{120.23 - 120}{120.23} = 1.88\times10^{-3}$$

$$x_{yh} = \frac{(7.375)(1)}{(750)(1.88E-3)} = 5.23 \ \ inches$$

$$M_{yh} = \frac{0.85\times1}{4}(7.375 - 5.23)^2 = 0.978 \ \ kip-inch/inch$$

Substituting into Equation 34

$$W = 8\left(\frac{4.14}{180}\right)(240-180) + 8(4.14)\ln(2) + 8\left(\frac{0.978}{180}\right)\left(\frac{2.96}{5.23}\right)\ln\left(\frac{240}{240-90}\right)(240)$$
$$= 36.77\ kips$$

or

$$w = \frac{36.77 \times 1000}{240 \times 180} = 122\ \ lbs\ /\ ft^2$$

The out-of-plane strength of the infill for the case of moderate in-plane damage (Figure 6.8) is 122 psf. The out-of-plane strength of the infill for the case of severe in-plane damage is obtained by multiplying this value by the reduction factor from Table 6.3.

$$w = 122 \times 0.776 = 94.5\ lbs\ /\ ft^2$$

CHAPTER 7 SUMMARY, CONCLUSIONS AND RECOMMENDATIONS

7.1 Summary

Many buildings used by the U.S. Army are classified as reinforced concrete frames with masonry infill walls. There is therefore a need to develop reliable analysis tools to predict the real strength and the dynamic response of such infilled frames. For that reason, a comprehensive multi-year study was carried out by the staff of the U.S. Army Construction Engineering Research Laboratories (USACERL). In that study, several half-scale specimens consisting of reinforced concrete frames (bare and with masonry infill), were subjected to simulated earthquake motions using a shaking table. Both in-plane and out-of-plane motions were applied to virgin specimens, previously damaged specimens, and repaired specimens. In the study reported here (carried out at the University of Texas at Austin) no additional experimental work was performed. In this study, the experimental data obtained by the USACERL was used to evaluate both the in-plane and out-of-plane behavior of infilled frames. Load-displacement characteristics were obtained; and maximum loads, deflections and internal strains were measured and assessed. Dynamic response was predicted analytically, using various mathematical idealizations. Finally, simplified analytical idealizations were developed to predict the strength and stiffness of infilled frames.

7.2 Conclusions

7.2.1 General Conclusions Regarding Experimental Behavior of Specimens

Results from tests with low levels of base acceleration were not useful for evaluating the strength and stiffness of the specimens. Moreover, the forces generated in the specimens during such tests were usually just a fraction of the yielding and failure loads, and they induced generally minor damage in the specimens.

On the other hand, results from tests with higher base shears were generally useful for evaluating the strength and stiffness of the specimens. However, for some tests measured displacements were unrealistically large and therefore stiffness could not be evaluated accurately.

7.2.2 Conclusions Regarding the Behavior of Bare-Frame Specimens

1) The measured average backbone stiffness of the strong bare frame obtained from the load-displacement diagrams was 120 to 140 kip/inch (21.0 to 24.5 kN/mm). Maximum measured load and displacement were 20 kips (89.0 kN) and 0.3 inches (7.6 mm) respectively.

2) The measured average backbone stiffness of the weak bare frame was 47 kips/inch (8.2 kN/mm). Maximum measured load and displacement were 22 kips (97.9 kN) and 0.7 inches (17.8 mm) respectively.

3) The weak bare frame was excited up to yield; the strong bare frame was not.

4) Computer idealizations using DRAIN-2DX gave acceptable predictions of stiffness and maximum base shear (within 10%). Maximum tip displacement was less accurately predicted (it exceeded the experimental values by 30% in some cases of post-yielding behavior).

5) The computer idealizations exaggerate the effect of spikes in ground acceleration, especially if the structure is yielding. Predicted displacements and base shears resulting from spikes were generally higher than those measured by about 20%. Spikes in excitation while the structure was yielding caused an overestimation of tip displacement by about 50%.

7.2.3 Conclusions Regarding the In-Plane Behavior of Infilled-Frame Specimens

1) For the strong infilled frame, average stiffness could not be evaluated. Measured base shear levels were 30 to 40 kips (130 to 180 kN).

2) For the weak infilled frame, very low values of stiffness, ranging from 200 to 300 kips/inch (35 to 53 kN/mm) were measured. Base shears of 30 to 60 kips (133 to 267 kN) were measured.

3) Measured displacements from in-plane tests of infilled frames are unreasonable (drifts exceeding 12%), probably due to a failure of the displacement gages.

4) Infilled frames under in-plane excitation were not excited up to failure but some damage was induced in them.

5) The stiffness of the confining frame has significant effect on the response of the infilled frames. Finite element analysis showed that the infill in the strong frame will start cracking at higher forces because the contact area between the frame and the infill is higher than the case of the weak frame.

6) The response prediction using LPM/I had a similar pattern to the plotted using the test data. Maximum predicted base shear was close to that obtained experimentally (within 10%).

7) Computer idealization predicts the effects of spikes of shaking table acceleration on the response accurately (within 15%).

7.2.4 Conclusions Regarding the Out-Of-Plane Behavior of Infilled-Frame Specimens

1) Measured response accelerations were fairly uniform over the surface of the infills, with a slight tendency to increase with height.

2) No collapse occurred in any test. Therefore, measured load levels are only lower bounds to the strength of the specimens.

3) Strong-frame specimens results are as follows: the maximum base shear for the previously damaged specimen was about 1.2 kips (5.3 kN); the maximum base shear for the repaired infill was over 2.0 kips (8.9 kN); and the maximum base shear for the virgin infill was about 1.0 kip (4.4 kN).

4) For the weak infilled-frame specimen, the maximum out-of-plane base shear was 2.0 kips (8.9 kN), and the maximum displacement was 0.6 inches (15.2 mm). The average stiffness was estimated as 10 kips/inch (1.8 kN/mm).

5) Maximum lateral pressure levels (transverse inertia force per unit area) on the repaired specimen were almost twice those of the unrepaired panel for similar levels of damage.

6) The level of lateral pressure reached in the damaged infill was higher than in the virgin specimen. However, this may be due to the fact that the specimens were not excited up to their ultimate strength. Therefore, it is not possible to assess the real effect of the in-plane excitation on the out-of-plane strength of the panels.

7) The cracking pattern was X-shaped, similar to that obtained for correponding static tests.

8) Predicting the out-of-plane strength using one-way strips cracked at mid-span is not conservative.

7.3 Recommendations for Implementation

1) Dynamic analysis of infilled frames excited in-plane can be performed using equivalent single degree of freedom idealizations in conjunction with the computer program LPM/I, as described in Appendix B, give accurate results.

2) The initial lateral stiffness of infilled frames excited in-plane is most accurately predicted using Stafford Smith's second method "SS2" (as explained in Section 7.2.3). Under cyclic loads the stiffness will eventually degrade to half of this initial value.

3) The lateral strength of infilled frames excited in-plane is most accurately predicted using the "CERL" method (as explained in Section 7.2.4)

4) The out-of-plane strength of infills can be predicted using the yield line-arching theory (as explained in Section 7.3).

7.4 Recommendations for Further Research

1) Further experimental research is required to determine the effect of in-plane damage on the out-of-plane strength of infilled frames. Similarly, the effect of previous damage due to out-of-plane shaking on the in-plane strength must also be assessed.

2) Further experimental research is required to idealize the effect of the relative displacements between the cracked segments of an infill panel on its out-of-plane strength.

CHAPTER 8 REFERENCES

Al-Chaar, G., Angel, R., and Abrams, D. P. (1994), "Dynamic Testing of Unreinforced Brick Masonry Infills," Proceedings of the Symposium on Advances in Engineering for Concrete and Masonry Structures, April 24-28, 1994.

Allahabadi, R. and Powell, G. H. (1988), "DRAIN-2DX User Guide," EERC Report No. 88/06, University of California, Berkeley.

Anderson, C. (1984), "Arching Action in Transverse Laterally Loaded Masonry Wall Panels," The Structural Engineer, Vol. 62B, pp. 12-23.

Bashandy, T. R., Rubiano, N., and Klingner, R. E. (1994), "Behavior of Reinforced Concrete Infilled Frames under Dynamic Loading," Report to U.S. Army Construction Engineering Laboratory (USACERL), Phil M. Ferguson Structural Engineering Laboratory, The University of Texas at Austin, December 1994.

Carter, C. and Stafford Smith, B. (1969), "Structural Behavior of Masonry Infilled Frames Subjected to Racking Loads," Designing, Engineering, and Constructing with Masonry Products, F. B. Johnson, ed., 1969, pp. 226-233.

Dawe, J. L. and Seah, C. K. (1990), "Out-of-Plane Resistance of Concrete Masonry Infilled Panels," Journal of the Canadian Society of Civil Engineering, January 1990, pp. 854-864.

Eremin, A. A. (1956), "Discussion of Arching Action Theory of Masonry Walls," Journal of the Structural Division of the American Society of Civil Engineers, Vol. 82, pp. 1067-27 - 1067-40.

Ewing, R. D., El-Mustapha, A., and Kariotis, J. C. (1987), "FEM/I: A Finite Element Computer Program for the Nonlinear Static Analysis of Reinforced Masonry Building Components," Report No. 2.2-1 EKEH (Revised 1990).

Farahany, M. M. (1983), “Computer Analysis of Reinforced Concrete Cross-Sections,” Master’s Thesis, The University of Texas at Austin, December 1983.

Holmes, M. (1961), “Steel Frames with Brickwork and Concrete Infilling,” Proceedings of the Institution of Civil Engineers, Vol. 19, No. 6501, August 1961, pp. 473-475.

Holmes, M. (1963), “Combined Loading on Infilled Frames,” Proceedings of the Institution of Civil Engineers (25), pp. 31-38.

Kanaan, A. E. and Powell, G. H. (1975), “DRAIN-2D,” EERC Report No. 73-6 and 3-22, University of California, Berkeley.

Kariotis, J. C., Rahman, A. M. D., Wafqi, O. M., and Ewing, R. D, (1992), “LPM/I Version 1.03 A, Computer Program for the Nonlinear, Dynamic Analysis of Lumped Parameter Models,” Report No. 2.3-4, EKEH.

Liauw, T. C. and Kwan, K. H (1982), “Nonlinear Analysis of Multistory Infilled Frames,” Proceedings of the Institution of Civil Engineers, Part 2, No. 73, pp. 441-454.

Liauw, T. C. and Kwan, K. H (1983a), “Plastic Theory of Non-Integral Infilled Frames,” Proceedings of the Institution of Civil Engineers, Vol. 75, September, pp. 707-723.

Liauw, T. C. and Kwan, K. H (1983b), “Plastic Theory of Infilled Frames with Finite Interface Shear Strength,” Proceedings of the Institution of Civil Engineers, Vol. 75, December , pp. 707-723.

Liauw, T. C. and Kwan, K. H (1985), “Unified Plastic Analysis of Infilled Frames,” Journal of Structural Engineering, ASCE, Vol. 111, No. 7, July 1985.

Mahin, S. A. and Bertero, V. V. (1977), “RCCOLA: A Computer Program for Reinforced Concrete Column Analysis, User’s Manual and Documentation,” Department of Civil Engineering, University of California, Berkeley, August 1977.

McDowell, E. L., McKee, K. E., and Sevin, E. (1956), "Arching Action Theory of Masonry Walls," Journal of the Structural Division of the American Society of Civil Engineers, Vol. 82, Paper 915, pp. 915-1 - 915-18.

Riddington, J. R. and Stafford Smith, B. (1977), "Analysis of Infilled Frames Subjected to Racking with Design Recommendations," Journal of the Structural Division, ASCE, Vol. 55, No. 6, June 1977, pp. 263-268.

Stafford Smith, B. (1962), "Lateral Stiffness of Infilled Frames," Proceedings of the institution of Civil Engineers, Vol. 88, No. 3355, December 1962, pp. 183-199.

Stafford Smith, B. (1966), "Behavior of Square Infilled Frames," Journal of the Structural Division, ASCE, Vol. 92, No. ST1, February 1966, pp. 381-403.

Stafford Smith, B. (1967a), "The Composite Behavior of Infilled Frames," Tall Buildings, A. Coull and B. Stafford Smith, eds., Pergamon Press, London, 1967, pp. 481-495.

Stafford Smith, B. (1967b), "Methods for Predicting the Lateral Stiffness and Strength of Multi-Storey Infilled Frames," Building Science, Pergamon Press, Vol. 2, November 1967, pp. 247-257.

Stafford Smith, B. (1969), "A Method of Analysis of Infilled Frames," Proceedings of the institution of Civil Engineer, Vol. 44, No. 7218, September 1969, pp. 31-48.

Stafford Smith, B. and Riddington, J. R. (1978), "The Design of Masonry Infilled Steel Frames for Bracing Structures," Journal of the Institution of Structural Engineers, Vol. 56Bm, No. 1, Mar 1978, pp. 1-8.

Thomas, R. D. and Klingner, R. E. (1990), "Behavior of Infilled Frames," Chapter 4 in Limit States of Masonry, The Masonry Society, Boulder, Colorado.

APPENDIX A: DESCRIPTION OF COMPUTER PROGRAMS AND ANALYTICAL IDEALIZATIONS

In this Appendix the principal assumptions and the procedures used in the computer programs and in the preparation of the analytical idealizations are summarized.

A.1 RCCOLA (Mahin 1977, Farahany 1983)

RCCOLA is a program for the analysis of reinforced concrete beam-column sections. It was used to calculate the moment curvature behavior of the beams and columns for both the strong (Model #1) and the weak (Model #6) bare frames.

The stress-strain relationship proposed by Park and Kent was used for the concrete, assuming f'_c equal to 5000 psi (Al-Chaar 1994). The steel yield strength was assumed to be 62.5 ksi (personal contacts with Al-Chaar). The analysis considered the side slab connected to the beam. For both the column and the beam, the initial section only was analyzed. There was no need to analyze the confined section because the level of loading was much lower than that causing the loss of cover.

A.2 DRAIN-2DX (Kanaan 1975, Allahabadi 1988)

DRAIN-2DX is a general-purpose computer program for the static and dynamic analysis of inelastic planar structures. It was used to analyze the response of both the weak and strong bare frames, loaded with the ground accelerations obtained from the shaking table data.

The beam-column element was used to model the columns and the beams of the frames. This element uses the parallel-component model, with axial and flexural deformations. Flexural shearing deformation is also considered. Yielding can take place only in concentrated plastic hinges at the element ends. Strain hardening is approximated by assuming that the element consists of elastic and inelastic components in parallel. The hinges in the inelastic component yield under constant moment, but the moment in the elastic component continues to increase. For the L shaped beams of these specimens, the positive and negative yield moments differed. Yield moments for the beam and the interaction diagram for the columns were obtained from RCCOLA analysis of the initial sections, because the level of loading was much lower than that causing the loss of cover.

Masses were assumed to be concentrated at the nodes of the beam-column connections. Rotational mass was assumed to come only from the beam and column self weight, and was obtained assuming a cubic deflormed shape for the elements. Translational mass was the calculated using the frame's self-weight, plus the concentrated mass on the top of the slab.

Equivalent viscous damping was assumed as 5% of critical. Rayleigh damping was used, and values of mass and stiffness-proportional damping were obtained using the fundamental period of the undamped structure.

A.3 FEM/I (Ewing, 1987)

The FEM/I program is a finite-element program for the nonlinear static analysis of masonry walls. Finite elements were used to represent the masonry infill and the reinforced concrete frame. The analytical models and constitutive relations used for the elements consider the various biaxial stress states that can exist in the structure, as well as the pre- and post-cracking behavior. The program uses an initial stiffness formulation with an incremental solution method that is reliably convergent for softening systems when prescribed displacements are used as the primary excitation.

The problem is dominated by material nonlinearity; geometric nonlinearities are assumed negligible. The model assumes that tension cracks are smeared over the integration points of each finite element. The model includes compressive strength reduction after tensile cracking occurs in orthogonal directions. This model does not incorporate any stiffness degradation. Masonry and concrete strengths were assumed to be 5 ksi, and the steel yield strength was assumed to be 62.5 ksi. Figure (A.1) shows the finite-element mesh used for the analysis of the specimen under investigation.

A.4 LPM/I (Kariotis, 1992)

LPM/I is a computer program for the nonlinear dynamic analysis of lumped-parameter models subjected to external forcing functions and kinematic boundary conditions. The infilled frame was modeled using a nonlinear, hysteretic, degrading envelope spring element (Element 11), which was originally formulated for masonry cantilever shear walls (Figure 6.8). The characteristics of this element are described by force-deformation relations based on analysis and observation of cyclic experiments of reinforced masonry walls.

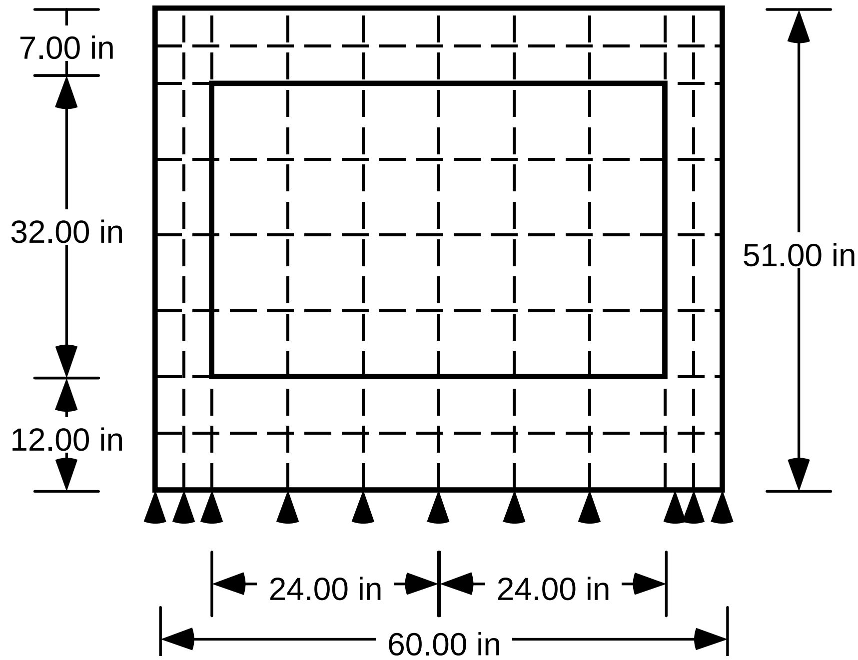

Figure A.1 Finite Element Mesh used for FEM Analysis

The force-deformation relations include an envelope curve, defined by the following characteristics: initial stiffness; stiffness softening to a peak strength; deformation at peak strength; and strength degradation after peak strength. Additionally, the hysteretic behavior is defined by the following characteristics: degrading unloading stiffness; rules for reloading; and pinch force. The values of these parameters were obtained from the output of the push-over analysis performed with FEM/I. Viscous damping was neglected, because the nonlinear model had been calibrated neglecting viscous damping. The effect of this approximation is expected to be insignificant, because the effect of viscous damping is negligible with respect to hysteretic damping.

APPENDIX B: EFFECT OF MASONRY STRESS-STRAIN RELATIONSHIP ON OUT-OF-PLANE PANEL STRENGTH, CONSIDERING ARCHING ACTION

In this Appendix the lateral strength of masonry, (including the effects of arching action) will be computed assuming a rectangular stress distribution for masonry as obtained in Section 6.3. Those results will be compared with the lateral strength calculated assuming a parabolic stress-strain distribution, and also with the results obtained from tests on the static behavior of brick beams under lateral loads (McDowell, 1956).

A parabolic stress-strain distribution similar to that used in reinforced concrete analysis is used to describe the stress distribution over regions of contact of the masonry segments. This stress-strain distribution is shown in Figure (B.1) , and is given by the following equation

$$f_c = f'_c \left[\frac{2\varepsilon}{\varepsilon_o} - \left(\frac{\varepsilon}{\varepsilon_o} \right)^2 \right] \tag{B.1}$$

Where

f_c = stress

f'_c = maximum compressive stress

ε = compressive strain

ε_o = compressive strain at maximum stress

The deflected shape of a half-strip segment is shown in Fig. (B.2). From simple geometric relations the decrease in contact length, b, is related to the segment rotation by

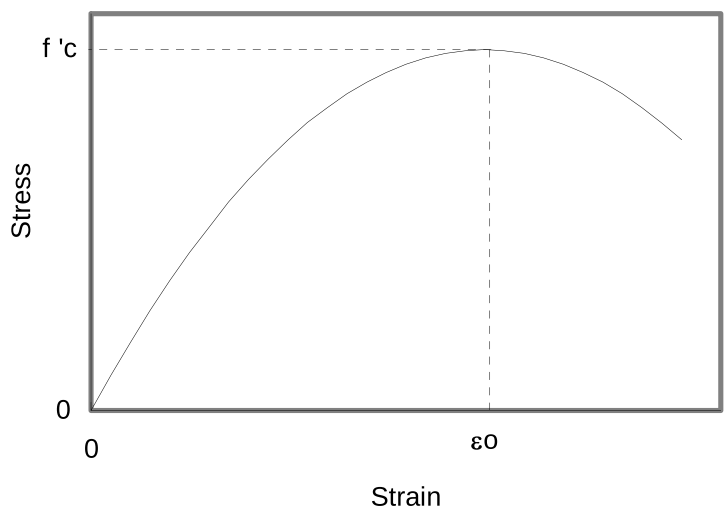

Figure B.1 Assumed Stress Strain Relationship for Masonry

$$b = \frac{h}{4}\left(\frac{1-\cos\theta}{\sin\theta}\right) \tag{B.2}$$

The center deflection, d, is given in terms of the rotation by

$$d = h\left(\frac{1-\cos\theta}{\sin\theta}\right) \tag{B.3}$$

From Equations (B.2) and (B.3), the decrease of contact length and the center deflection are related by

$$b = \frac{d}{4} \tag{B.4}$$

and the contact length, c, is given by

$$c = \frac{t}{2} - \frac{d}{4} \tag{B.5}$$

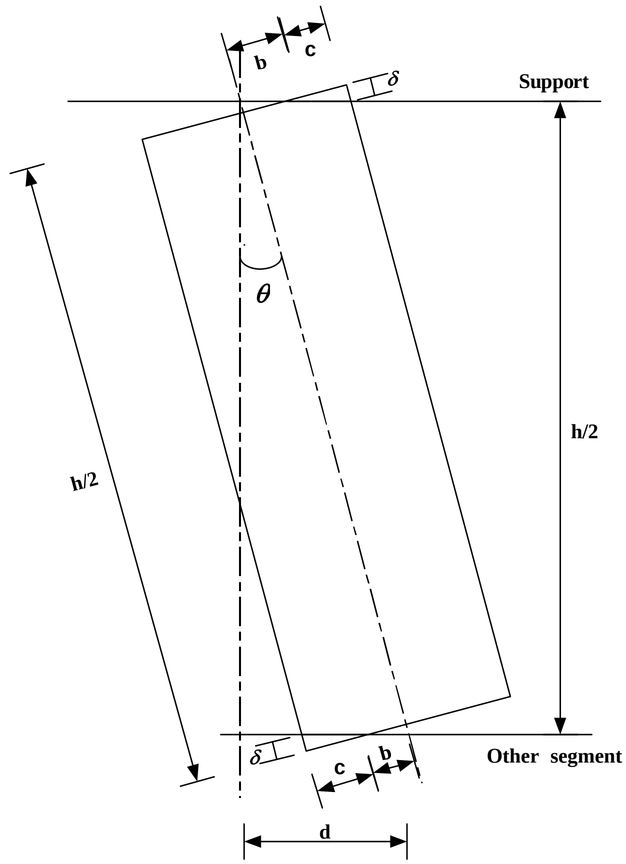

Figure B.2 Deflected Shape of Half Strip Segment

The shortening at one end of the masonry segment, δ, is given by

$$\delta = c \cdot \tan\theta \tag{B.6}$$

or

$$\delta = \left(\frac{t}{2} - \frac{d}{4}\right)\frac{2d}{h} \tag{B.7}$$

$$\delta = \left(t - \frac{d}{2}\right)\frac{d}{h} \tag{B.8}$$

The strain in the masonry segment is given by

$$\varepsilon \approx \frac{2\delta}{h/2} \tag{B.9}$$

$$\varepsilon \approx \left(2t-d\right)\frac{2d}{h^2} \tag{B.10}$$

The resultant compression force due to a contact length c, and a maximum strain ε, can be obtained by integrating Eq. (B.1) as follows

$$F = \int_0^c f_c\,dx = f'_c \int_0^c \left(\frac{2\theta x}{\varepsilon_o} - \frac{\theta^2 x^2}{\varepsilon_o^2}\right)dx \tag{B.11}$$

$$F = f'_c\,\frac{\varepsilon}{\varepsilon_o}\,c\left(1-\frac{\varepsilon}{3\varepsilon_o}\right) \tag{B.12}$$

The distance from the neutral axis to the line of action of resultant compression force, x_c , can be obtained from the following equation

$$x_c\ F = \int_0^c f_c\ x\ dx \tag{B.13}$$

Substituting the expression above for F (Eq. B.12), and rearranging terms, the distance from the neutral axis to the line of action for the resultant compression force is

$$x_c = c\left(\frac{8\,\varepsilon_o - 3\varepsilon}{12\,\varepsilon_o - 4\varepsilon}\right) \tag{B.14}$$

The resisting moment corresponding to a deflection d is given by

$$M = F\left[t-d-2\left(c-x_c\right)\right] \tag{B.15}$$

The lateral strength of the segment is obtained by substituting the value of this moment in Equation 25.

Figure B.3 compares the resistance function described above and that obtained using an equivalent rectangular stress block, with the MIT Test Beam 8-3. The rectangular stress block resistance function calculates the lateral strength assuming uniform stress equal to $0.85f'_c$ over a portion of the contact length. The ratio between the length of the stress block and the contact length does not affect the lateral strength because the contact length is chosen so that the lateral strength would be maximum. The function assume linear load-deflection relationship up to the lateral strength.

The resistance function obtained using a parabolic stress strain distribution is very close to test results. Lateral strength and deflection at the lateral strength are estimated with an error less than 2%. The equivalent rectangular stress block method shows less accuracy. However, the computed lateral strength and deflection at the lateral strength are still close to the test results (the difference is about 6%). The inaccuracy of the equivalent rectangular stress block method results from assuming a linear load-deflection relationship. Because the contribution of the lateral resistance of a masonry infill is mostly from segments reaching the deflection at maximum strength, and because the equivalent stress block method simplifies the estimation of the total lateral strength of an infill with an "X" yield line pattern (as described in Section 6.3), the method is considered acceptable.

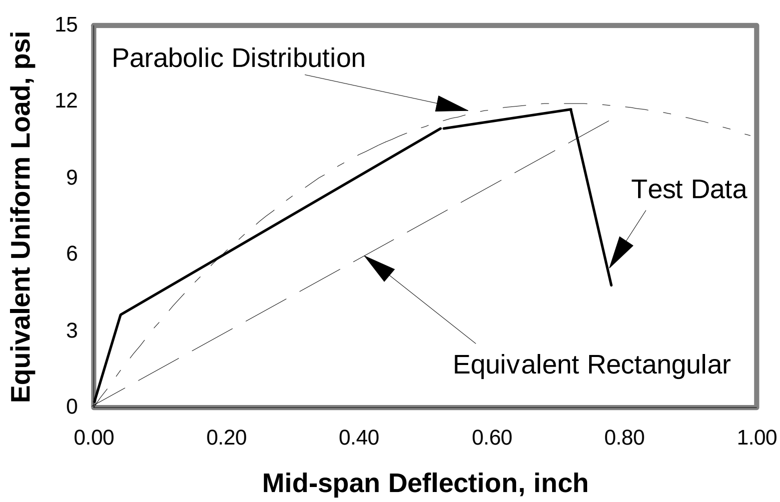

Figure B.3 Comparison of Resistance Functions Using Different Stress Distributions with Test Data